DEVELOPMENT OF A HIGH SENSITIVITY RADON EMANATION DETECTOR

by

Stephen Robert Hanchurak

A thesis submitted in partial fulfillment of the requirements for the degree of

Master of Science

Department of Physics

University of Alberta

Abstract

Within the last few decades, experiments in particle physics have developed a need to produce radio-pure experiments. These experiments are designed to search for new physics that involves low event rates. Due to the event rates as low as 1 event/kt/year, these experiment must take precautions that reduce background radiation in the detector. A significant source of background radiation comes from radon-222 produced from the uranium decay chain. Radon-222 is gaseous and can be emanated from the surface of materials and propagate throughout a detector contaminating the experiment. Measuring the emanation rate of radon from materials has become an important area of study to enable the construction of low background environments. This thesis will present the ongoing development and analysis of a high sensitivity radon detector at the University of Alberta with a sensitivity of 4 ± 2 radons/hr at 68% confidence.

Acknowledgements

Many may view a thesis as the work of single person. I for one do not. I could not have completed this long and arduous journey alone. The completion of this thesis could not have been achieved without the help of many. I would like to thank those who have had an enormous influence on my work and my time spent here. I would like to thank my supervisor Dr. Carsten Krauss. Without his guidance and immeasurable contribution to my work, I could never have hoped to finish. I would also like to thank Carsten for the opportunity he has given me. My particle physics group for all their help, insight and knowledge of an field I can only hope to understand. The electronics shop for their help with any electronics questions/problems I encountered. Aksel Hallin for his vast experience, knowledge, and willingness to help in any way he could. Richard Soluk and his assistance with the technical aspects of my research was invaluable to the completion of my thesis. Arash, Logan, Thomas, Sarah, Tania, Pitam, Pawel and Kamal for the help in keeping my sanity alive. Without them the late nights would have been an unbearable torture. My close friends Brett, Dom, Garret and Matt. Their willingness to listen to my angry rants and ability to bolster my confidence at times when I felt desperately overwhelmed was a foundation of my success. Finally I would like to thank my family who have supported me through my entire academic career. Without them I would never have dreamed of being where I am today.

Contents

List of Tables

List of Figures

List of Abbreviations

List of commonly used abbreviations

Rn	Radon
Po	Polonium
Bi	Bismuth
Pb	Lead
U	Uranium
Th	Thorium
Ra	Radium
N_2	Nitrogen Gas
ADC	Analog to Digital Converter
AMU	Atomic Mass Unit (1.66×10^{-27} kg)
DAQ	Data Acquisition
eV	electronVolt, 1.6×10^{-19} Joules
FWHM	Full Width at Half Maximum
MeV	Mega-electronVolt
HV	High Voltage
ESC	Electro-Static Chamber
mBar	milli-Bar, 100 Pascal
ROI	Region of Interest
WIMP	Weakly Interacting Massive Particle
TPC	Time Projection Chamber
AV	Acrylic Vessel

PMT	Photomultiplier Tube
SNO	Sudbury Neutrino Observatory
PIN Photodiode	Positive-Intrinsic-Negative Photodiode
UPW	Ultra-pure water
MSPS	Million Samples Per Second
KSPS	Thousand Samples Per Second
kt	Kiloton

List of Symbols

List of commonly used symbols

β	Electron
γ	Photon
α	Alpha particle
Θ	Angle of Incidence
ϵ	Efficiency
ν	Neutrino

Chapter 1

Introduction

With the advent of neutrino experiments and dark matter searches extremely sensitive particle detection systems have been developed. These sensitive detection systems detect particles through their interactions with a target material within the detector. These interactions result in the deposition of energy in the target materials[1]. The deposited energy can be observed as detectable radiation, ionization, vibrations, temperature changes, or even secondary particle creation. From these observation it is possible to identify a type of particle and ideally infer how it was produced. This method of detection however is very sensitive to the effects of background radiation which also interacts within the target material. Background radiation can result in energy depositions and interactions which produce signals that are consistent with the particle of interest. Background radiation can come in many forms for example alpha, beta and gamma radiation from nuclear decays of radioactive isotopes and cosmic rays. This background radiation obscures the signal from the particle of interest. This makes it necessary to find methods of determining and minimizing signals caused by backgrounds within a detector.

A significant source of background radiation comes from radioactive decays of naturally occurring uranium-238 and thorium-232 which produce radon in a chain of decays. These decay chains can be seen in figure 1.1 where uranium-

238 produces radon-222 and thorium-232 produces radon-220. Radon is a noble gas that has no stable isotopes. Because it is gaseous it is very volatile and can be emitted from the surface of many materials causing background radiation in the subsequent decays of radon. This thesis focuses on a particle detector which has been constructed at the University of Alberta that can measure radon-222 emanation. Radon emanation is the process where gaseous radon is emitted from the surface of materials arising from uranium and thorium contamination. This detector has been used to measure radon emanation in various materials used in the construction of particle detectors. The following chapter, Chapter 2 will introduce radon and radon daughters. Chapter 3 will introduce other experiments and their methods of radon detection. A summary of the working principles and designs of the University of Alberta's radon detector will be given at the end of this chapter. In Chapter 4 the analysis techniques used to extract radon emanation rates from the data obtained from the detector will be covered. In addition to the description of analysis techniques the calibration process and efficiency determination will be described. Chapter 5 will report on results obtained from the detector and a short summary of a fully analyzed detector run. The final chapter will provide a short summary of the emanation analysis, along with the projected sensitivity of the detector. In closing an outline for improvements to the detector will be presented.

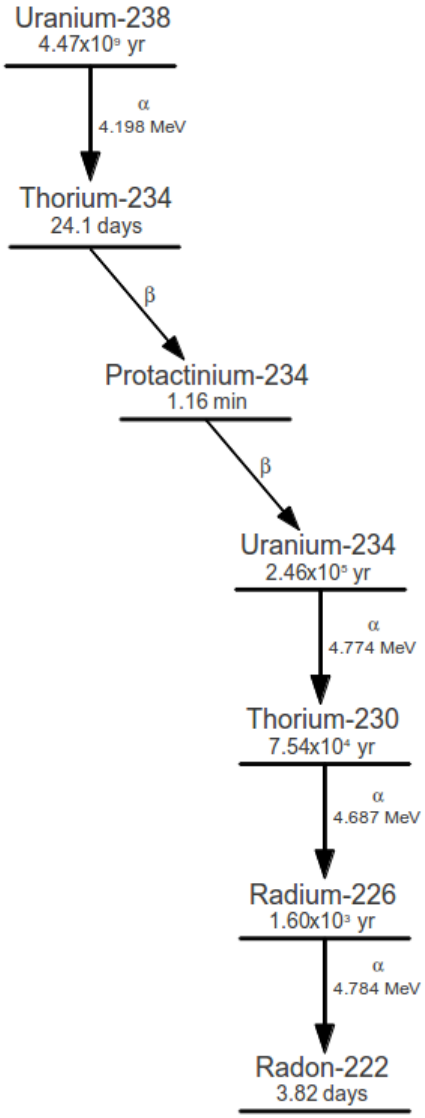

(a) Uranium decay chain.

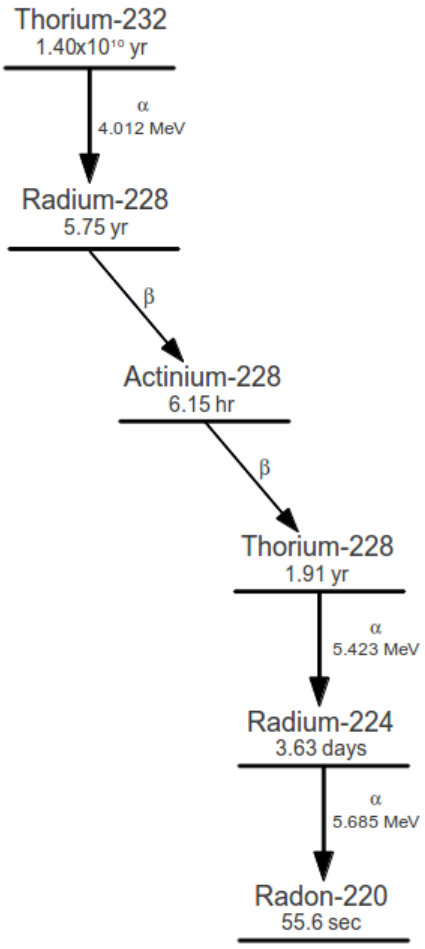

(b) Thorium decay chain.

Figure 1.1: The decay chain for (naturally occurring) uranium and thorium up to radon. Data obtained from [2].

Chapter 2

Radon

Radon is an element that is produced from the decay chains of naturally occurring uranium and thorium. It has become commonly accepted that radon was first discovered in 1900 by Friedrich E. Dorn in Germany[3]. Radon has an atomic number of 86 and is the heaviest of all the noble gases. It has a low boiling point of $-61.8\,^{\circ}\mathrm{C}$[4] and therefore at room temperatures (298 K) radon is gaseous and is distributed evenly throughout the air. All radon isotopes are radioactive, while its most common and stable isotope is radon-222 with a half-life of 3.82 days. Due to the gaseous nature of radon and relatively long half-life, radon can become a significant source of radioactivity in atmospheric air. Gaseous radon is produced from the surface of many construction materials which contain trace amounts of naturally occurring uranium and thorium, its parent nuclei. The production of radon[1] is so considerable that over 50% of the total natural radiation a human is exposed to is a result of radon exposure/inhalation[5]. As a result radon constitutes a considerable health risk which has lead to radon monitoring of buildings throughout the world[6]. Radon decays via alpha decay with MeV scale Q values and can result in decay products embedding themselves in the surface of materials[7, 52]. It is

[1]This includes natural production of radon within the environment along with radon produced from manufactured materials.

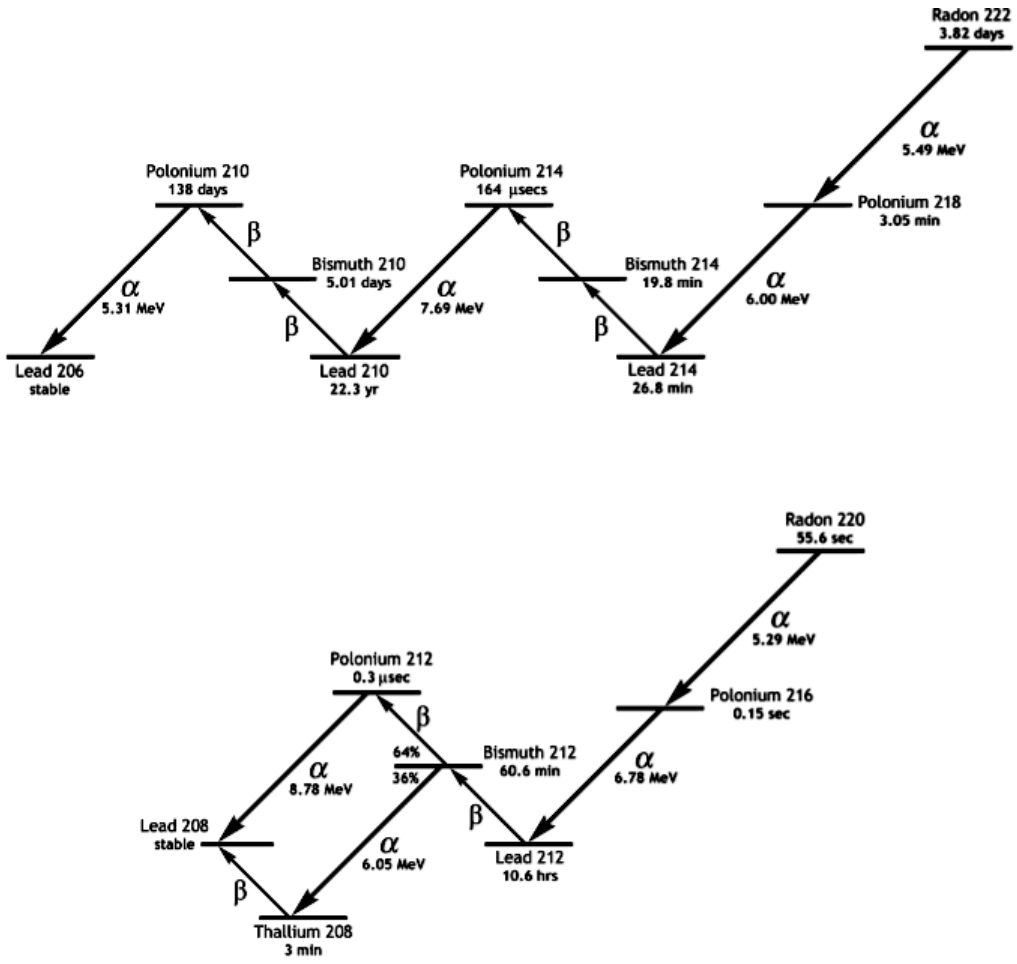

Figure 2.1: Decay sequence of two common radon isotopes[8]. Radon-222 is produced from uranium decays and radon-220 is produced from thorium decays.

these properties of radon which makes it an important research subject in low background experiments and will be discussed in this section.

2.1 Decay Chain of Radon

Radon is produced naturally from both the uranium and thorium decay chains. There are two naturally occurring radon isotopes both of which decay by alpha emission. The decay chain of these isotopes is shown in figure 2.1.

The most important and abundant radon isotope is radon-222. Radon-

222 alpha decays into polonium-218, which further decays into polonium-214. These radon daughters can then be used for the indirect detection of radon-222. This is possible due to the short half-life of these isotopes relative to radon-222 which allow secular equilibrium between radon and its daughters to be reached. As a result of secular equilibrium, the abundance of these isotopes is determined by the quantity of radon-222 producing them and directly reflects the activity of radon-222. The polonium isotopes have decay energies of 6.00 MeV (polonium-218) and 7.69 MeV (polonium-214) and are predominantly positively charged when produced[9]. The alpha decay of polonium-214 result in the creation of lead-210 and polonium-210. These isotopes have a half-life of 22.3 years and 138 days respectively and it is these specific long-lived isotopes that make the control of radon exposure important for low-background experiments, which will be discussed in the following section.

In addition to radon-222, a common radon isotope is radon-220 historically known as thoron. Radon-220 decays into polonium-216, polonium-212 and bismuth-212. These nuclei all decay through alpha decays with energies ranging from 6-9 MeV. These nuclei including, radon-220 are short-lived and as a result decay away quickly and do not pose as significant a background problem for low background experiments as radon-222.

2.2 Why is Radon Important?

Radon is an important source of background radiation for low-background experiments. These experiments require extremely low levels of background radiation as the particular physics they investigate only produces a small number of events[2]. This small number of events can be easily obscured by even low levels of background radiation resulting in difficulties in distinguishing events of interest from background events. Thus attempts to significantly lower background

[2]The number of events produced can be as low as only a few events per year.

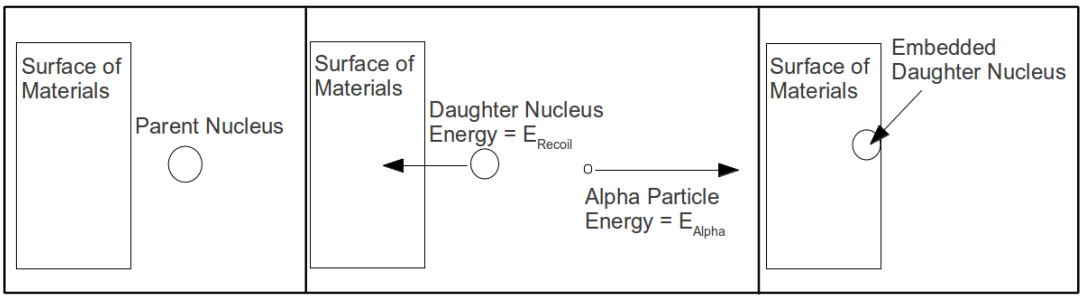

Figure 2.2: The embedding process of radon and its daughter nuclei in materials.

radiation sources are required.

Many construction materials contain trace amounts of uranium and thorium. Due to radon production from uranium and thorium decays such materials release gaseous radon into their surroundings. This can result in high concentrations of radon in the air as a result of its long half-life. Increasing the radon concentration in the air increases the radioactivity of the air. This causes an increase in background radioactivity which directly counters the purpose of low-background experiments. This makes the control of radon concentrations in air essential as a means of lowering background radiation in low-background experiments. Radon present in atmospheric air however is not the only problem associated with radon and low-background experiments. Since radon decays through alpha emission its daughters become charged radioactive nuclei that can become attracted to the surface of materials due to electrostatic attraction. As these charged radioactive daughters become attracted to the surface of materials they can further decay which can cause the daughter nuclei to become embedded within a thin layer below the surface of the material as shown in figure 2.2. The embedded daughter nuclei can then further decay to long lived nuclei.

The daughter nuclei of specific importance are the polonium-210 and lead-210. These nuclei have a half-life of 138 days and 22.3 yrs respectively. This poses an issue as the longer a material is exposed to air containing a high

radon concentration, the larger the surface build-up of polonium-210 and lead-210. Even in an environment free from radon it is impossible to wait until all surface contamination decays due to the long lifetimes. This method has been employed with ancient lead recovered from sunken Roman ships. The lead recovered was found to have low levels of radioactivity and has been used as radio pure shielding in experiments such as CUORE[10]. There is an additional option available which is to remove a small surface layer of the material which contains the embedded nuclei. This presents a difficult task for many operating detectors as this surface contamination slowly increases over time and would require a detector to be disassembled. Disassembling of an operational detector is impractical due to non-reversible construction techniques, such as acrylic bonding which can make areas inaccessible after.

There is an additional property of radon that can lead to the issues described above. Since the majority of construction materials contain trace amounts of uranium and thorium, this results in the materials emanating radon from the surface of the material. This is an intrinsic property of each material and cannot be lowered, even with the use of an environment free from radon[3]. This creates an additional problem for low-background experiment in which construction materials must be carefully selected based on its radon emanation. However manufacturing processes can vary from different manufacturers and as a result each material must be tested individually for radon emanation rates and only low emitters can be chosen. It is this property of radon that is studied in this thesis.

[3]It is a property defined by the uranium/thorium concentration throughout the material producing the radon and the diffusion properties of radon within the material.

Chapter 3

Low Background Experiments

3.1 Motivation

In low background experiments such as dark matter and neutrino experiments event rates are substantially lower than most other experiments. As a result a detailed understanding of all background radiation sources must be gained for each low event rate experiment. The background radiation sources must be fully understood as they can imitate the signals of interest and prevent significant measurements.

A significant source of background radiation comes from radon. For low background experiments the following routes of radon induced backgrounds are most relevant:

- radon inherent in atmospheric air can be introduced into detector components.
- emanation of radon from the surface of detector materials.
- surface deposits of radon daughters.
- internal contamination with uranium and thorium.

These sources produce background radiation which can have a significant effect on the detection of the signals of interest.

For low background experiments such as dark matter searches, radon and its daughters decay and produce nuclear recoils within the target materials. The nuclear recoils are an important background in direct detection dark matter searches, where these experiments aim to detect dark matter through its collision with target nuclei producing a nuclear recoil. The nuclear recoils produced from radon decays can imitate the signals for a dark matter recoil event. This can introduce difficulties in distinguishing nuclear recoils produced from radon decays from recoils initiated from dark matter interactions. In addition to nuclear recoils from the decays of radon and its daughters, the neutrons from (α,n) reactions are a strong source of background. The alphas emitted from radon decays can initiate nuclear reactions within nuclei causing the ejection of a neutron. As neutrons have no charge, they interact within the target material in the same way as dark matter, producing a nuclear recoil signal once they interact with the surrounding nuclei. The neutron recoil signal is therefore indistinguishable from a dark matter signal[1]. As a result, the activity from radon and radon daughters present in the detector needs to be minimized and monitored.

In addition to dark matter searches, neutrino experiments are sensitive to the effects of radon backgrounds. Unlike dark matter experiments, nuclear recoils are not a predominate concern for neutrino experiments. Alpha particles produced from radon decays can undergo alpha quenching in which energy is lost as they travel through matter[1]. Once they reach the target material of the detector the alpha particles can appear to have a small fraction of their original energy. They can therefore produce a signal that is within the ROI for neutrinos and act as a background signal. The decays of the radon chain can produce

[1]Neutron sources have been used as calibration sources for dark matter experiments[11, 12, 13].

γ radiation in addition to the alpha emissions. In the SNO experiment the γ radiation from these decays could cause photo-disintegration of D_2O resulting in free neutrons. The resulting signal from the free neutrons can imitate a neutrino signal as neutrinos interact under the same principle which cause the photo-disintegration of D_2O[14]. This introduces an additional background signal from the radon decay chain decaying through gamma emission.

These are the reasons that radon control measures must be taken to lower radon contamination and radon exposure in low background experiments. This can be achieved through the careful selection of materials with low radon emanation, low contamination of uranium and thorium and by limiting the detector exposure to radon in air using a radon free environment. For these reasons radon is an important research subject and motivates this thesis.

3.2 SNO

The Sudbury Neutrino Observatory(SNO) was a neutrino experiment in the Creighton mine near Sudbury, Ontario, Canada. It was first proposed in 1984 and was designed to solve the solar neutrino problem[15]. The solar neutrino problem resulted from a deficit of neutrinos that were detected when compared to the number of neutrinos that should be produced in the Sun according to solar models[16]. The one-third deficit in neutrinos was theorized to be a result of neutrino oscillations. Massive neutrinos can oscillate between three different flavor states. This explains the one-third deficit observed in the number of detected neutrinos. The observed deficit of solar neutrinos was a result of the method used to detect solar neutrinos which was only sensitive to one flavor state, the electron-neutrino and could not detect muon or tau neutrinos. SNO was designed and constructed to allow the detection of all three flavor states[17]. The SNO detector consisted of a 12 m diameter acrylic vessel (AV) with an 8 m long, 2 m diameter neck. The AV was placed at a depth of $\sim$2040 m within

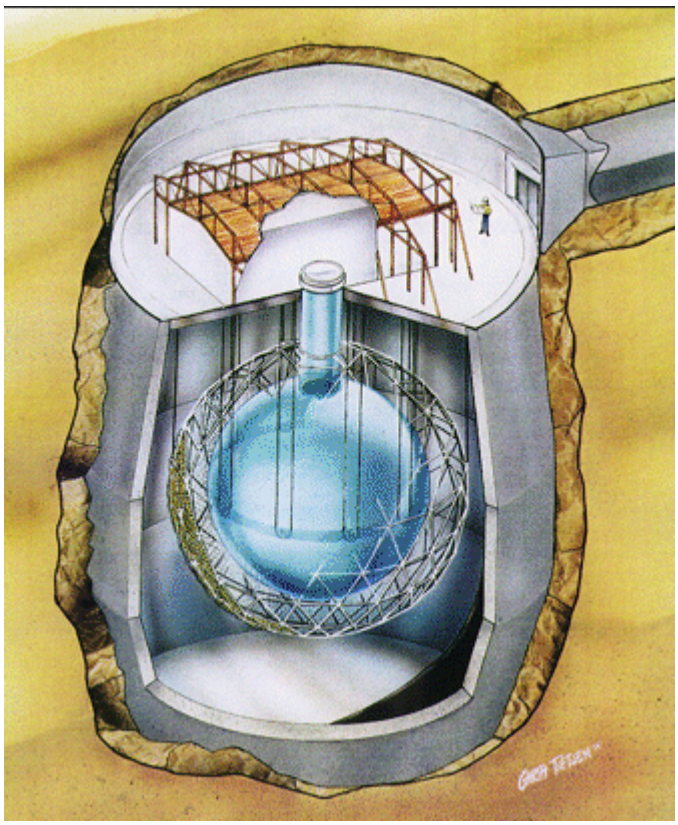

Figure 3.1: Artist's rendering of the SNO detector in its excavated cavern[18].

the Creighton mine to shield SNO from the effects of cosmic rays. In addition, the acrylic vessel was submerged in light water which acts as shielding from neutron and gamma radiation produced from the surroundings. The vessel was filled with heavy water (D_2O) which was used as the target material for neutrino interactions. Surrounding the AV was an array of PMTs with light concentrators[2] which were used for the detection of Cherenkov light from the neutrino interactions[17]. An artist's rendering of the SNO detector can be seen in figure 3.1.

The SNO detector was unique in its use of D_2O as the target material. D_2O allowed for sensitivity to interactions of all three neutrino flavors through three

[2]Using the light concentrators, it was possible to obtain a photocathode coverage of 54%[17]

types of particle interactions. The first was the charged current reaction which is sensitive to only the electron-neutrino. This interaction involves the weak force in which an exchange with the W boson occurs in the D_2O and changes a neutron from the D_2O target material into a proton and electron. The electron receives the majority of the neutrino energy due to its much smaller mass. As a result the electron propagates through the heavy water at speeds faster than light in heavy water resulting in Cherenkov radiation. The Cherenkov radiation can then be detected by the arrays of PMTs surrounding the AV. The second interaction is the neutral current reaction in which a neutrino interacts with the D_2O nucleus through the exchange of the Z boson. This interaction breaks apart the D_2O nucleus and the freed neutron scatters within the heavy water until it is captured by another nucleus. The capturing of the neutron by a nucleus produces a gamma ray emission that scatter electrons producing Cherenkov radiation that is detected by the PMT array. This interaction is sensitive to all three flavors of neutrinos. The third interaction is known as elastic scattering in which a neutrino elastically scatters off electrons surrounding a nucleus imparting energy to the electron. The energy transferred to the electron is sufficient to cause Cherenkov radiation that is detected by the PMT array. This interaction is not unique to heavy water, in fact this interaction process is used in light water detectors. This interaction is sensitive to all three flavors however it is strongly dominated by the electron-neutrino.

The standard solar models predicts only 63 events in the SNO detector per day from the contributions of all three interactions. As a result all sources of background need to be understood and accounted for. Radon presents a significant source of this background radiation and measurements of its concentration and effects within the SNO detector were required in order to accurately detect the low number of neutrino events. This prompted the development of the SNO Electrostatic Chamber (ESC) which was used to measure radon levels in the SNO detector[19].

3.2.1 SNO Electrostatic-chamber

The SNO Electrostatic Chamber(ESC) was developed as a means of measuring the radon levels in the heavy and light water of the SNO detector[19]. Even after a careful selection of ultra-low radioactive materials used to construct the SNO detector, trace amounts of uranium and thorium were present. Radium produced from the decays of uranium and thorium can dissolve within the water and be transported throughout the detector. As a result monitoring the amount of radon produced from the dissolved radium was required and led to the development of the ESC. The water in the SNO detector passed through a column filled with MnO_2 coated acrylic beads that captured the radium dissolved in the water with ∼90% collection efficiency[19]. The column of acrylic beads had nitrogen bubbled through it and the radon produced from the radium decays was transported with the nitrogen into the ESC detection system. The ESC system is shown in figure 3.2.

The ESC consists of a windowless silicon photo-diode used as an alpha particle detector. The diode has an intrinsic capacitance of 400 pF when depleted to more than 90% depletion[3] which occurs at about 70 V. Since the daughters produced from radon decays are predominately charged nuclei[9], a high voltage of -(1000-1500) V was applied to the diode producing an electric field between the detector walls and the photo-diode. The electric field is used to attract and collect the charged daughters to the photo-diode thereby significantly increasing the detection efficiency of the ESC system. In addition to an electric field to improve efficiency, an improved geometric design was used which minimize areas of low collection electric field strengths. The low electric field areas result in dead spots where collection of the daughter nuclei through the drift field would have been insufficient and would not attract the charged daughters to the diode before they decay. With the improved design of the de-

[3]The depletion layer is a biased voltage dependent volume within the diode which is void of free electrons.

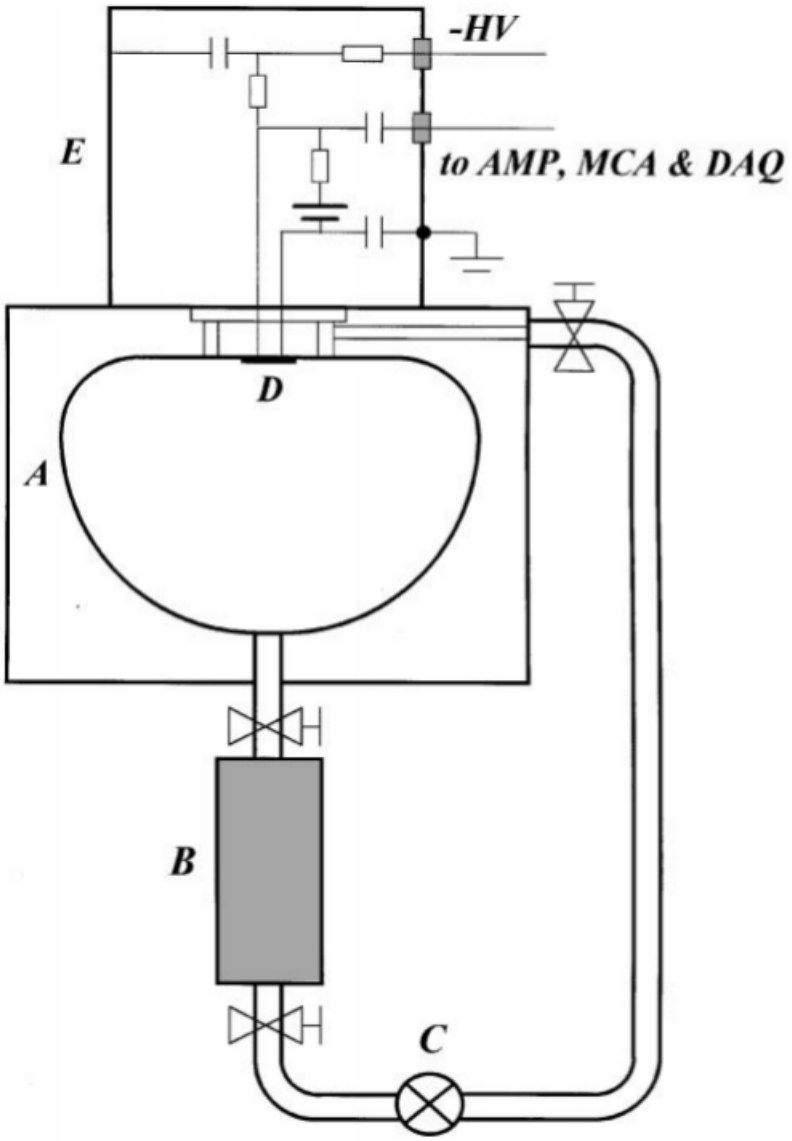

Figure 3.2: Schematic representation of the second step of water radioactivity measurement. The column (B) containing Ra and Th after water sampling is dried and connected to the chamber (A). A diaphragm pump (C) is used to circulate nitrogen gas and carry radon into the chamber. The positively charged polonium ions from radon decays are collected on the detector (D) by the electric field. The signals from α-decays are sent to the electronic data acquisition system[19].

tector an efficiency of 35% was achieved for radon-222 and 22% for radon-220 with an electric potential of -1000 V at 30 mBar[19] with a sensitivity limit of the order of 10^{-10}g Th(U)/m^3 (1.24 μBq/m^3) in water[20]. The efficiency was a significant improvement over previous electrostatic radon detectors which achieved efficiencies of $\sim$10% for radon-222 and $<$1% for radon-220[9, 21, 22].

3.3 Borexino

The Borexino experiment is a neutrino detector which was designed as a real-time detector. The detector's purpose was to conduct measurements of low energy solar neutrinos fluxes. It was originally proposed in 1989 by R.S. Raghavan and was initially called the BOREX experiment[23]. Its initial purpose was the detection of boron-8 solar neutrinos using trimethylborate ($C_3H_9BO_3$) liquid scintillator. This was to be achieved through detection of the neutral current reactions which lead to nuclear de-excitation of boron-11 in the scintillator. In addition to the neutral current reactions, the detection of neutrinos was also measured through charged current neutrino capture reactions. This reaction produces carbon-11 causing the emission of a positron which produces light through electron-positron annihilation in the scintillator. The 4-ton prototype for BOREX was called Borexino and it was later determined that through sufficient scintillation purification it would be possible to instead observe the beryllium-7 neutrinos. The shift in focus from detecting boron-8 neutrinos to beryllium-7 neutrinos was a result of the significantly increased rate of beryllium-7 neutrinos produced from nuclear processes within the Sun. This evolution of the detector was preferred and thus the Borexino detector remained. The Borexino detector was constructed and began taking data in May 15, 2007[23].

The Borexino detector is located at the Laboratori Nazionali del Gran Sasso(LGNS) in Gran Sasso, Italy. Borexino is 1500 m underground providing

$\sim$3800 m.w.e shielding from cosmic rays. Borexino consists of 100 tons of liquid scintillator that is a mixture of pseudocumene (PC, 1,2,4-trimethylbenzene, $C_6H_3(CH_3)_3$) as a solvent and PPO (2,5-diphenyloxazole, $C_{15}H_{11}NO$) as flour, at a 1.5 g/l concentration[23]. The scintillator converts energy deposited by neutrino interactions into light which is then detected through arrays of PMTs surrounding the scintillator vessel. There are 2212 8" ETL-9351 PMTs used to achieve coverage of the detector. The scintillator that acts as the fiducial volume of the detector is contained within a transparent spherical nylon membrane with a diameter of 8.5 m and a thickness of 125 μm used to prevent radon contamination of the fiducial volume. This is then partially surrounded by an additional nylon vessel that contains pure pseudocumene plus dimethylphtalate, in a 5 g/l solution[23]. The second layer was added as an additional means of lowering radon diffusion into the inner vessel which contains the fiducial volume of the detector. The second layer contains a scintillator mixture similar to the inner vessel. The mixture was chosen to balance the hydrostatic pressure between the inner and outer vessel and minimize chances of distortion of the spherical shape of the nylon vessel as well as limit any possibility of mechanical ruptures of the nylon vessel. The outer vessel is produced of the same nylon as the inner vessel with a larger diameter of 12.6 m and the same thickness. The outer vessel layer is then surrounded by an additional stainless steel sphere with a diameter of 13.7 m and a thickness of 8-10 mm. Along the walls of this stainless steel sphere the PMTs are mounted. This stainless steel sphere is then submerged in ultra-pure water contained within a stainless steel tank. The inner walls of this tank as well as the outer wall of the spherical stainless steel vessel are covered with Tyvek sheets which is a highly reflective material that enhances muon detection by maximizing light collection. The final layer of ultra-pure water acts as additional shielding for the detector from radiation produced from the surroundings. The design of this detector resembles the layering of an onion in which every layer further toward the center becomes

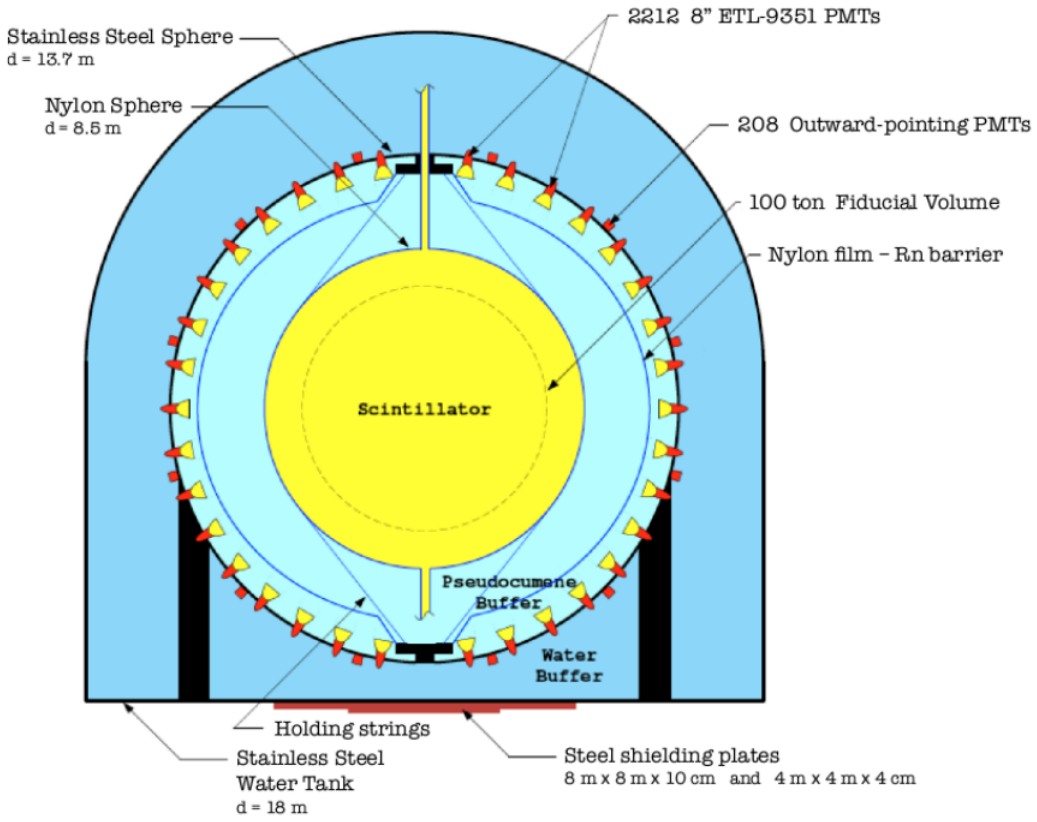

Figure 3.3: Schematic representation of the Borexino detector. The onion concept of the detector is easily visible[23].

increasingly radiopure. This is shown in figure 3.3

3.3.1 Counting Test Facility

The Borexino experiment required the measurements of radioactive contamination in the materials used to construct the detector. Borexino like the SNO detector required measuring and minimizing internal radioactivity of their scintillator in addition to limiting radioactivity of the materials used in the detector construction. The Borexino experiment developed a detector that could be used to measure the radioactive contamination of these materials, however unlike the SNO ESC this detector used completely different principles. Unlike the

development of a system which uses electrostatic attraction of radon and alpha spectroscopy as a means of detecting radon, the Counting Test Facility(CTF) uses the same concept on which Borexino operates[24]. The CTF was designed as a prototype of the Borexino detector, and was used to test and improve many aspects of the detector design before the development and operations of the Borexino detector. The CTF detector has undergone two upgrades and is in its second stage of upgrades known as CTF 3. As of December 2013 CTF 3 is still actively taking data[25]. The CTF design is shown in figure 3.4. A brief overview of its design will be covered as it closely matches a scaled down version of the Borexino detector.

The CTF detector is based on the principle of graded shielding like Borexino. The CTF consists of a nylon sphere which holds the liquid scintillator used as the active volume of the detector. The scintillator is a similar mixture of pseudocumene and PPO used by Borexino. The CTF has an active material of $\sim$4.3 tons. The spherical inner nylon vessel also reduces radon diffusion into the active material. Surrounding the inner nylon vessel is an additional nylon sphere for the same purpose of limiting radon diffusion into the active material and is known as the CTF shroud. Between the shroud and inner nylon vessel ultra-pure water is contained. The ultra-pure water serves to shield the active material from radiation from the surroundings. Around the surface of the CTF shroud is an inward facing array of PMTs for light detection. The CTF shroud and PMT array are then surrounded by a cylindrical stainless steel tank and submerged in water. This outer layer of water acts as additional shielding from surrounding radiation. In addition to the use of the Borexino onion style shielding, a refill piping system is used in which each nylon vessel which can be drained and refilled separately through pipes running at the top and bottom of the nylon vessels.

The CTF detects particles through the scintillation light produced in particle interactions. From the reconstructed event energies, vertex reconstruction

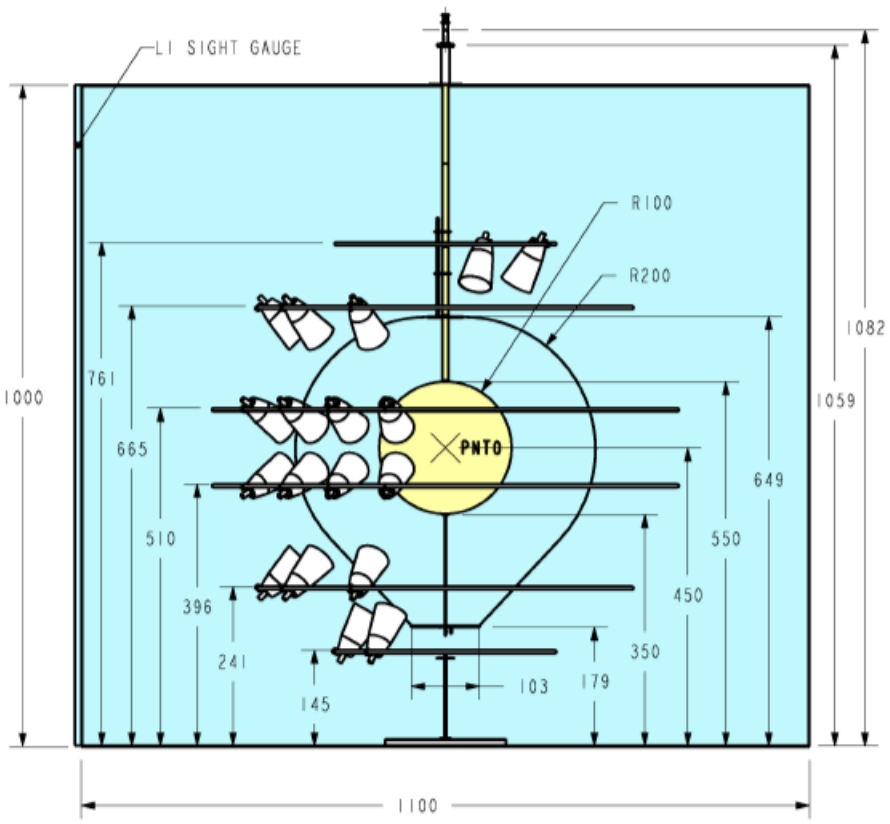

Figure 3.4: Side view of the design of the CTF 2 and CTF 3. The vessel (labeled R100 in this drawing) and shroud (R200) are shown, as well as the six rings of PMTs, the cylindrical tank, and the tubes used for filling and draining the vessel. The point PNT0 is the nominal center of the sphere of PMTs and of the CTF vessel. Water-filled volumes are shaded blue, while scintillator-filled volumes are shaded yellow. Dimensions are given in cm[24].

and event time tagging it is possible to determine the type of particle decays and initial particle identities. From this it is possible to determine radioactive contamination levels in the scintillator and test the scintillation purification process. The CTF has a sensitivity limit of $<1\text{x}10^{-9}$ Bq/kg for uranium and thorium decay products dissolved in the liquid scintillator[26]. The CTF can therefore be used to sample liquid scintillator radio-purity. However, solid samples cannot be tested because they need to be placed within the inner nylon shell which cannot be opened and only a liquid scintillator circulation system is installed.

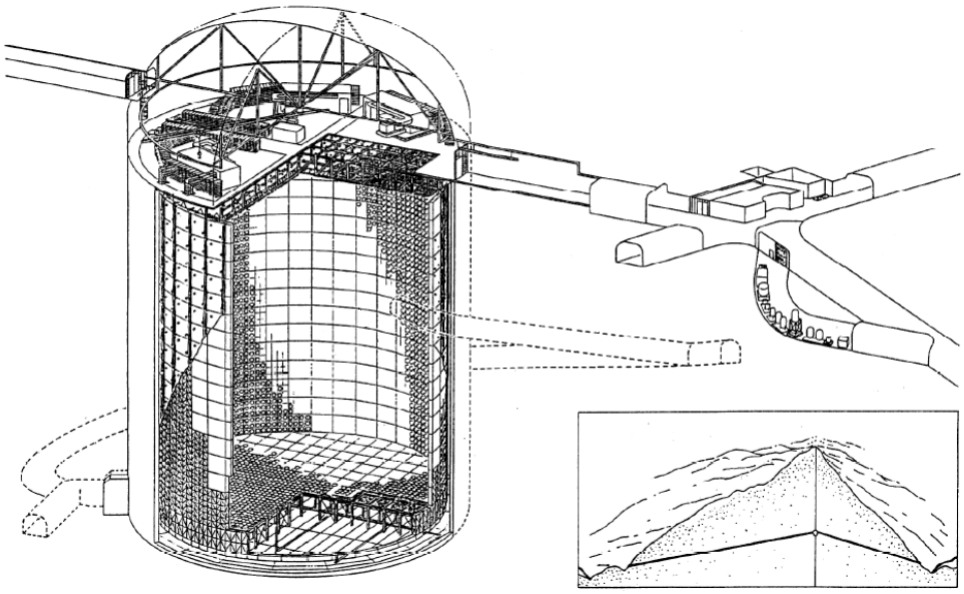

Figure 3.5: A cross-sectional view of the Super-Kamiokande detector in place under Mountain Ikenoyama. Inset at the bottom shows the location within the mountain[29].

3.4 Super-Kamiokande

The Super-Kamiokande (Super-K) experiment is a neutrino experiment constructed in 1991 and has been in operation since 1996[27]. It consists of a large stainless steel tank, 39 m in diameter and 42 m in height that is filled with 50,000 tons of ultrapure water(UPW), purified almost to the chemical limit of 18.24 MΩcm[28]. Along the walls of the tank there are 13,000 photomultipliers installed. The Super-K detector is located underground in the Kamioka-mine in Mountain Ikenoyama, Hida-city, Gifu, Japan. It is approximately 1000 m($\sim$2700 m.w.e) below the surface. A schematic of the Super-K detector can be seen in figure 3.5. The 1000 m of overhead rock acts to shield the detector against cosmic ray muons that act as background in the detector. The overhead rock allows for a reduction in cosmic ray muon flux of 5 orders of magnitude in comparison to the flux on the Earth's surface[27]. The Super-K detector detects particles using Cherenkov radiation. The collected Cherenkov

radiation can be used to determine particle trajectories, energies and particle identification.

The main motivation of the Super-K experiment is to search for nucleon decays and to study various types of neutrinos which include atmospheric neutrinos, solar neutrinos, neutrinos from supernovae and neutrinos from other astrophysical sources. In addition, due to the large detector volume the Super-K detector is also used as a target for neutrino beams in long-baseline neutrino oscillation experiments. The Super-K experiment detects these neutrinos through the elastic scattering interaction. A neutrino can elastically scatter off an electron imparting a portion of its energy to the electron. The electron then traverses the water at speeds greater than the speed on light in water, producing Cherenkov radiation.

Since the Super-K experiment deals with neutrino interactions, the expected event rates are very low. This necessitates the construction of a detector that is radiopure in order to minimize the effect of backgrounds in the detector. Not only is it necessary to minimize the radioactivity of the materials the detector is constructed from, the 50,000 tons of ultra-pure water in the detector require constant filtering and monitoring. Radium produced from the uranium and thorium decay chains can become dissolved in the ultra-pure water thereby slowly contaminating the water and increasing background in the detector. Radon monitoring and control of the air surrounding the detector is required so that radon is not introduced into the stainless steel tank should it be opened. To achieve this, two radon detection systems were designed. The first was designed to measure radon levels in the air within Super-K and the other was built to measure radon concentrations in the ultra-pure water. Both work under the same principles, however to measure radon concentrations in water radon must be extracted from the water, this requires additions to the detector as well as differences in volume and geometry of the detector vessel. A discussion of both detectors is given below, however the section referring to the water

detector will focus on the differences of this radon detector.

3.4.1 High Sensitivity Radon Detector for Air

Radon contamination can come from either emanation from detector materials, or exposure of the ultra-pure water to radon contaminated air when the holding tank is opened to mine air. The design of the radon detector is shown in figure 3.6. The radon detection vessel is constructed from stainless steel with a dimension of 50 cm diameter and 35 cm in height resulting in a total volume of ∼70 liters. The stainless steel vessel is electropolished in order to reduce surface contamination. The silicon PIN photodiode is electrically isolated from the stainless steel vessel walls using an acrylic plate and a ceramic feed-through. The silicon PIN photodiode is a Hamamatsu Photonics S3204-06 with passivation finish[30]. The glass cover was removed to enable sensitivity to alpha particles due to the alphas inability to penetrate the glass cover. The PIN photodiode has a detection area of 18 mm x 18 mm with a depletion layer thickness of 500 μm and a 80 pF capacity[31].

The radon detector works on the principle of electrostatic collection of radon daughters. It was previously found that over 90% of polonium-218, one of the radon-222 daughter, nuclei are positively charged when produced from radon decays[33]. The radon detector uses an electric drift field as a means of collecting the charged daughters from the decay of radon to the silicon PIN photodiode. This is achieved by using a high voltage of roughly -1.5 kV applied to the the silicon PIN photodiode which produces an electric drift field between the photodiode and the detector walls. The -1.5 kV voltage was chosen for the stability of the electronics. Using the measured rate of polonium-214 decays, the radon concentration can be found. The polonium-214 decays were chosen because of the purity of the signal. Since no other decays from radon and radon daughters occur near the 7.69 MeV decay, the signal is entirely polonium-214 decays. The detector could also detect the polonium-218 decays however

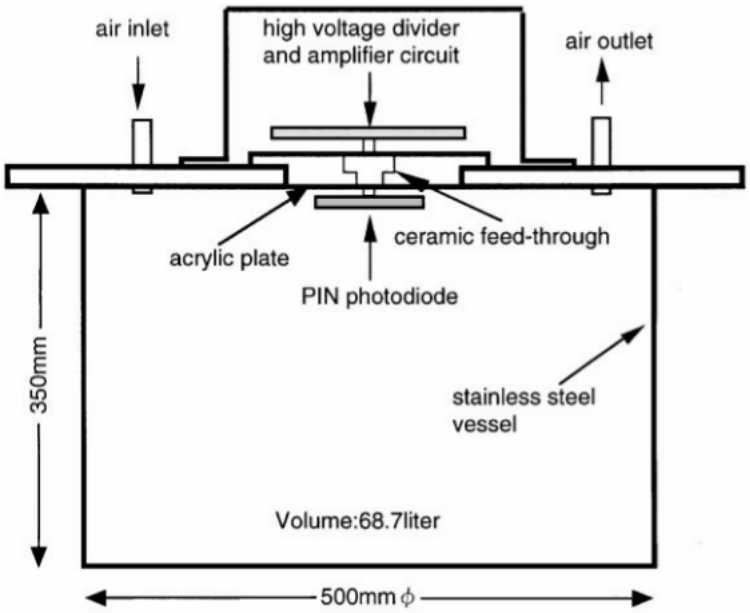

Figure 3.6: A schematic view of the high sensitivity radon detector for air. Image obtained from reference [32].

this decay has an energy of 6.00 MeV which also overlaps with the decays of bismuth-212 from radon-220. As a result this signal is polluted and separation between the two alpha peaks is not possible. Polonium-214 is also chosen due to the increased collection efficiency of this decay. The polonium-214 nuclei have more time to attract to the PIN photodiode before they decay due to its delayed production in the radon chain thus it is expected that the polonium-214 efficiency is larger than the polonium-218 efficiency. Using the polonium-214 decay channel the radon detector for air has a sensitivity limit of $\sim$1.4 mBq/m^3 with a calibration factor of 2.2 $\pm$ 0.2 (counts/day)/(mBq/m^3)[32]. Where the calibration factor is defined as:

$$\text{CF} = \frac{\text{number of detected counts per day}}{\text{radon concentration (mBq/m}^3\text{)}} \tag{3.1}$$

3.4.2 High Sensitivity Radon Detector for Water

The radon detector designed for water is essentially the same detector as the one used for measuring radon in air. It operates under the same principle of electrostatic attraction of radon daughters to the PIN photodiode. A schematic view of the high sensitivity radon detector for water is shown in figure 3.7. The stainless steel vessel is nearly identical however the bottom of the vessel has a hole which is covered by a mesh. This mesh allows the electric drift field to be entirely isolated within the stainless steel vessel. The radon contaminating the ultra-pure water is then showered into the diffuser vessel. The showering of the ultra-pure water occurs just below the stainless steel mesh in the diffuser vessel. The ultra-pure water then falls under gravity through the diffuser vessel containing plastic balls which assist in allowing the dissolved radon in the water to diffuse out and into the air within the diffuser vessel during this fall. This is due to an increase in surface area of the ultra-pure water that the plastic balls cause. The air in the diffuser vessel then diffuses up into the stainless steel vessel and the radon is then detected using the same principles as the radon detector for air. In addition, the sensitivity of the water detector is similar to the air detector limit of $\sim$1.4 mBq/m^3 however it has a larger calibration factor of 3.6 $\pm$ 0.5 (counts/day)/(mBq/m^3)[32].

3.5 Emanation Chamber Detector

At the University of Alberta a emanation chamber detector was developed for measuring radon emanation from materials. The emanation chamber is a custom made stainless steel cylindrical vessel similar to the one used by Super-Kamiokande. The emanation chamber dimensions are a diameter of 0.598 m and a height of 0.609 m resulting in a total detector volume of 0.171 m^3. A delrin feed-through is installed in the lid of the emanation chamber with a Hamamatsu S3204-09 silicon PIN photodiode attached to the bottom

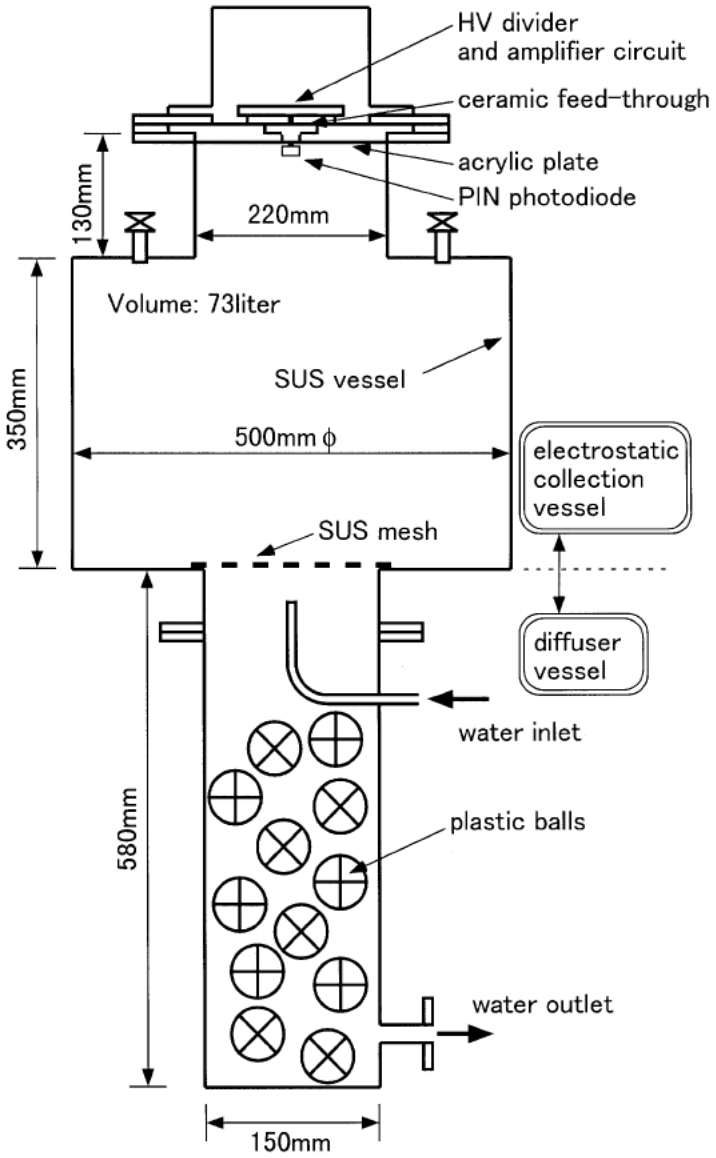

Figure 3.7: A schematic view of the high sensitivity radon detector for water. It is important to note that the water inlet pipe is higher than the outlet pipe, so the water falls down through the plastic balls to the outlet pipe. SUS is synonymous for stainless steel. [32].

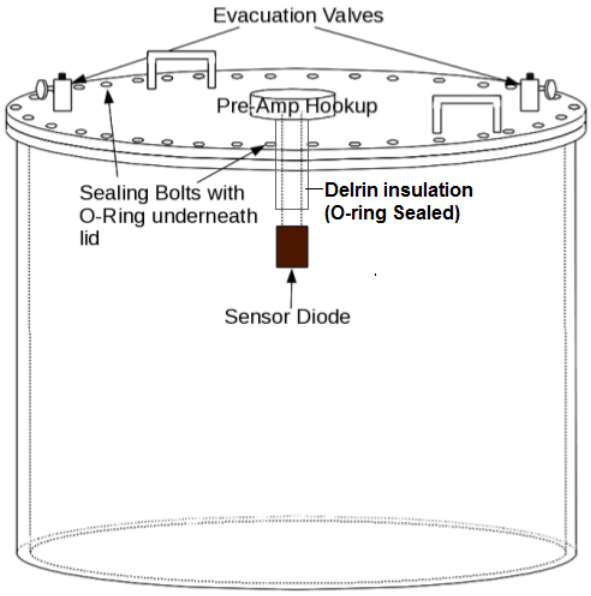

Figure 3.8: A schematic view of the high sensitivity radon emanation detector.

of the feed-through[30] and both the lid and the feed-through are sealed using butyl o-ring seals. The PIN photodiode is surrounded by a ceramic mount and is located ∼10 cm from the top of the stainless steel vessel. The emanation chamber uses of an electric drift field to collect radon daughters. A high voltage of approximately +5 kV is applied to the detector walls causing the positively charged radon daughters to be electrostatically attracted to the PIN photodiode which is kept at ground potential. The photodiode is biased to ∼40 V to achieve a depletion zone within the PIN photodiode. A schematic of the emanation chamber is shown in figure 3.8. Due to the high voltage applied to the outer walls of the detector, the emanation chamber vessel is surrounded by a Faraday cage that is not shown in figure 3.8. In figure 3.8 the emanation tank has two ball valves which will be discussed in section 3.5.1.

The upper and bottom portion of the emanation chamber's stainless steel tank required welding for construction. It is known that tungsten welding rods

contain thorium and so non-thoriated welding rods were used to minimize radioactive contamination of the vessel[34]. This was insufficient and the welds still contained measurable amounts of thorium and increased the radon emanation from the detector walls. This increased the background radioactivity of the emanation chamber. A chemical surface treatment was developed to lower the background levels within the detector and the details and results of this treatment will be discussed in Chapter 4.

3.5.1 Principles and Operation of the Emanation Detector

The emanation chamber detector operates using the method of electrostatic collection of charged radon daughters. This is achieved using of an electric collection field which acts as a drift field attracting the positively charged radon daughters to the surface of the PIN photodiode. The electric drift field is an essential part of the detector and without the drift field the detector efficiency would be very small and only radon daughters in the immediate volume around the PIN photodiode would be detected. The photodiode is used to detect the energies of alpha particles which deposit their energy in the depletion region of the PIN photodiode. Due to their charge and mass, alpha particles have a very short path length and deposit all their energy within a short range, therefore the depletion region of the diode can be very thin. This also means the alpha particles do not travel far in the detector. As a result only alpha particles produced from decays near the PIN photodiode can be detected. This led to the use of the electric drift field to collect the daughters to the surface of the PIN photodiode thereby significantly increasing the number of alpha particles which can deposit energy within the PIN photodiode. This is the same principle as used by both the ESC detector for SNO and the high sensitivity radon detector for Super-Kamiokande to achieve maximum particle detection.

The emanation chamber may work on the same principle as other radon detectors however it measures something fundamentally different. Other detectors are used to measure radon levels in the air or the water that becomes contaminated from radon emanation from materials. The emanation chamber is designed to specifically measure the radon emanation from materials. The measurement of radon emanation is accomplished using the ball valves shown in figure 3.8. Radon emanation is the amount of radon emanating from the surface of a material. To measure radon emanation, all ambient radon must be removed from the detector volume. This is achieved by evacuating the detector with a rotary vacuum pump attached to the ball valves. The chamber is then refilled with nitrogen gas which acts as a radon free buffer gas. A gas is required to prevent breakdowns due to the +5 kV applied to the chamber walls. At low pressure the breakdown voltage is low and as a result electrical arcing can occur within the detector which prevent the diode from collecting data and can damage electronics. The nitrogen purging is performed a total of three times to remove the ambient radon in the detector. Any radon detected within the emanation chamber will then comes from either the surface of the detector walls or the surface of the sample materials. Through measuring intrinsic detector emanation and testing sample materials it is possible to measure the amount of radon emanating from a test sample.

Samples are introduced in a holding tank, which circulates the nitrogen buffer gas between the emanation chamber detector and a sample holding tank. The addition of a holding tank decreases the efficiency due to an increased total volume, while the sampled volume is kept constant[4]. The sample holding tanks where chosen because they allow an easy exchange of sample materials. The full schematic of the emanation system can be seen in figure 3.9.

[4]The sample volume is constant because at any point in time only the air within the emanation chamber vessel is being sampled.

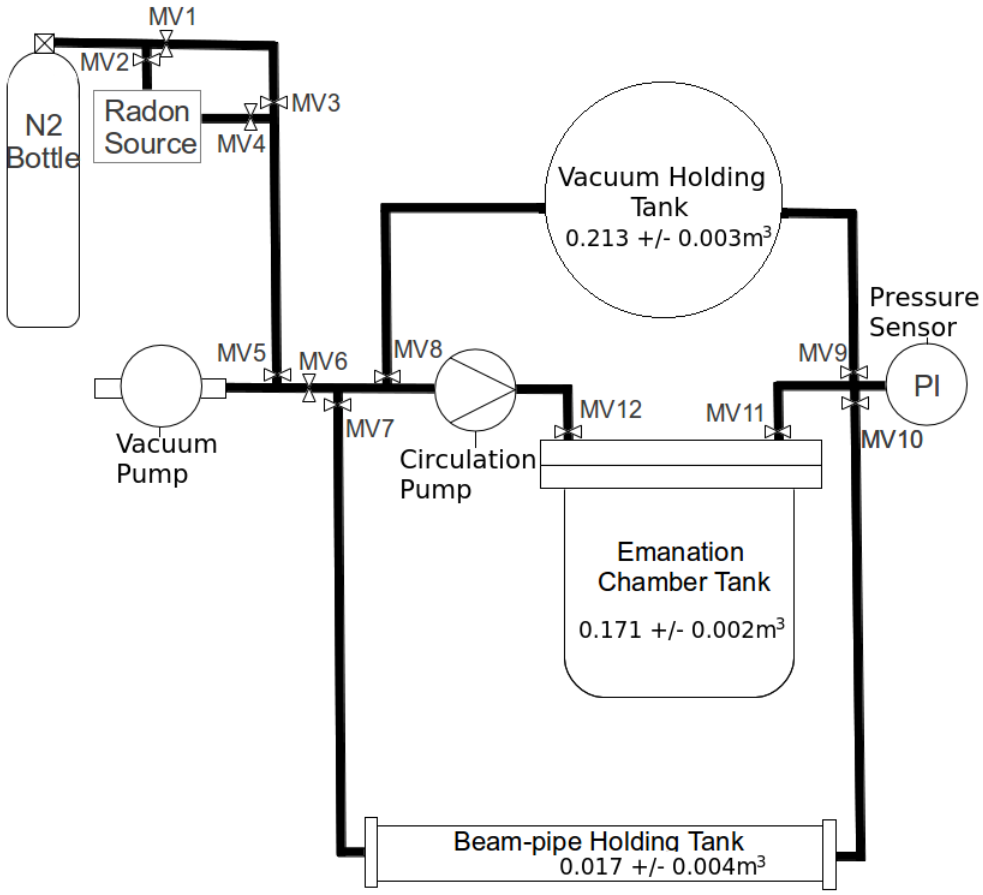

Figure 3.9: A schematic view of the emanation system which includes the emanation chamber and the sample holding tanks. MV1,...,MV12 are ball valves.

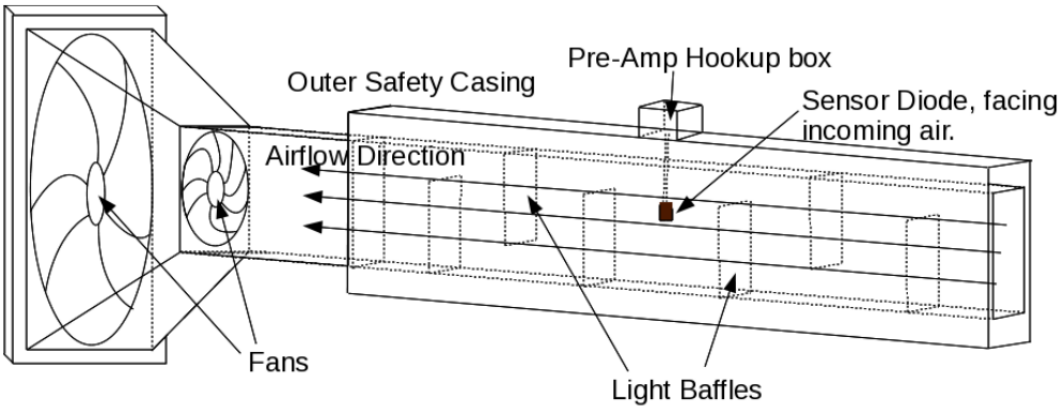

Figure 3.10: A schematic view of the tunnel detector which is the current prototype for the radon monitors for the radon-cleanroom.

3.6 Tunnel Detector

In addition to the emanation chamber, there is the tunnel detector used to monitor the radon levels in atmospheric air. This was designed as a high sensitivity radon monitor for use in a clean-room currently being constructed at the University of Alberta[5]. The tunnel detector is currently in a prototype phase however smaller versions of this detector are being built that will monitor radon levels in the clean-room. The purpose of this detector is to monitor the radon levels in air with high flow rates to sample large volumes. A schematic of the current tunnel detector prototype is shown in figure 3.10.

The detector consists of a long air-duct with a feed-through located in the center between the air-duct ends. Attached to the feed-through is a the silicon PIN photodiode and its housing. The silicon PIN photodiode is the same model PIN photodiode as used in the emanation chamber. The photodiode is placed in the center of the air-duct and faces the flow of incoming air. The tunnel detector uses an electric drift field like other radon detectors however unlike the emanation chamber where the voltage is applied to the walls of the detector, the

[5]A short discussion of the clean-room can be found at the end of this chapter.

voltage is applied to the PIN photodiode. The typical voltage used is -2.5 kV. Increasing the voltage drives electronic noise in the detector that significantly reduces the resolution of the detector within the region of interest of the radon daughters. The air-duct also contains light baffles as can be seen in figure 3.10. The PIN photodiode is light sensitive and any stray light incident on the diode is detected and adds additional noise which the light baffles aim to prevent. In addition the air-duct walls were anodized black so that there are no reflective surfaces for stray light to penetrate past the light baffles. The light baffles do not completely stop all stray light however they are sufficient in minimizing its effect. The detector is designed for large volume sampling which is accomplished by pulling air in through the end of the air-duct with the assistance of two high volume fans shown in figure 3.10. As of writing this, no limits on the sensitivity or detection efficiency of the detector have been determined.

3.6.1 Principles and Operation of the Tunnel Detector

The tunnel detector operates under the same principle as the emanation chamber, ESC, and high sensitivity radon detector from Super-Kamiokande. The detector uses an electric drift field which collects charged radon daughters to the PIN photodiode thereby significantly increasing the detection efficiency of radon. However unlike the emanation chamber the tunnel detector applies the voltage to the PIN photodiode. The tunnel detector also uses a 40 V bias voltage that is applied across the diode in order to produce the depletion zone used for particle detection, similar to the emanation chamber. The purpose of this detector however is more closely related to the ESC and high sensitivity radon detector as opposed to the emanation chamber. Its purpose is to monitor radon concentrations in the air.

3.7 UofA Low Background Clean-room

A radon free environment is currently under construction at the University of Alberta. The clean-room is being built for low background detector fabrication. The clean-room minimizes exposure to radon which greatly reduces the potential build-up of the long lived daughters produced in the radon-222 decay chain. In figure 3.11 the current layout of the clean-room is shown. The clean-room will use both cryogenic and pressure/vacuum swing carbon adsorption techniques to strip clean-room air of radon. The air will be filtered and dried to 70C dewpoint using a dessicant drier[36]. It is then cooled to -65 °C and passed through carbon columns. The carbon colums consist of five stainless steel tanks each filled with approximately 200 kg of coconut carbon. Under normal operations, three of the carbon tanks will be maintained at -60 °C for radon adsorption and two will operate at room temperature while in a pressure/vacuum swing configuration. The circulation system and all other major components will be automated and will be managed with process control software.

The clean-room uses a modular wall design that is constructed of aluminum materials produced by CleanAir Solutions. All seams are sealed with butyl caulking with an additional layer of aluminum foil backed butyl tape. This provides an additional layer of sealing and covers the butyl caulking that is non-hardening. It consists of a two stage air lock system in which every subsequent airlock lowers radon concentration within the air. This minimizes the possibility of introducing radon into the clean-room when entering/exiting the clean-room. The clean-room contains HEPA filters used in the air circulation system and a radon monitoring system in the clean-room will be based on a more compact design of the tunnel detector discussed in section 3.6. The clean-room will have a target of a class 1000 clean-room.

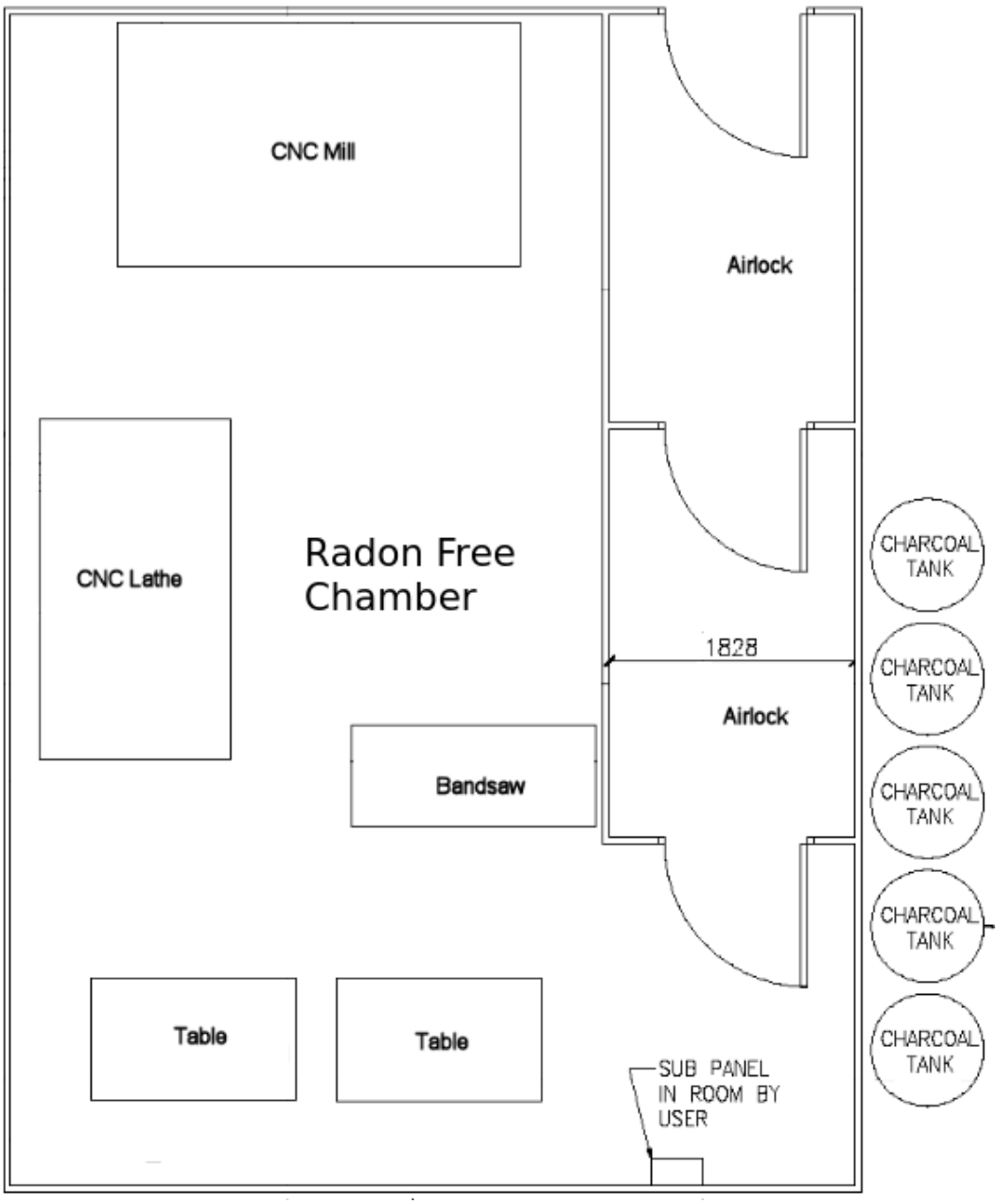

Figure 3.11: Layout of the radon clean-room at the University of Alberta[35].

Chapter 4

Data Analysis

This chapter will introduce the data acquisition and the analysis software that is used for the emanation system. In addition, this chapter will also provide a detailed description of the analysis techniques such as the calibration method, efficiency determination, and emanation rate determination.

4.1 Data Acquisition Software

The data acquisition software used in the emanation system uses the Labview programming environment[37]. The data is acquired with a custom 8 channel multi channel analyzer (MCA) designed by the University of Alberta electronics shop. The 8 channels have an input voltage range of 0-2V with a sampling frequency of 50 MSPS (million samples per second) and a 12 bit resolution. In addition, 12 secondary "slow" data channels are used for monitoring slowly varying information such as pressure and high voltage. The 12 secondary channels have an input voltage range of 0-5V with a sampling frequency of 10 KSPS (thousand samples per second) and a 10 bit resolution.

The information is sent via a USB connection that uses the QuickUSB library as a means of communication between the MCA hardware and the data acquisition software[38]. The DAQ program uses a custom C++ library

to write the data to a ROOT file saving the data organized into single event packets. This allows easy data access using the ROOT C++ libraries used in the analysis that will be discussed later in section 4.2[39]. A full description of the software setup required to run both the data acquisition software and the data analysis software is given in the appendix.

4.1.1 Data Structure

This section will cover the data structure of the emanation system data. The data is saved in one of four ROOT TTrees that are associated with different detector information. The four TTrees are the FPGA information, run comments, slow adc data and event data[40]. Each TTree and its data format are shown below, along with a short description of what each TTree stores.

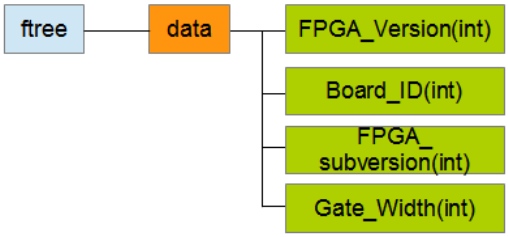

Figure 4.1: Structure of data stored in the FPGA TTree.

Figure 4.1 represents the TTree associated with the FPGA/electronics data. This TTree stores information pertaining to the electronics of the emanation system. This data records electronic changes such as hardware replacement that can introduce changes to the detector that require detector re-calibration. Figure 4.2 represents the TTree associated with the operators comments about specific information pertaining to the detector run. This information may be a description of the sample tested, variation from normal operating conditions[1] or any other information not automatically recorded that is considered impor-

[1] A description of the normal operating conditions are detailed in section 4.2

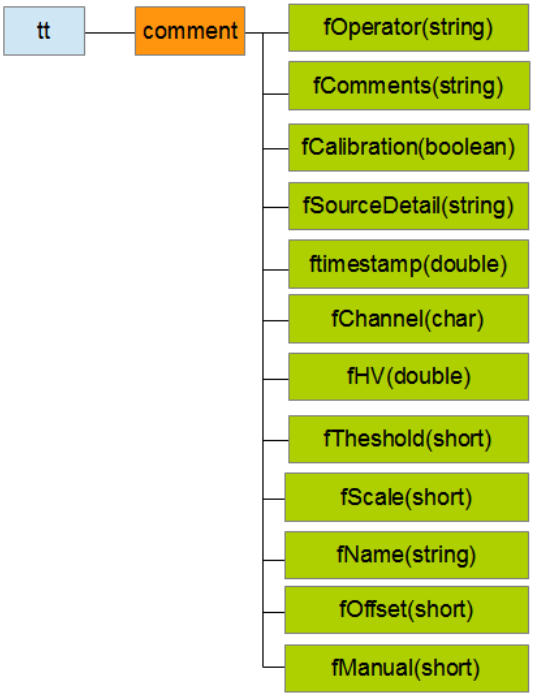

Figure 4.2: Structure of data stored in the run comments TTree.

tant by the operator. In addition this TTree is used to determine the initial start time and end time of a run[2]. Figure 4.3 represents the data structure as-

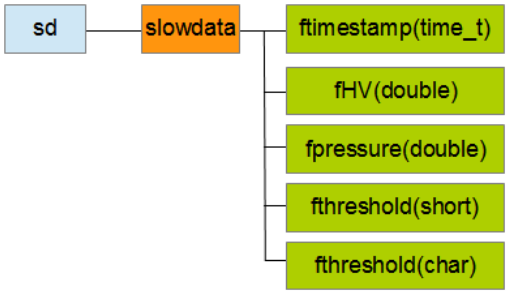

Figure 4.3: Structure of data stored in the slow adc TTree.

sociated with the SlowADC TTree. This TTree records various slowly varying information that may correlate to changes in the detector. This can be information such as pressure, temperature, humidity, etc. Figure 4.4 represents the

[2]The start-time is determined from ftimestamp and the end-time is determined from the last recorded event or from ftimestamp of the subsequent run, which ever occurs first.

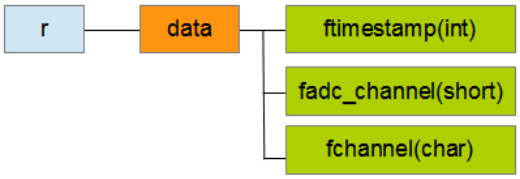

Figure 4.4: Structure of data stored in the detector data TTree.

data structure of events measured in the emanation system. The TTree shown in figure 4.4 is used extensively and is the TTree that stores the data which pertain to each recorded event such as event occurrence time, event energy, and which detector the event is associated with. This data is the primary focus of the analysis that obtains radon emanation rates.

4.2 Data Analysis Software

This section will cover a description of the software used to analyze the data from the emanation system. In addition, the different emanation system run types that are analyzed, why they are important, how they relate to each other and a detailed explanation of the analysis techniques will be described.

The data analysis software used to analyze the emanation system data is a C++ based code that uses the ROOT C++ library. Using ROOT allows the retrieval of the data from the saved ROOT files generated by the data acquisition system. A ROOT file was chosen to reduce the storage space required by automatically packing the files on disk. ROOT is also used to analyze the data through fits and calculations. The ROOT based software is called time_analysis and was written by myself based on an older version by Dr. Carsten Krauss and Patrick Galloway. It consists of four main files and 2 additional files created on software compilation. The main code is time_analysis along with its associated makefile. The classes performing the data analysis are stored in the two files MCAclasses.cxx and MCAclasses.hh. MCAclasses.cxx contains all

the analysis operations and outputs all required information determined from the analysis. The file MCAclasses.hh acts as a single header file for MCAclasses.cxx and defines the analysis functions and structures created and used by MCAclasses.cxx.

The analysis code analyzes three different types of detector runs. The three types of detector runs that are handled by time_analysis are calibration runs, background runs, and emanation runs. The runs are normally acquired under these conditions:

- the system is run at (850 ± 40) mBar. Lower pressure causes increased wear and damage to the circulation pump diaphragm increasing the risk of vacuum leaks. A lower pressure also increases the efficiency[3].
- the temperature is at (23.5 ± 1.0) °C.
- the system undergoes three nitrogen purges to remove ambient radon introduced during the insertion of samples.
- calibration runs have radon gas introduced into the system by flushing nitrogen through a radon source into the system at pressures between 600mBar and 850mBar. This minimizes the pressure gradient across the radon source while drawing all radon from the source into the emanation system.

Calibration runs are taken when no samples are inside the system. The system is evacuated and refilled using nitrogen gas flowing through a Pylon model Rn-1025 radon source with an equilibrium activity of 930 Bq[41]. Although the radon source activity is known at equilibrium, the radon source requires ∼27 days to reach 99.9% equilibrium activity. It is not always practical to

[3]Although efficiency is increased at lower pressures, the possibility of introducing radon from a diaphragm failure is detrimental to sample runs.

wait 27 days between calibration runs, so the times when the radon source is opened/closed are recorded.

$$A_{Rn}(t) = A_{Ra}(1 - e^{-\lambda_{Rn}t}); \tag{4.1}$$

Using the recorded times and equation 4.1 with $t=t_{Opened}$-$t_{LastClosed}$ the activity of the radon source can be found. The entire volume of radon from the source is flushed into the emanation system and the activity within the emanation system is equal to the source activity calculated using equation 4.1. The calibration runs can be used to determine the emanation system's detection efficiency with respect to the radon-222 daughter nuclei. In addition, the high radon activity produces a clear signal from its daughter nuclei. Using the decay signals from the daughter nuclei, it is possible to perform an energy calibration on the radon spectrum. This removes the radon spectrum's dependence on the detector electronics. In addition, hardware replacement becomes easier and only requires a re-calibration of the detector. The analysis of a calibration run does not require any previous run information.

The background run is the second run type. Background runs are used to determine the intrinsic contamination of the detector. The contamination causes radon emanation from the detector materials resulting in a constant source of radon emanation. A background run is taken after nitrogen purging the emanation system and then operating the system while it does not hold a sample. Any radon that is detected comes from within the detector. This intrinsic background will pollute every sample's signal. The background activity must be minimized in order to improve the sensitivity of the detector which is directly related to its background emanation. The analysis of background runs requires the knowledge of the detection efficiency of the radon-222 daughters determined from the calibration runs. Background runs also require the calibration parameters extracted from calibration runs to perform an en-

ergy calibration. Due to the design of the emanation system, the detection efficiency of each daughter and the energy calibration parameters will remain constant under normal operational conditions and can be applied to other runs. These parameters however can change if there are system malfunctions such as pressure leaks or changes in the electronics of the system.

The last run type is an emanation run. To analyze an emanation run, parameters extracted from both the calibration runs and the background run are required. This run is acquired with a sample placed in one of the holding tanks. The system is then evacuated and purged with nitrogen gas. The emanation run requires background rates measured from previously analyzed background runs. In addition, the energy calibration and efficiency parameters are determined from calibration runs. The background run is used to perform a background subtraction to determine the emanation rate of the sample. The above is a simple overview of the analysis process that extracts information from the different run types. A comprehensive discussion of what is performed will be given in the following sections.

4.2.1 Radon Spectrum

In a detector run the generated data is stored event by event with their associated information tags such as ADC channel, the time of the event, pressure, etc. Using the information from the events a radon spectrum can be obtained. The spectrum represents the raw data where each bin represents an ADC channel that contains the number of events with that ADC channel representing the amount of energy of these events. The number of channels used in the emanation system is 4096 ADC channels. A radon spectrum can be seen in figure 4.5. The spectrum is not calibrated and reflects the raw data from the emanation system. This spectrum was chosen to show the distinguishable peaks that represent the signals from the different radon daughters. A clear separation between all four peaks is observed. The four peaks from left to right are

polonium-210 centered at ∼1300, polonium-218 centered at ∼1470, polonium-214 centered at ∼1870 and polonium-212 centered at ∼2125.

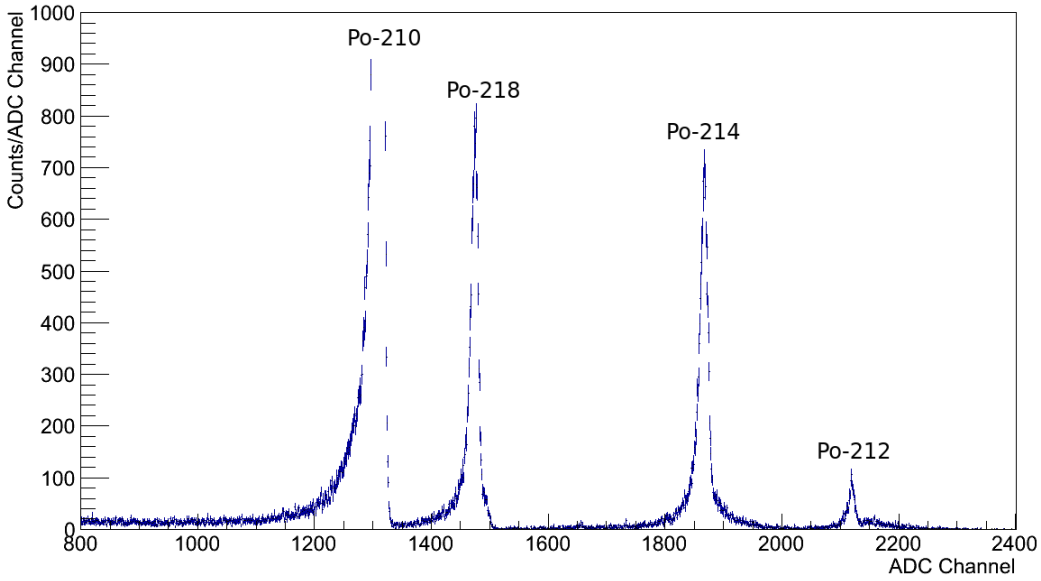

Figure 4.5: A non-calibrated radon spectrum produced from the emanation system. This spectrum is from run 1031 consisting of five toolbox wheels and black foam mats. Run duration of ∼380 hours using the vacuum tank emanation system.

The peaks shown in the spectrum that are the focus of the analysis are polonium-218 and polonium-214. The decay times for the radon daughters are much shorter than the 3.82 day half-life of radon. Due to the large difference in the decay times in comparison to radon-222, secular equilibrium between radon-222 and its daughters can be reached within several hours[42]. Therefore the polonium-218 and the polonium-214 exist in secular equilibrium with the radon-222 and reflect the radon-222 activity and can be use to determine the radon-222 emanation rate from a sample.

The lowest ADC channel peak visible in the radon spectrum corresponds to polonium-210 decays. The polonium-210 peak is a decay product of the radon-222 decay chain. Polonium-210 has a half-life of ∼138 days and is pro-

duced from lead-210 which has a very long half-life of ∼22.3 years. Due to the large half-life of polonium-210 and lead-210 secular equilibrium cannot be reached with radon-222 within the timescale of a run. As a result the activity of polonium-210 does not reflect the activity of the radon-222 emanating from a sample. Although not useful for radon measurements, polonium-210 builds up on the diode surface due to a long half-life and can be used as an indication of the radon exposure of the diode[43, 20]. The significant activity of calibration runs accelerates the build up of polonium-210 caused by exposure to high amounts of radon. The build up of polonium-210 can be seen in terms of its hourly activity in figure 4.6. The figure shows the hourly activity of polonium-210 for ∼300 days of data. Each data point corresponds to a single detector run with calibration runs marked as vertical line to show their occurrences. It is apparent from figure 4.6 that the activity of polonium-210 increases as the diode is exposed to radon.

For comparison, the expected rate of increase based on the amount of lead-210 introduced from calibration runs is shown in blue. The equation plotted is contructed from the following equation:

$$A_{Po}(t) = \frac{\lambda_{Bi}\lambda_{Pb}N^0_{Pb}[(\lambda_{Po}-\lambda_{Bi})e^{-\lambda_{Pb}t} + (\lambda_{Pb}-\lambda_{Po})e^{-\lambda_{Bi}t} + (\lambda_{Bi}-\lambda_{Pb})e^{-\lambda_{Po}t}]}{(\lambda_{Bi}-\lambda_{Pb})(\lambda_{Po}-\lambda_{Pb})(\lambda_{Po}-\lambda_{Bi})} \tag{4.2}$$

where λ_x is the decay constant of the given isotope, and N^0_{Pb} is the amount of lead introduced during a calibration run. The curve shown in figure 4.6 is constructed by adding equation 4.2 for each subsequent calibration run to the initial polonium-210 rate increase such that the following equation is obtained:

$$\begin{aligned} A^{Total}_{Po}(t) = A_{Po}(t>0, N^0_{Pb} = N_{Cal0}) \ + \ A_{Po}(t>54, N^0_{Pb} = N_{Cal1}) + \\ A_{Po}(t>124, N^0_{Pb} = N_{Cal2}) \ + \ A_{Po}(t>252, N^0_{Pb} = N_{Cal3}) \end{aligned} \tag{4.3}$$

where N_{Calx} (x=0,1,2,..) is the amount of lead-210 introduced during the calibration run determined from the number polonium-214 decays. One assump-

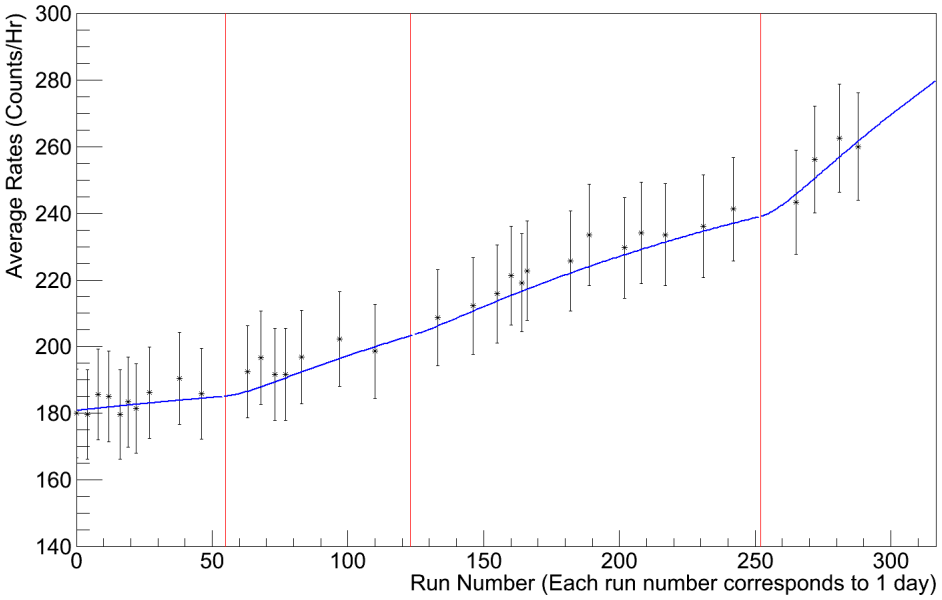

Figure 4.6: The average hourly activity of polonium-210 over ∼300 days. As time increases it is apparent that the polonium-210 activity increases due to polonium 210 build-up on the diode surface. The vertical red lines correspond to calibration runs. The data points shown consist of all runs within the 300 days excluding calibration runs. The first calibration runs occured approximately -180 days on this time axis.

tion that was made is that the increase in lead-210 is caused by the lead-210 introduced during calibration runs and assumes the radon emanation from samples during subsequent runs has a negligible effect on the overall increase of lead-210 and polonium-210. The expected rate increase agrees well with what is observed in the detector.

In figure 4.5, at channel ∼2125 a small peak exists corresponding to polonium-212 which is a daughter of radon-220. Because polonium-212 is a radon-220 daughter it is not useful in directly determining radon-222 emanation rates. The polonium-212 can be used to determine radon 220 emanation rates. This can be accomplished using a radon-220 calibration source for radon 220 calibrations. However, it is assumed that due to the short half-life of radon 220 and its

daughters the collection efficiency is expected to be low. This can be seen from the lack of decay peaks corresponding to other radon-220 daughters. Most of the radon-220 daughters decay before they are collected and this results in the low collection efficiency. Because of the long half-life of polonium-210 and lead-210 it is more important to measure radon-222 contamination. Radon-220 and its daughters decay away more rapidly than radon-222 daughters and do not build up on the surface of materials to appreciable levels. However, polonium-212 can be used as a tool to remove signal contamination from a radon-222 signal channel caused by radon-220.

The polonium-218 peak in figure 4.5 also contains contributions from the bismuth-212 decay from the radon-220 decay chain. Bismuth-212 has an alpha decay energy that is close to the polonium-218 decay energy. The close energy separation between the two decay energies causes the bismuth-212 to overlap the polonium-218 signal. The integral around the polonium-218 is therefore not solely related to the radon-222 emanation rate as is the case with polonium-214. This makes the polonium-214 signal the ideal choice for determining emanation from radon-222 rather than the polonium-218 signal. This is due to a polonium-214 signal that is free of contamination from other decays[31, 32]. This however does not mean that the polonium-218 signal cannot be of use for determining radon-222 emanation rates. A method to separate the bismuth-212 from the polonium-218 signal to obtain radon-222 emanation rates as a consistency check for the polonium-214 signal will be given in section 4.2.4.

4.2.2 Calibration of the Radon Spectrum

To allow interpretation of the data an energy calibration is applied to the detector data. This translates the data from the raw ADC channels to an energy space that is independent of the electronics. This is achieved by using a linear response of the detecting diode. A linear relationship between the ADC channels and the energies associated with each polonium decay is extracted

from the calibration data. In Table 4.1 an example of associated ADC channels and the corresponding decay energies can be seen.

Table 4.1: A table of the isotopes that can be observed in the radon spectrum from the emanation chamber. It shows the typical associated ADC channel and the decay energy of each isotope. Bismuth-212 has a 35% branching ratio for the alpha decay channel which is split up between two closely separated decay energies[2].

Isotope Name	Associated ADC Channel	Decay Energy (MeV)	Radon Parent Isotope
Polonium 210	∼1300	5.304	Radon 222
Polonium 218	∼1415	6.002	Radon 222
Bismuth 212	∼1420 ∼1424	6.051(25.13%) 6.089(9.75%)	Radon 220
Polonium 214	∼1870	7.686	Radon 222
Polonium 212	∼2125	8.954	Radon 220

Using the values shown in table 4.1 it is possible to perform an energy calibration of the raw spectrum. A linear equation is extracted from the associated peak ADC channel and their corresponding decay energies. The equation used to determined the calibration factors is as follows:

$$\mathrm{ADC}(\mathrm{E}_{\mathrm{decay}}) = \mathrm{E}_{\mathrm{decay}} \cdot \mathrm{scale} + \mathrm{offset} \tag{4.4}$$

The scale variable represents the scaling factor between the ADC channels and decay energies. The spectrum can stretch/compress resulting from changes in the electronics. This factor applies the corrections to compensate for the stretching/compressing effect on the spectrum caused by the electronics. The spectrum can also undergo a translation to higher or lower ADC channels. The effect of the translation is corrected with an offset factor. The offset factor contains the effects of the translation of ADC channels introduced by electronic changes in addition to the effect caused by a dead-layer on the surface of the diode. The dead-layer results in energy losses that at best is partially detected by the diode and is dependent upon the angle of incidence of the alpha particle

with the diode[44, 45]. The dead-layer and its effects are discussed later in this section.

The parameters extracted from equation 4.4 are unique to the electronic setup and the geometry of the detector used for each calibration. Figure 4.7 shows a comparison between calibration parameters extracted through calibration runs where peaks are well-defined versus calibration parameters extracted from runs where all four peaks are visible but not well-defined. The two method extract consistent calibration parameters and the parameters from calibration runs are chosen due to well-define peak locations. The calibration parameters extracted from calibration runs result in a scaling parameter of 234.5 $\frac{\text{ADC}}{\text{MeV}}$ with an offset value of 71.9 ADC for the calibration run 920 taken on Oct 7, 2012. From the parameters it can be seen that the energy bin width of 1 ADC channel is 4.26 keV. Using these parameters with equation 4.4, the ADC channels are converted to their energy equivalent values to energy calibrate the radon spectrum. The polonium-212 and polonium-210 peaks are not used when determining the calibration parameters from calibration runs because they lack statistics.

The calibration parameters are obtained from calibration runs because they have high radon-222 activity producing well-defined polonium-218 and polonium-214 peaks. The peak locations are determined with a peak finding class included in the ROOT C++ library known as TSpectrum[46]. The polonium-218 and polonium-214 isotopes have well established peak locations as seen in figure 4.8. However due to the strength of these peaks, the polonium-210 and polonium-212 lack defining statistics and are not easily observed. This is a result of the high activity causing long tails from the polonium-218 and polonium-214 decays which overlap into the regions where the polonium-210 and polonium-212 are located and make these signals statistically insignificant.

It is important that the calibration parameters remain constant over long

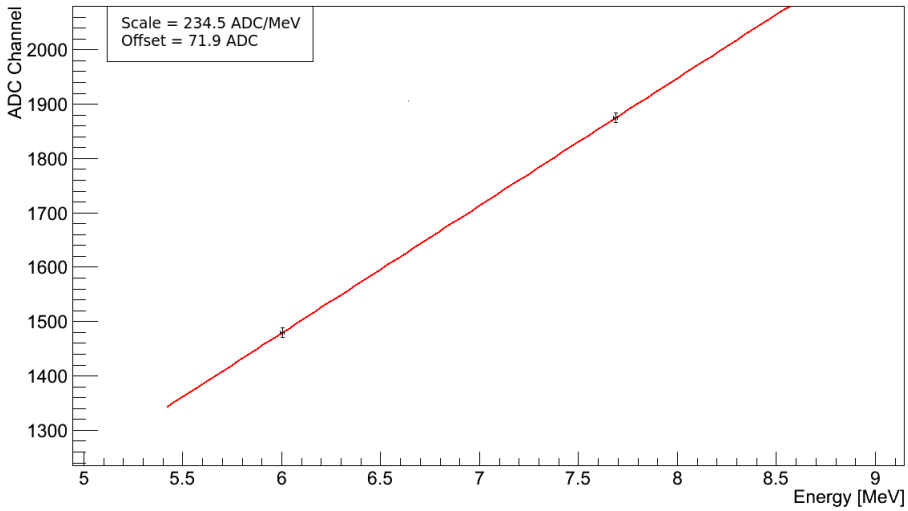

(a) Two point calibration plot.

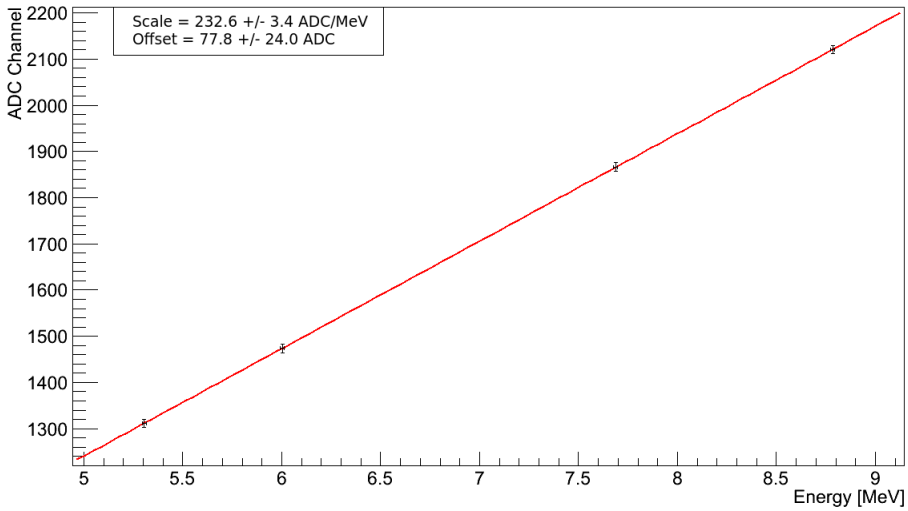

(b) Four point calibration plot.

Figure 4.7: A two peak calibration plot using a calibration run with high activity(930 Bq) and a non-calibration run used to show a 4 point fit for comparison. The calibration parameters are extracted from the well-developed polonium-218(6.00 MeV) and polonium 214(7.686 MeV) peaks observed in calibration runs. Errors in the ADC channels correspond to the uncertainty in determining the peak locations.

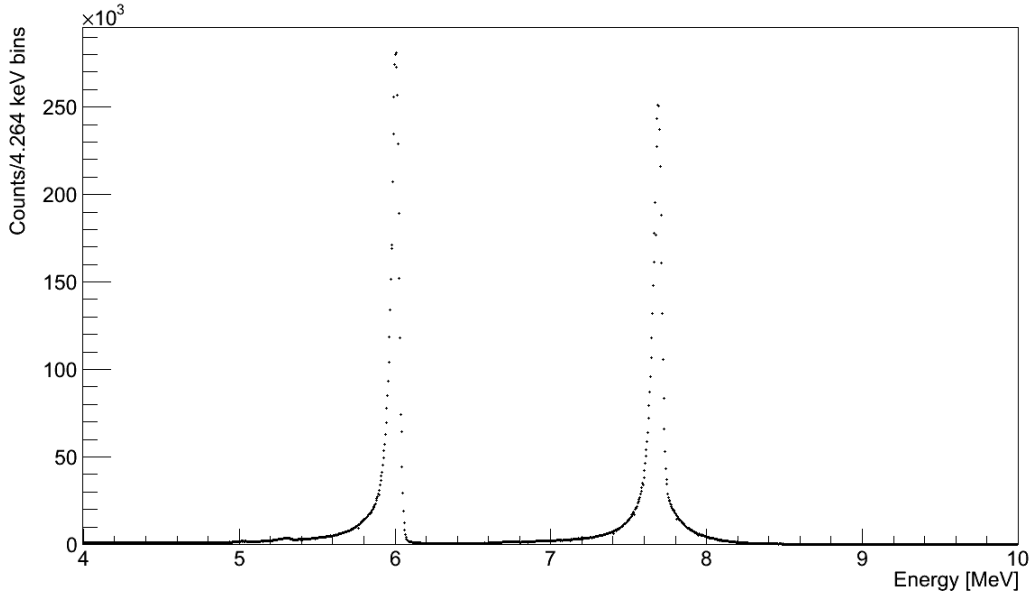

Figure 4.8: An energy calibrated spectrum that is produced from calibration run 920. The polonium-218 and polonium-214 peaks are easily observed.

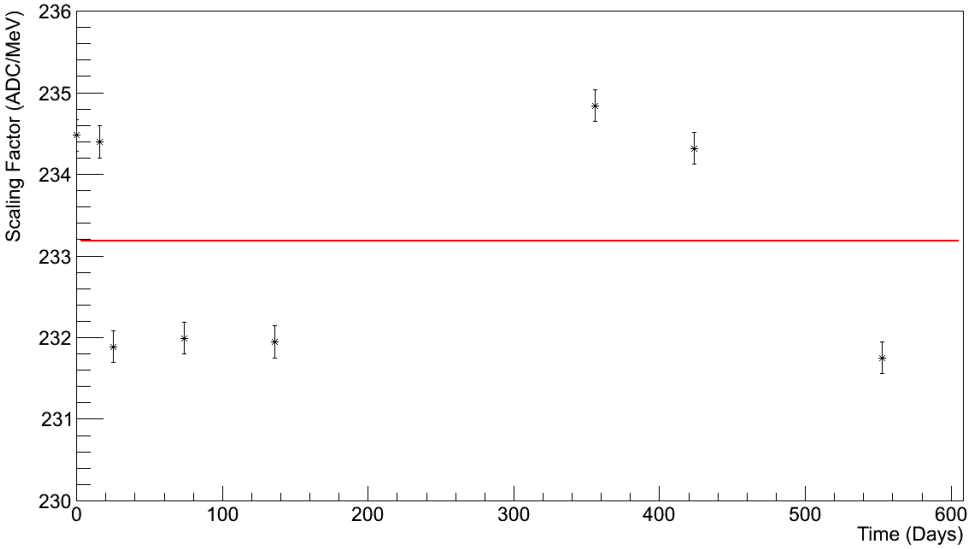

Figure 4.9: The time evolution of the scaling factors determined from calibration runs using equation 4.4.

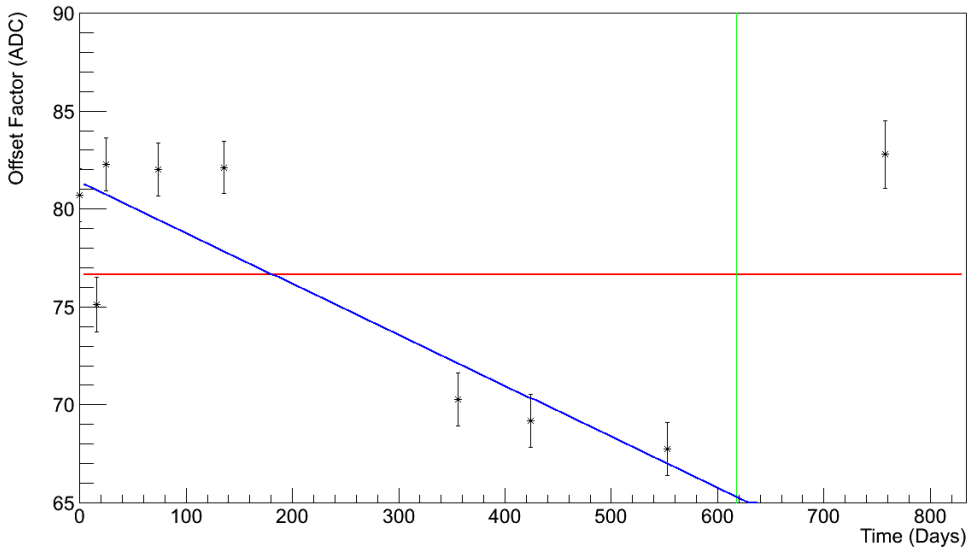

Figure 4.10: The time evolution of the offset factors. The red line is a constant fit for reference. The blue line is the fit assuming a dead-layer increase. The green vertical line marks a time when the detector was modified and in the process the diode was wiped clean to remove dust.

periods of time. If these parameters were to vary significantly during a detector run, it would result in added systematic uncertainties in the emanation rate. Figure 4.9 shows that there is variation in the scaling factor parameter in a period of 600 days. The stability of the offset factor can be seen in figure 4.10. The offset is shown with a constant fit for reference, however the factor appears to steadily decrease. The decrease in the offset factor can be modeled as an increase in the dead-layer of the diode due to a build-up of dust on the surface of the diode and is shown as the linear fitted blue line. Assuming this effect, the rate of increase in the dead-layer thickness can be calculated. Assuming a dust composition of mainly steel and concrete dust a thickness increase of $\sim(0.34 \pm 0.02)$ nm/day is determined[47]. The vertical green line shows a time when the diode was wiped clean and this removed the dust and the offset factor increased. As a result this point is not included in the fit shown as the blue line. This model however is not conlusive and further study of the change in the

offset factor and scaling parameters is needed. This is because these changes can also be a result of electronic effects such as changes in the gain of the diode due to variations in the bias voltage which is not monitored. However to minimize the variations observed in the calibration parameters the parameters are taken from the most previous calibration run data from the run analyzed.

Peak Range Discussion

The radon spectrum such as that shown in figure 4.8 represent the sum of all events within specific energy channels over the detector run. In emanation runs very low rates are expected, therefore regions within the spectrum are identified for each relevant decay. With stably defined regions of interest (ROI) for specific radon daughter decays, it is possible to extract the time evolution of these decays. Specifically, the number of decays of a particular radon daughter in a given time window within the defined region of interest can be extracted. The ROI for each peak is defined such that the majority of the peak is contained within this range. This however does not mean that all events of a specific decay are contained within the ROI. A dead-layer present on surface of the diode creates a low energy tails in each peak distribution which trails off to lower energies. This can cause peak overlap between two different decays. This means a selection for the ROI is maximally constrained by the presence of nearby peaks to minimize peak overlap resulting in misidentified events.

Table 4.2: The region of interest chosen for each polonium decay that is observed. Closely spaced peaks have bounds which nearly overlap. Peak deposition energy obtained from[2].

Isotope Name	Deposition Energy(MeV)	Lower Energy Bound(MeV)	Upper Energy Bound(MeV)	Events Within ROI
Polonium-210	5.304	4.9	5.5	97.1%
Polonium-218	6.002	5.5	6.2	98.8%
Polonium-214	7.686	7.0	8.2	99.4%
Polonium-212	8.784	8.3	9.1	95.5%

The energy range specified for the polonium-210 decay channel is defined

by a lower bound that is unaffected by peak overlapping. The lower bound for polonium-210 was chosen as 4.9 MeV to contain the majority of the polonium-210 peak while minimizing the influence from low energy electronic noise in the spectrum[4]. The upper bound however is constrained by the overlap of the polonium-218 peaks low energy tail. The upper bound was chosen as 5.5 MeV and is based on a polonium-210 main deposition energy of 5.304 MeV. The peaks quickly drops off at energies larger than the main deposition energy and it was decided that an upper bound of 5.5 MeV would not significantly overlap the low energy tail of the polonium-218 peak. The choice for the bounds determined for the other three peaks are based on similar constraints which minimize peak overlap. The ROI for each polonium isotope can be seen in Table 4.2 along with the fraction of total events contained within the ROI.

The four polonium decay peaks can be seen in figure 4.11 and figure 4.12 with the majority of each peak contained within their ROI. The overlapping of the polonium-218 decay channel with bismuth-212 decays is still present and therefore the polonium-218 ROI includes bismuth-212 decays. Of the four polonium ROIs the most important is polonium-214 which provides an α background free signal from radon-222 and is the focus of the radon analysis. In addition, attempts at using the polonium-218 ROI for radon analysis can still be made with attempts to separate the bismuth-212 signal from the polonium-218 signal. A technique to seperate the two decays will be presented in section 4.2.4. The polonium-210 and polonium-212 are not useful to directly determine a radon-222 signals, however they can be used for other purposes. The polonium-210 ROI shows the effects which make the measurement of radon-222 relevant, that is the long half-life of radon daughters resulting in surface radiation build up. The polonium-212 signal will be used to seperate polonium-218 and bismuth-212 events.

[4]The electronic noise will be discuss in section 4.2.6.

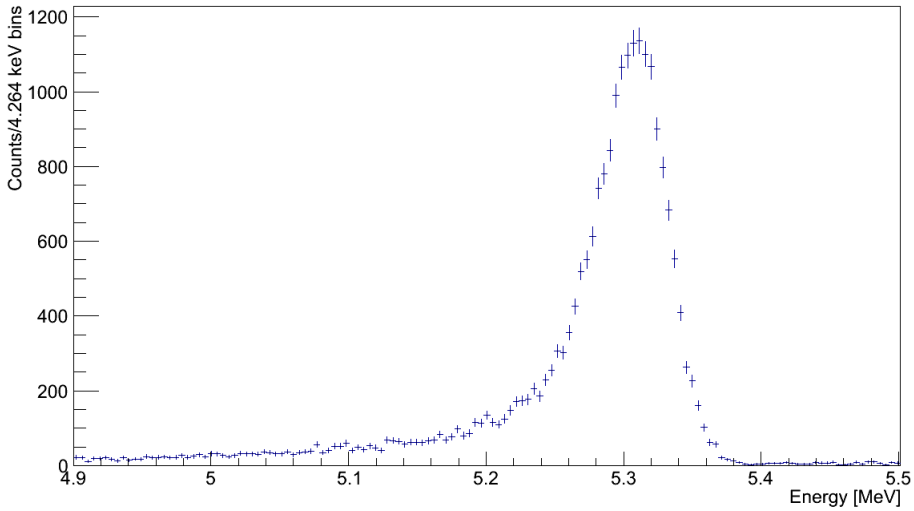

(a) Polonium-210 peak in the ROI

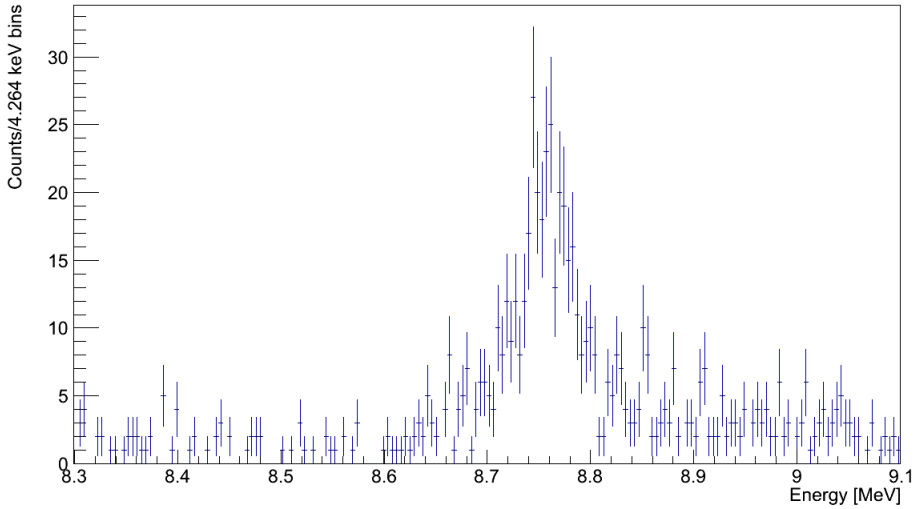

(b) Polonium-212 peak in the ROI

Figure 4.11: Peak distributions within the region of interest for polonium-210 and polonium-212 isotopes. Run 1054 consists of ∼91 hours run-time testing radon emanation off a 40' 4-conduit SNO+ cable.

Peak Fitting Models

Since the physics of the emanation system remains constant, the peaks in the calibrated spectrum can assist in the extraction of radon emanation rates. One

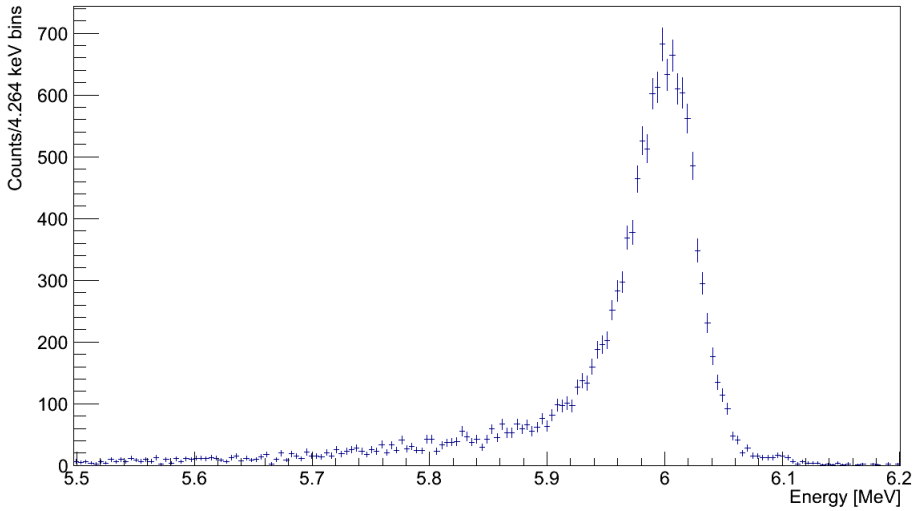

(a) Polonium-218 peak in the ROI

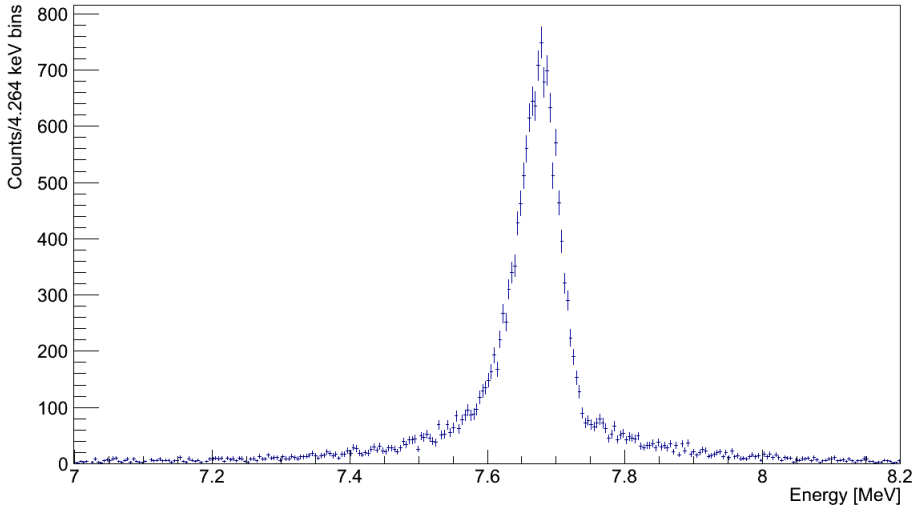

(b) Polonium-214 peak in the ROI

Figure 4.12: Peak distributions within the region of interest for polonium-218 and polonium-214 isotopes. Run 1054 consists of ∼91 hours run-time testing radon emanation off a 40' 4-conduit SNO+ cable.

technique used is the fitting of peak distributions with models which best describe the observed radon spectrum. Specifically, models are chosen which produce stable fits and describe the peak shapes well. Some processes and their

effects on the spectrum are not described from first principles accurately[5] and as a result the models are constructed empirically. Many samples exhibit low levels of radon emanation which yield limited statistics in the relevant peaks and the goal of the emanation system is to give an absolute number of detected radon, even for very low event counts. To determine the number of events in a peak the expected peak distributions from best fit models can be extrapolated from high statistic data samples by constraining the parameters of the fit. This is possible due to the stability of the line shape. The line shape for the peaks within the calibrated radon spectrum do not vary as they are produced from physical processes within the emanation system. There are two models which have been used to fit the peak distributions. Of the two models described, only one model was chosen due to superior fitting results. The model chosen is contructed from the first model, with additions that improve the fit to the peak line shapes.

The line shape observed in the emanation system is generated by the geometry of the diode used for particle detection. The diode is a window-less photodiode designed for the detection of optical photons. Unlike photons the detection of alpha particles produces a peak distribution that does not follow a Gaussian distribution. In order for the diode to operate as an alpha particle detector it must be reverse-biased so that all free charges are removed and a fully depleted zone is produced. However, a thin layer near the diode surface is needed to contact the diode and therefore is not active. This region must be traversed by the alpha particles before they can be detected within the depletion zone. This thin layer, known as a dead-layer causes a low energy tail skewing the expected Gaussian distribution. The low energy tail is formed due to the energy loss in the dead-layer region which is dependent on the angle of incidence of the incoming particle[44, 45]. The alpha particles traversing the

[5]Process such as radon mixing between detector chamber and sample chamber, small circulation speed variations, small temperature(pressure) variations, etc.

dead layer will lose more energy if the alpha particle travels into the diode at an angle which is not normal to the diode surface. An estimate can be placed on the dead-layer thickness for the diode. The KATRIN experiment tested the same diode that is used in the emanation system and reported a dead-layer thickness of (122 ± 10) nm[48]. A small variation in the thickness is expected due to different bias voltages[6], however the voltage dependence of the depletion layer was not studied. The dead-layer effect can be seen visually in figure 4.13. It can be seen that the effective dead-layer thickness Δh increases as:

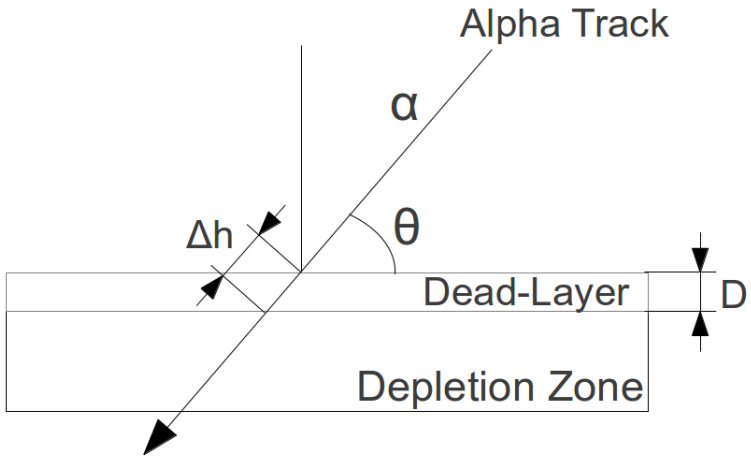

Figure 4.13: The dead-layer and its effective increase due to the angle of incidence of the alpha particle. The minimum energy loss of an alpha occurs when Θ is 90 ° and D is the dead-layer thickness estimated at (122 ± 10) nm[48].

$$\Delta h(\Theta) = \frac{D}{\sin(\Theta)} \tag{4.5}$$

As a result of the energy loss the expected distribution is no longer Gaussian and another model must be chosen.

A Landau distribution reflects energy loss through matter and can be used to model the effective energy loss[49, 50]. An analytical approximation to the Landau distribution was adopted to remove the need for a numerical lookup

[6]No report on the diode's bias voltage used in the KATRIN tests.

table required by the Landau fitting in ROOT. The Moyal approximation for a Landau distribution was chosen as the analytical approximation[51]. Fitting the Moyal equation to a polonium peak produces a fit that follows typical energy loss, however the fit results were not satisfactory. The Moyal fit can be

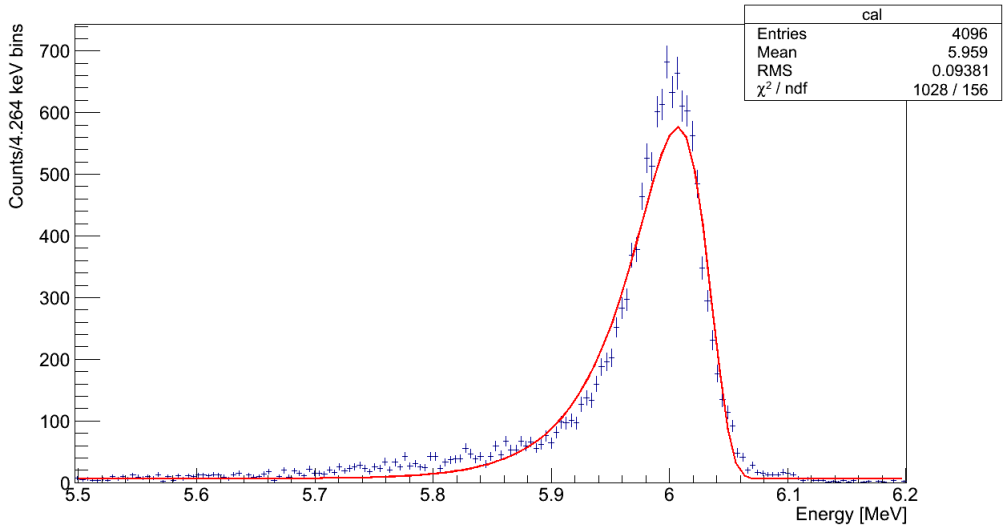

Figure 4.14: Moyal fit performed on the polonium-218 peak distribution. The function does not describe the data, but the main peak line-shape approximately follows this distribution.

seen in figure 4.14 where the Moyal equation is as follows:

$$\mathrm{F(E)} = \frac{P_0}{\sqrt{2\pi}} \exp\left(\frac{E - P_1}{2P_2} + \exp\left(\frac{E - P_1}{P_2}\right)\right) \tag{4.6}$$

where P_0 is the amplitude of the peak, P_1 is the peak location in MeV, and P_2 is the width of the distribution.

Although not satisfactory, the Moyal model approximately fits the low energy tail of the peak distribution caused by the dead-layer energy loss. However, the Moyal model does not model effects observed in the polonium-214 peaks. The Moyal model cannot accurately model this peaks due to a small high energy tail seen in the polonium-214 peak that can be produced from two effects.

The first effect is from nuclear recoils from alpha decays which cause nuclei to become embedded within the dead-layer[52]. Using SRIM a maximum embedding distance of ∼46 nm is calculated[47]. When embedded nuclei decay they can observe a thinner dead-layer resulting in a smaller energy loss for the emitted alpha particle from the decays. This effect can be seen in figure 4.15.

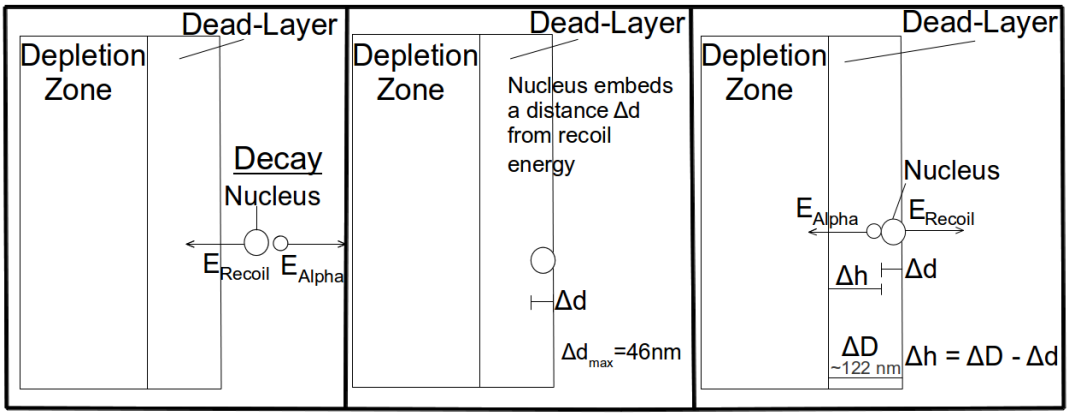

Figure 4.15: Model of the embedding of the polonium-214 nuclei that can lead to a smaller apparent dead-layer thickness Δh. The maximum distance that a polonium-214 nuclei can become embedded from a nuclear recoil is ∼46nm.

In addition to embedded nuclei, the high energy tail can be caused by the detection of multiple coincidence events. That is, multiple decays can occur almost simultaneously and the energy of the decays are summed together resulting in a single higher energy event. This effect is relevant to decays which can produce coincidence events. The radon-222 daughter isotope that is detected which can produce this effect is polonium-214 and is a result of the short polonium-214 half-life. This effect is strongly observed for the radon-220 daughter polonium-212[19] however radon-220 is not the focus of the radon analysis and so no fits to the polonium-212 peak are performed.

The Moyal equation cannot model these effect and as a result a new fit was constructed empirically to describe these effects. The fit equation is based on the Moyal equation, however two exponentials are included to fit the tails of the peaks multiplied by an error function to terminate the exponentials as

they approach the peak locations. The distribution that was constructed can be used to fit the peak distributions and is constructed as follows:

$$\begin{aligned} F(x) = P_0[\ & \frac{1}{\sqrt{2\pi}} \exp\left(\frac{1}{2}\frac{(x - P_1)}{P_2} + \exp\left(\frac{(x - P_1)}{P_2}\right)\right) \quad + \\ & P_3 \exp\left(P_4(x - (P_1 - P_8))\right) \cdot (1 - \mathrm{erf}((x - P_1)P_5)) \quad + \\ & P_6 \exp\left(-P_7(x - (P_1 - P_9))\right) \cdot (1 - \mathrm{erf}((x - P_1)P_{10}))\ ] \end{aligned} \tag{4.7}$$

where P_i represents parameter i(i=0,1,2,....,10) determined from the fit.

This purely empirical model fits the peak distribution of the radon-222 daughters well. A fit to the polonium-218 and polonium-214 peak can be seen in figure 4.16. This model is fitted to high statistic runs such as calibration runs to determine the line shape of the polonium peaks. From the fit parameters it is possible to constrain this model and only scale down its total amplitude P_0 to fit to peak distributions where there is limited statistics. This process will be used in section 4.2.4 to attempt to separate polonium-218 and bismuth-212 decays which have overlapping energy regions.

4.2.3 Emanation Equation

During the operation of the emanation system radon daughters are produced by radon emanation within the system. Initially no radon is present allowing to predict how the radon emanation should behave within the emanation system. Because there is no radon in the emanation system, any rates from radon is caused by radon emanation, thus we have:

$$\frac{dN_{Rn}}{dt} = -\lambda_{Rn} N_{Rn} + E_{Rn} \tag{4.8}$$

Where E_{Rn} is the radon emanation rate and $-\lambda_{Rn} N_{Rn}$ is the decay rate of radon. Equation 4.8 represent the change in the radon rate ($\frac{dN_{Rn}}{dt}$) due to radon emanation. From this it follows that the number of radons produced

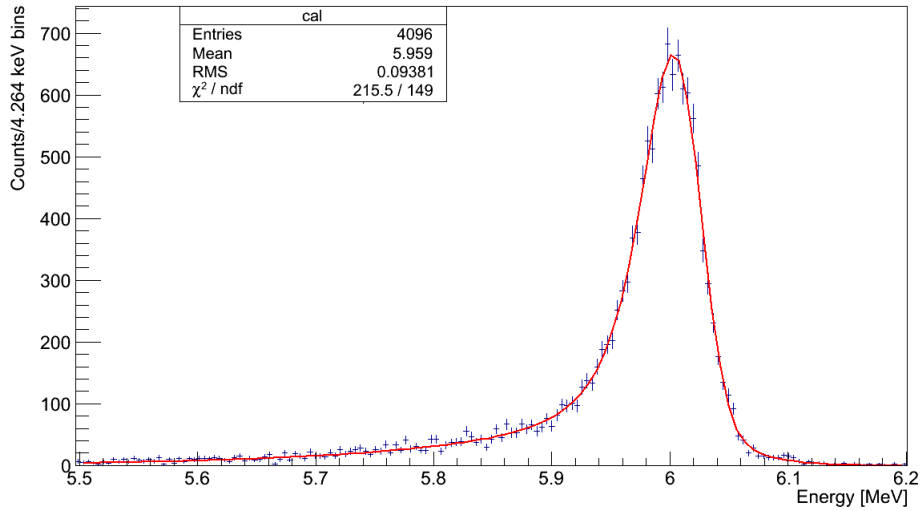

(a) Polonium-218 peak fit.

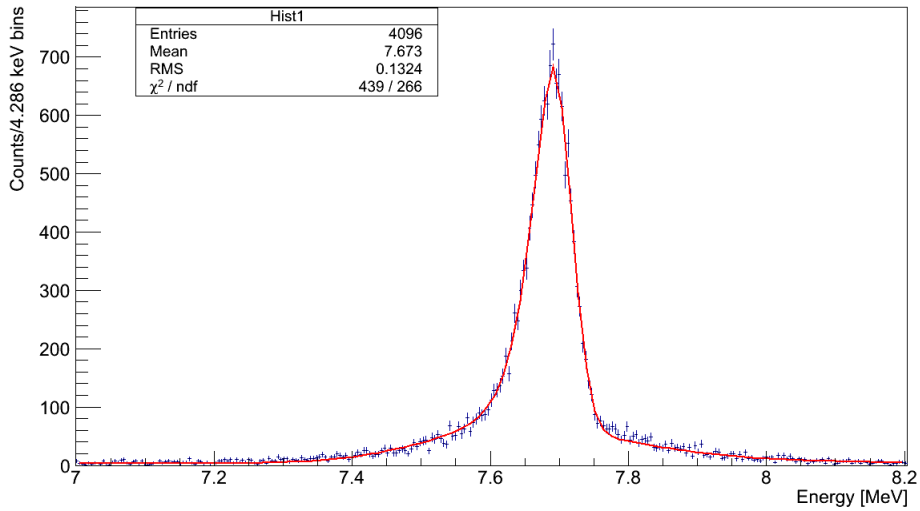

(b) Polonium-214 peak fit.

Figure 4.16: Best fit model result on the same data as in figure 4.14.

from radon emanation behaves as:

$$N_{Rn}(t) = \frac{E_{Rn}}{\lambda_{Rn}}(1 - e^{-\lambda_{Rn} t}) \tag{4.9}$$

This equation represents the expected behavior of radon emanation in which radon is produced from constant radon emanation. A more apropriate form of this equation in terms of radon activity is:

$$\lambda_{Rn} N_{Rn}(t) = A_{Rn}(t) = E_{Rn}(1 - e^{-\lambda_{Rn} t}) \tag{4.10}$$

This form can be directly applied to the data which represents the activity within the emanation system and thus equation 4.10 represents the expected behavior of the data from the emanation system. Using equation 4.10 the radon emanation rate of the samples can be extracted from the data.

4.2.4 Background Determination

Measurements of radon emanation rates from samples require an understanding of the backgrounds within the emanation system. The background radiation is intrinsic to the detecting system. In order to measure the radon emanation rates from samples, the influence of the background radiation must be removed. The only detectable radiation comes from alpha or beta radiation from nuclear decays within the emanation system. The detection of beta radiation does not pose a significant problem for the emanation system. Beta radiation deposit energies much lower than the energies associated with the radon signals and thus do not act as a source of background for the radon signals. This only leaves backgrounds from alpha emissions in nuclear decays having energies at or above 5 MeV where the radon signal exists.

The materials the emanation system is constructed from produce some amount of radon emanation due to uranium and thorium contamination. The contamination of the detector material give rise to the alpha backgrounds present in the emanation system. Due to the purging operation of the emanation system any detectable alpha radiation in the absence of a sample comes from the detector materials or the nitrogen gas used in purging. In addition,

any vacuum leaks within the emanation system can draw radon contaminated air into the system producing a signal that is indistinguishable from radon emanation.

From the detector emanation it is possible to determine the background radon emanation rate as it follows the emanation equation 4.10. Once the background radon emanation rate is known it can be subtracted from the overall radon emanation rate of a tested sample. With the background rate subtracted the radon emanation rate for the tested sample is obtained. A discussion of the background determination of the emanation system for both the polonium-214 and polonium-218 isotopes along with improvements in background rates will be the focus of this section.

Pressure Tests

To achieve a stable background in the emanation system, all sources of background must be understood. The backgrounds due to detector emanation are intrinsic to the emanation systems and will not vary unless modifications are made to the detector. Another possible source of radon background depends on the operational method of the emanation system. The emanation system is purged multiple times and continuously run slightly below atmospheric pressure. The negative pressure differential can introduce radon through leaks in the emanation system's many NPT and Swagelok connections. In addition, the emanation chamber is sealed with a large lid that uses a 24" diameter o-ring seal and a Delrin feed-though that uses one 3" diameter outer o-ring and two $1\frac{1}{8}$" inner o-rings. The feed-through was initially sealed with one inner o-ring, however this did not provide an adequate seal. Leaks allow ambient radon from outside the emanation system to be drawn into the system. Radon leaks produce a signal consistent with radon emanation. This can be seen in the

equation describing radon leaks:

$$\frac{dN_{Rn}}{dt} = -\lambda_{Rn}N_{Rn} + E_{Rn} + L_{Rn} \tag{4.11}$$

where N_{Rn} is the amount of radon, λ_{Rn} is the decay constant for radon-222, E_{Rn} is the radon emanation rate, L_{Rn} is the radon leakage rate and t is time.

Applying the approximation that any leak rate within the detector is small and constant over the detector runtime allows the solution of the time evolution of the radon within the emanation system to be derived. Equation 4.12 accounts for the effects of both radon emanation and radon leakage. A comparison to equation 4.10 shows that a constant radon leak will produce a signal indistinguishable from radon emanation.

$$\lambda_{Rn}N_{Rn}(t) = A_{Rn}(t) = (E_{Rn} + L_{Rn})(1 - e^{-\lambda_{Rn}t}) \tag{4.12}$$

Small leaks were found to have a strong effect on determining radon emanation rates. A run was performed comprising of a monitored pressure leak that was caused by a damaged circulation pump diaphram. The pressure sensor used to monitor the pressure is a INFICON PCG550[53]. The data was used to verify the effect that vacuum leaks can have on the measurements of radon emanation rates. By assuming a constant leak rate of ambient radon contaminated air into the emanation system, it is possible to compare the measured value for the factor $E_{Rn} + L_{Rn}$ to the expected value of L_{Rn}. The expected value of L_{Rn} was found from the monitored pressure and radon activity of the air surrounding the emanation system. The pressure changes observed during this run can be seen in figure 4.17. Using the linear fit parameters extracted from figure 4.17, an estimated radon room air activity of $\sim(6.76 \pm 0.18)\ \frac{Bq}{m^3 atm}$ [7] and an emanation system volume of $(0.3837 \pm 0.0037)\ m^3$ an estimate of

[7]This was measured in July 2013 using the emanation system when it was open to room air approximately 20 days after this background run.

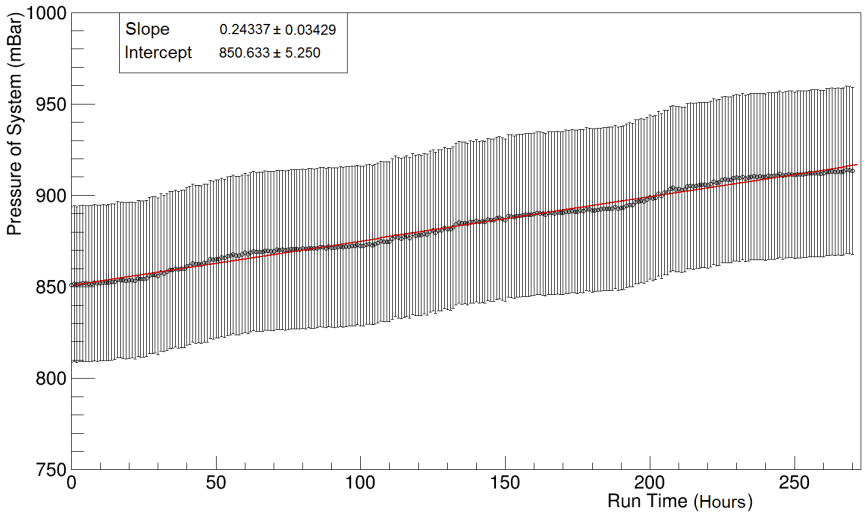

Figure 4.17: Pressure during background run 1195 in which a leak was found. The error bars are based on pressure sensors stated uncertainty of 5% in the operational pressure range[53].

the radon leak rate L_{Rn} can be determined. Using the above information, the expected radon leak rate into the emanation system was calculated to be (320 ± 48) radons/hr. This was calculated using the following equation:

$$L_{Rn} = \frac{L_{Rate} V_{Detector} A_{Air}}{\lambda_{Rn}} \tag{4.13}$$

where L_{Rn} is the radon leak rate in radons/hr, L_{Rate} is the pressure leak rate in mBar/hr, $V_{Detector}$ is the vacuum system volume and A_{Air} is the radon activity concentration and λ_{Rn} is the hourly decay constant of radon-222.

Unit conversions from s^{-1} (Bq) to hr^{-1} were applied to match the detector data. The value for the total radon emanation and radon leakage ($E_{Rn} + L_{Rn}$) was measured to be (391 ± 21) radons/hr. This shows that over 80% of the measured radon rate can be attributed to ambient air leaking into the emanation system.

Small leaks in the range of 0.2 mBar/hr can have a significant impact on

the E_{Rn} factor. For radon emanation runs, a stable low radon background activity is needed. E_{Rn} is intrinsic to the emanation system and is difficult to lower. As a result it is important to eliminate the influence of ambient radon leaking into the emanation system. The effects from L_{Rn} can be minimized by sealing the emanation system making this factor negligible. To achieve this a systematic sealing procedure of leak testing individual components before additional connections were introduced was conducted on the emanation system to minimize leaks. In additon a helium leak test was also conducted. This minimized the effects from radon leaking into the emanation system within the uncertainty of the pressure monitoring.

Background of the Polonium 214 Channel

The materials the emanation system is constructed from contain small amounts of uranium and thorium contamination leading to radon emanation. The emanation system's background radon emanation for the polonium-214 decay channel can be determined and must be minimized to optimize the sensitivity of the emanation system within the polonium-214 channel. The background activity can be seen in figure 4.18.

A fit is applied to the data shown in figure 4.18 which follows equation 4.10. To constrain the fit, the parameter representing the decay constant of radon is fixed to its hourly value of 0.0075605 hr^{-1}[2]. This allows for a single parameter fit which determines the background radon emanation rate for the polonium-214 channel. The background radon emanation rate was measured to be (101 $\pm$ 11) counts/hr. The measured background activity is high and limits the sensitivity of the emanation system. This led to a search for the sources of the background in an attempt to lower the background level. Because radon emanation can come from all parts of the emanation system, as many pieces as practical were tested and replaced in order to improve the background activity. The improvements will be discussed in section 4.2.5.

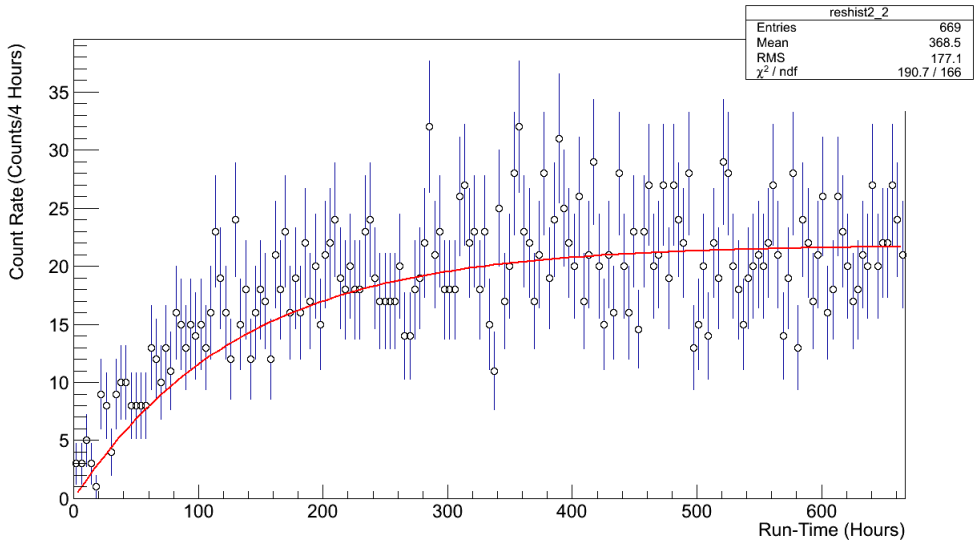

Figure 4.18: Background run 1153 in which the intrinsic radon background was measured from polonium-214 decays.

Background of the Polonium-218 Channel with the Bismuth-212 Separation Method

In addition to using the polonium-214 decay channel to obtain a radon-222 signal, the decays of polonium-218 can be used as a consistency check with the polonium-214 channel. However this decay channel can contain signal pollution from bismuth-212 decays. Due to the decays of radon-220 from the thorium-232 decay chain, the bismuth-212 daughter can be detected through its alpha emission.

The bismuth-212 alpha decays (6.05 MeV) act as a strong signal contamination in the polonium-218 channel (6.00 MeV). With only a 0.05 MeV energy separation the method of counting within the polonium-218 ROI requires additional analysis. The signal overlap can be removed using the good energy resolution of the detector. The peak separation of the two signals can be seen in figure 4.19, where the low energy tail from the bismuth-212 decay overlaps with the polonium-218 decays leading to the signal contamination in the ROI.

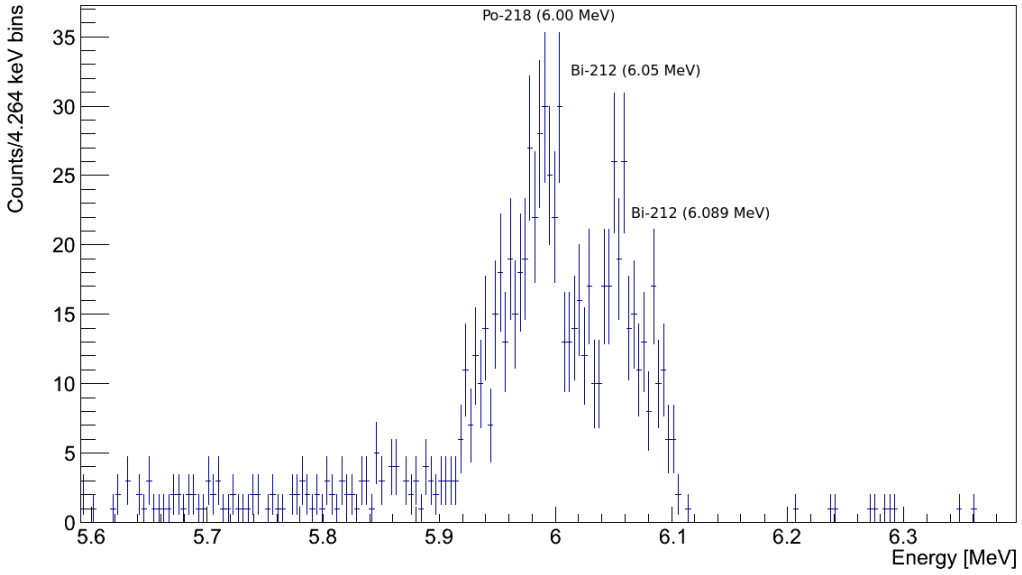

Figure 4.19: A calibrated background run spectrum in the region of interest around the polonium-218 peak. Two decay signals are visible, the polonium-218 and bismuth-212 peaks are located at 6.00 MeV and 6.05 MeV respectively.

This results in a combination of events from both polonium-218 and bismuth-212 decays in the ROI.

The two decay rates are separated by performing a fit within the polonium-218 ROI. The fit applies the best peak fit model discussed in section 4.2.2. The peak line shapes are intrinsic to the detector system and the fit can be constrained with the data from high statistic run while rescaling the amplitude to low statistics runs where the peak separation can be observed. The separation analysis can be applied to emanation runs in which the bismuth-212 and polonium-218 signals are comparable in magnitude. Using this analysis, a proportionality constant which relates bismuth-212 and polonium-212 can be extracted which makes the separation of polonium-218 and bismuth-212 possible and will be discussed below.

Bismuth-212 can decay via two alpha branches with energies of 6.05 MeV

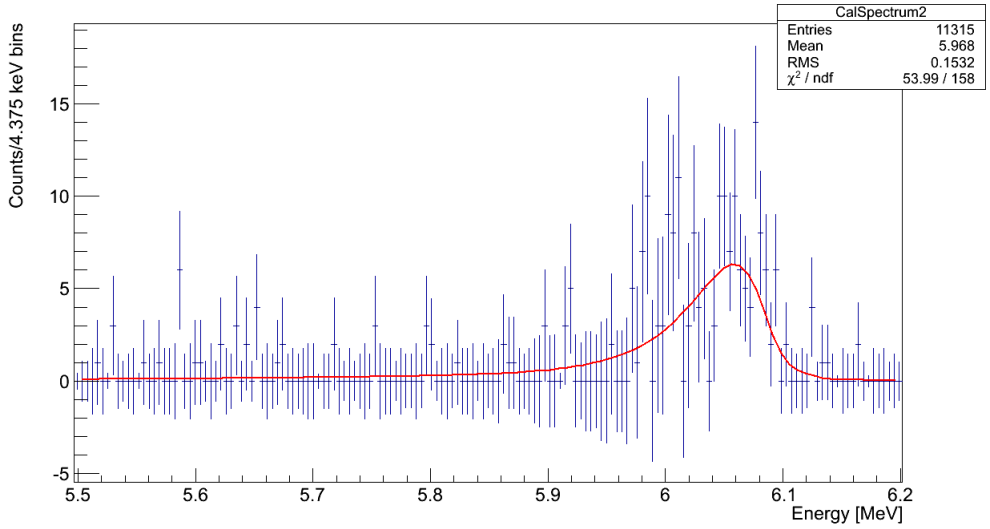

Figure 4.20: Double peak fit to bismuth-212 peak region with polonium-218 signal removed. Only the amplitude is fitted, peak location and line shaping parameters are constrained.

and 6.089 MeV with branching ratios of 25.13% and 9.75% respectively. As a result the polonium-218 ROI contains a combination of three peak distributions. The polonium-218 peak can be removed through fitting within this region with the empirical line-shape determined in section 4.2.2. The fit constrains the shaping parameters to the parameters extracted from the data of high statistic runs while the amplitude of the polonium-218 peak is determined through the fit. The fitted polonium-218 peak is subtracted from the spectrum leaving only bismuth-212 events. The ROI is then fit with two bismuth peaks that are associated with the two branching decay energies of the bismuth-212. A fit is performed to minimize any effects from polonium-218 still present within the ROI that was not removed through the fit subtraction. Using the bismuth-212 fit, a total number of bismuth-212 events can be extracted. The fit can be seen in figure 4.20, where the majority of the polonium-218 events have been removed.

In addition to the bismuth-212 decay signal from thorium contamination, a

polonium-212 decay signal is observed. The polonium-212 decay signal occurs in a region free of peak overlap from other decays. As a result the polonium-212 is a clear signal that is proportional to the bismuth-212 decays. From this proportionality it is possible to predict the bismuth-212 signal based on the signal from polonium-212 decays. A proportionality parameter can be extracted from the ratio of total counts of bismuth-212 and polonium-212 decays. The proportionality between bismuth-212 and polonium-212 is defined as follows:

$$\frac{\mathrm{C_{Bi-212}}}{\epsilon_{\mathrm{Bi-212}}\mathrm{B}_{\alpha-\mathrm{mode}}} = \frac{\mathrm{C_{Po-212}}}{\epsilon_{\mathrm{Po-212}}\mathrm{B}_{\beta-\mathrm{mode}}} \tag{4.14}$$

where $\mathrm{C_x}$ represents total counts of isotope "x", $\mathrm{B}_{\alpha-\mathrm{mode}}$ and $\mathrm{B}_{\beta-\mathrm{mode}}$ are the branching ratios of the decay modes of bismuth-212 (0.36 and 0.64 respectively) and ϵ_{x} is the detection efficiency with respect to bismuth-212 and polonium-212.

Rearranging equation 4.14 to solve for the ratio between the total counts of bismuth-212 and polonium-212 gives:

$$\frac{\mathrm{C_{Bi-212}}}{\mathrm{C_{Po-212}}} = \frac{\epsilon_{\mathrm{Bi-212}}\mathrm{B}_{\alpha-\mathrm{mode}}}{\epsilon_{\mathrm{Po-212}}\mathrm{B}_{\beta-\mathrm{mode}}} \tag{4.15}$$

The parameters $\mathrm{B}_{\alpha-\mathrm{mode}}$ and $\mathrm{B}_{\beta-\mathrm{mode}}$ are known constants, while ϵ_x are constant and defined by the emanation system. A naive assumption can be made that both bismuth-212 and polonium-212 have the same detection efficiency. The half-life of polonium-212 is very small (0.3μsec) and as a result it will not be strongly influenced by the electric collection field. In this case no additional polonium-212 will be collected at the diode and the polonium-212 detected will have come from bismuth-212 decays that occurred on the diode. As a result, the efficiency for polonium-212 will be approximately equal to the bismuth-212 efficiency. A proportionality constant can then be determined and used to separate events from bismuth-212 and polonium-218. The assumption that the detection efficiency of polonium-212 and bismuth-212 are equal must be verified. This can be accomplished by experimentally measuring the ratio be-

tween the total bismuth-212 and polonium-212 counts. If the ratio is consistent with our assumption, then the proportionality constant can be used to separate bismuth-212 and polonium-218 events for any sample strength.

The total bismuth count is obtained from integrating the peak fit shown in figure 4.20. The total bismuth-212 count extracted from the fit is (160 ± 13) counts. The number of total polonium-212 counts is found through summing within its energy range and is (308 ± 18) counts. This results in a ratio with a value of (0.52 ± 0.05). The value expected is 0.56 and is consistent with our assumption. As a result the proportionality parameter can be obtained from the ratio of the branching ratios of beta and alpha decay modes of bismuth-212. Verifying the proportionality parameter determines a proportionality constant between polonium-212 decays and bismuth-212 decays.

With the proportionality constant obtained, a radon-220 emanation curve can be constructed for bismuth-212 and polonium-212 decays. The criteria for secular equilibrium ($\lambda_{Bi212} >> \lambda_{Po212}$) between bismuth-212 and polonium-212 is met. As a result deriving the radon-220 emanation curve observed in bismuth-212 decays also provides the curve for polonium-212. Due to the operation of the emanation system an approximation can be made that simplifies the curve. The duration between subsequent run is approximately half the decay time for lead-212; the radon-220 daughter with the longest half-life and which produces bismuth-212. In addition, the lead-212 is at equilibrium from radon-220 emanation when a detector run ends. Because of the short duration between subsequent runs, the amount of lead-212 does not significantly decay away and can be treated as approximately constant. This means that the activity of bismuth-212 and polonium-212 can also be treated as approximately constant. Using this approximation a model can be constructed which reflects a constant activity. Therefore the model that is used to describe bismuth-212

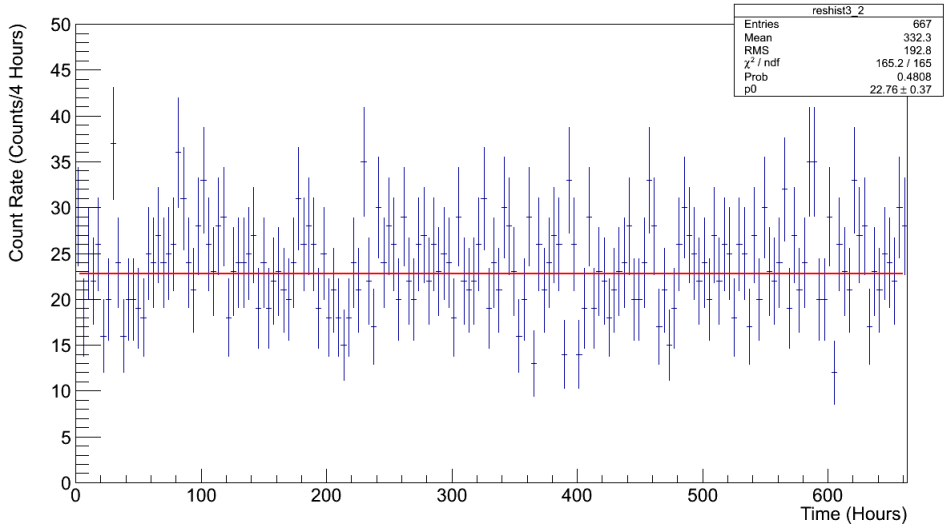

Figure 4.21: Polonium-212 rates fitted with the expected constant activity that follows equation 4.16.

and polonium-212 is as follows:

$$A(t)_{Bi(Po)} = A^0_{Bi(Po)} \tag{4.16}$$

By fitting the polonium-212 decay channel with equation 4.16 the polonium-212 activity resulting from radon-220 is obtained. A fit to the polonium-212 data is shown in figure 4.21 and the data follows the assumption of a constant activity.

Rescaling the polonium-212 curve with the proportionality constant of 0.56 determines the expected bismuth-212 curve. With the bismuth-212 curve known the polonium-218 channel can be analyzed through adding a radon-222 emanation curve to the fixed bismuth-212 curve. Using the combination of the radon-222 curve and the fixed bismuth-212 curve the radon-222 emanation rate can be extracted from the polonium-218 data. The resulting fit to the polonium-218 channel can be seen in figure 4.22 where the combined emanation

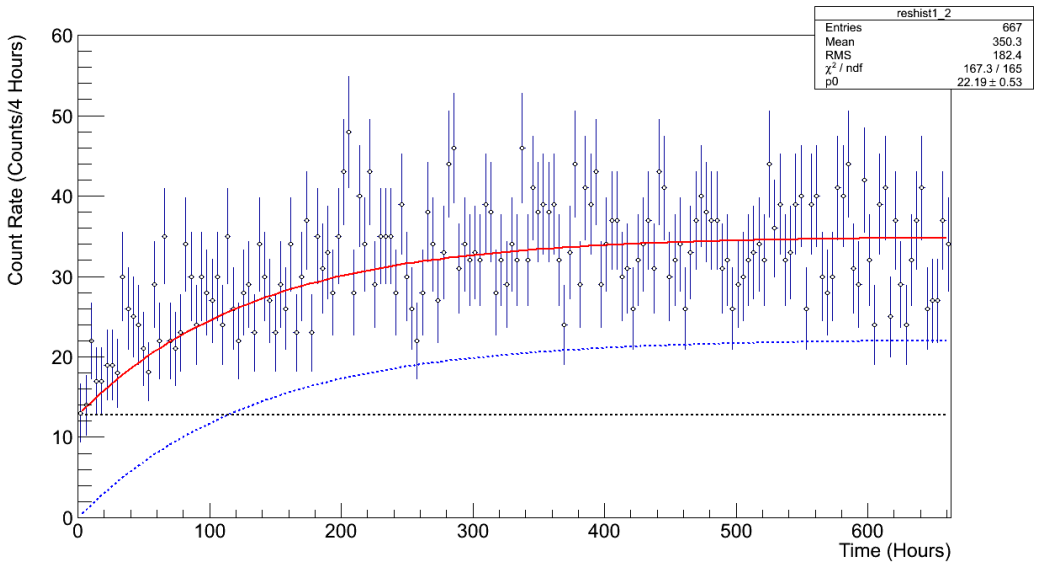

Figure 4.22: Fit to the polonium-218 decay channel using equation 4.17. The dotted blue line shows the contribution from radon-222 emanation. The dotted black line shows the contribution from the constant bismuth-212 activity.

curve is as follows:

$$A(t)_{Po218(Bi212)} = E_{Rn222}(1 - e^{-\lambda_{Rn222}t}) \; + \; P_{Bi/Po} \cdot A_{Po-212} \tag{4.17}$$

where $P_{Bi/Po}$ is the proportionality constant of 0.56, λ_{Rn222} is the decay constant of radon-222, E_{Rn222} is the radon-222 emanation rate and A_{Po-212} is the constant activity determined from polonium-212 rates.

Using the parameters from the fit, a background emanation rate for radon-222 of (119 $\pm$ 13) counts/hr using the polonium-218 decay channel is determined. This value is consistent with the background emanation rate of (101 $\pm$ 11) counts/hr determined through the polonium-214 decay channel and shows that the polonium-218 channel can be used as a consistency check for the polonium-214 channel.

Figure 4.23: The feedthrough components that were tested as possible radon emitters.

4.2.5 Background Improvements

During the operation of the emanation system it was found that the background emanation levels within the system are high. An attempt to lower the background activity and achieve a background level that allows for sensitive radon emanation measurements was made. To find the source of the background activity, vigoruous testing of the detector components was undertaken. Detector components which have exposed surface areas within the emanation system have been tested to determine the source of the radon emitter. All of the feed-through components have been tested by increasing the surface area of the component through testing a large quantity. Through testing, all the feed-through components have been measured and the results do not point to component contamination within the feed-through. A picture of the feed-through components can be seen in figure 4.23

Another possible source of the radon emanation can be attributed to the contamination of the stainless steel vessel. Any radon emanation from the

stainless steel was minimized through an extensive cleaning procedure performed on the internal surface area of the vessel. The procedure consists of ethanol wiping the stainless steel to remove dust and grease from its surface. In addition, the stainless steel was scrubbed vigorously using stainless steel brushes and a buffing disk. The purpose was to remove any dust or material that was strongly attracted to the surface of the steel which an ethanol wipe could not remove. Stainless steel passivation was also performed to minimize impurities on the stainless steel surface. The passivation was performed using a commercially available citric acid passivation solution called CitriSurf-2250 from Stellar Solutions Inc[54]. This solution was chosen due to a high viscosity which made passivation of the vertical surfaces possible. The solution had the added advantage of a non-hazardous, easy to use solution that could not exhibit a so called flash attack. A flash attack causes discoloration and surface degradation of the stainless steel[55]. The effect a flash attack can have on radon emanation has not been studied thus avoiding this possibility was advantageous. Through cleaning the stainless steel a background reduction of a factor of greater than three was achieved. The background of the emanation system was lowered from the value reported in section 4.2.4 of (101 $\pm$ 9) counts/hr to a value of (29 $\pm$ 4) counts/hr.

Materials produced from hydro-carbon based compounds can have uranium contamination which can lead to radon emanation[56]. This has always pointed at the possibility of the o-rings used to seal the emanation chamber as sources of radon emanation. Extensive testing of the emanation system o-rings have been performed, however each test involved replacing the o-ring and testing them *in situ* in the emanation system as opposed to emanating the o-ring as samples due to a lack of available materials. This produced no significant variation in background activity between o-ring materials. However tests have been performed using a large quantity of the o-ring materials tested as samples. The results imply that the current background activity of (29 $\pm$ 4)counts/hr can be

attributed to radon emanation from the o-rings used in the emanation system. The lack of significant variation in background activity from the different materials when tested *in situ* can be attributed to the manufacturer producing the o-rings. All o-rings tested came from the same manufacturer which can mean that the materials used to manufacture the o-rings such as the filler material of the o-rings are sources of the radon emanation. The filler material would be used in all the o-rings and would result in similar emanation rates from different o-ring materials. This can explain the lack of significant background variations when using the variety of o-ring materials. Attempts to minimize the radon emanation from the o-rings are currently on-going. Unfortunately radon emanation rates vary from manufacturers and limited data on radon emanation from o-rings can be found.

4.2.6 Detector Efficiency Determination

The emanation system can only detect a fraction of the radon daughters present in the volume of the emanation system. This efficiency loss is due to the geometric design of the detector, the radon daughter collection method which requires an electric drift field, as well as the diode which at most can detect ∼50% of the radon daughters due to the diode geometry. The efficiency is intrinsic to the design and operational parameters of the emanation system and must be determined experimentally in order for any measurements of radon emanation rates. The efficiency is strongly affected by the effective volume of the emanation system as the radon concentration decreases with an increased volume and only ∼50% of the volume of the emanation system is sampled when the sample holding tank system is used. The detection efficiency is therefore dependent on the volume of the detecting system. The emanation systems has two separate sample holding tanks. The first holding tank is the vacuum(largest) sample holding tank (see figure 3.9) with a volume comparable to that of the emanation chamber. The other system uses a "beam-pipe" holding tank which

has a volume approximately one tenth the volume of the emanation chamber. Due to the differences in volume of each system, the system efficiency must be determined for each of the two emanation systems.

Operating High Voltage

Electrostatic attraction of the charged radon daughters is used to significantly increase the emanation system efficiency. As a result, the dependence of the efficiency on the high voltage must be studied. This is important as any variation in the high voltage can have an effect on the detector efficiency. To minimize the effects of high voltage variations, the high voltage should be set at a value in the plateau where all possible charged daughters are collected through electrostatic attraction. The plateau presents a high voltage operating condition where small deviations have negligible effects on the collection efficiency. The high voltage plateau is shown in figures 4.24 and 4.25, where the fitted function follows $\epsilon(\mathrm{x}) = \epsilon_{\mathrm{Plateau}}(1 - \mathrm{e}^{-\lambda \mathrm{x}})$ and the parameter λ is a fit determined high voltage constant.

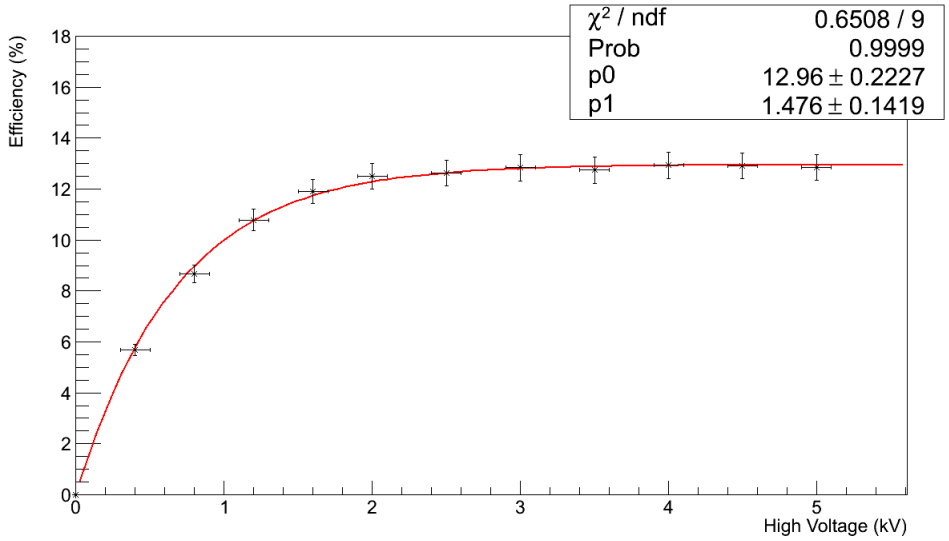

Figure 4.24: High voltage collection efficiency for the polonium-214 decay channel using the emanation chamber only.

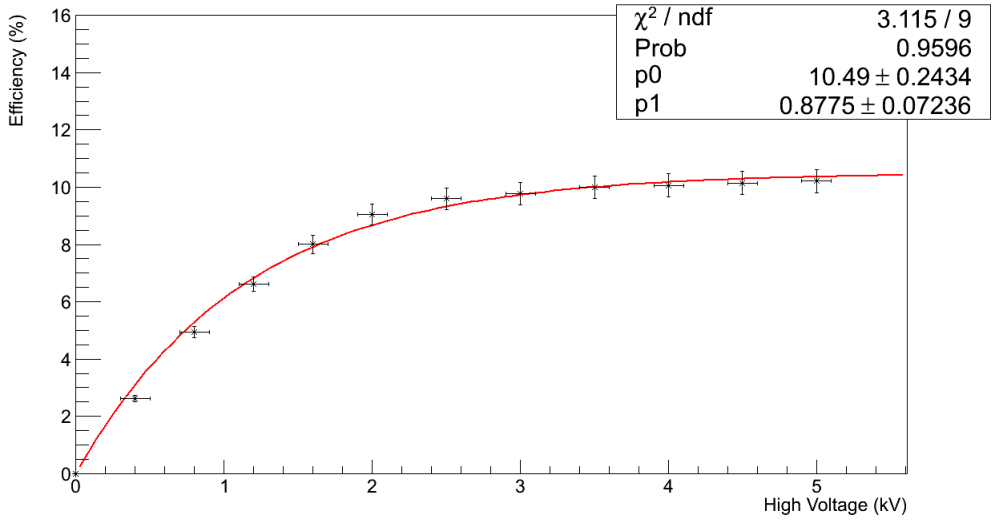

Figure 4.25: High voltage collection efficiency for the polonium-218 decay channel using the emanation chamber only.

From figure 4.24 and 4.25 the plateau is reached at approximately 2-2.5 kV for polonium-214 and about 4-4.5 kV for polonium-218. It was decided that operating at 5 kV was optimal to maximize collection efficiency of both radon daughters. This choice is also influenced by the additional affects that the high voltage has on the emanation system. Arbitrarily increasing the high voltage as high as possible risks damaging the electronics of the emanation system and increases the noise from microphonics within the radon spectrum. The high voltage noise produces a low energy tail that decreases exponentially with increasing energy. At voltages larger than 5 kV the low energy tail starts to approach the energy regions in which the radon daughters are present. This reduces the sensitivity for detecting radon daughters while gaining nearly no increase in efficiency. This led to the selection of +5 kV high voltage as the default operational setting.

Efficiency of the Vacuum Holding Tank System

The vacuum sample holding tank is the emanation system used the most extensively due to its large volume and easy accessibility. To determine radon emanation rates the efficiency of the emanation system with the vacuum sample holding tank is needed. The efficiency is experimentally determined from calibration runs used for the energy calibrations discussed in section 4.2.2. The radon-222 source at equilibrium is flushed into the emanation system using nitrogen gas to produce a total expected radioactivity of 930 Bq within the emanation system volume. The efficiency can then be determined from the detected activity. The detection efficiency of radon-222 through the polonium-214 decay channel was measured to be (5.502 +/- 0.002)% under the normal operating conditions described in section 4.2. This means that only 5.502% of the radon present in the emanation system is detected using the polonium-214 decay channel. The signal from one calibration run is shown in figure 4.26. The efficiency determined above is found using the radioactive decay law:

$$\mathrm{A(t)} = \mathrm{A_0 e^{-\lambda t}} \tag{4.18}$$

From the radioactive decay law the expected activity that should be detected with 100% detection efficiency can be determined at any time t. This allows the efficiency of the emanation system to be measured by using equation 4.19 shown below:

$$\epsilon(\mathrm{t}) = \frac{\mathrm{A_{Observed}(t)}}{\mathrm{A_{Expected}(t)}} \cdot 100\% \tag{4.19}$$

where ϵ(t) is the percent efficiency at time t, $\mathrm{A_{Observed}}$ is the detected activity of radon in the emanation system at time t, $\mathrm{A_{Expected}}$ is the expected radon activity at time t determined using equation 4.18 with the known radon activity. ϵ(t) should be constant as it does not vary as a function of time under normal operating conditions. This however is not entirely true due to the initial mixing of radon throughout both the sample holding tank and the emanation chamber.

This causes the efficiency to vary as a function of time until the radon concentration reaches equilibrium between both of the emanation system tanks. In addition to the radon mixing, there is a delay of several hours due to the time required for polonium-214 to reach secular equilibrium[42]. This produces a time dependent efficiency during the initial detector run-time. After the initial mixing and time required to reach secular equilibrium, the efficiency stabilizes and is constant.

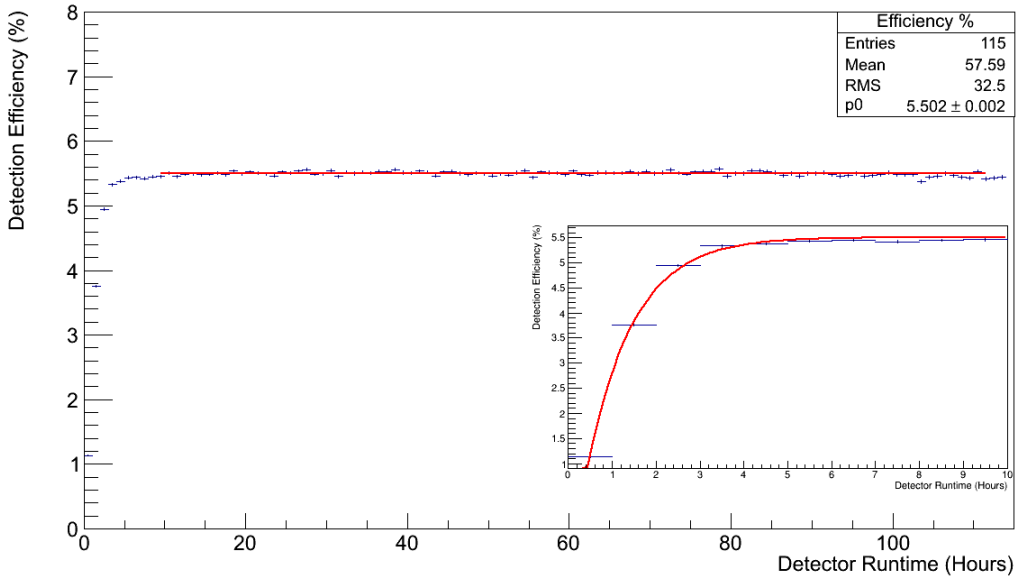

Figure 4.26: Efficiency of detecting radon-222 from the polonium 214 decay channel (Run 920 with a source activity of 421 Bq). The inset shows the effects of the initial radon mixing and delay for polonium-214 to reach secular equilibrium in the emanation system with a time constant of $(0.956 \pm 0.008)\text{hr}^{-1}$.

Due to the equilibrium delay at the beginning of calibration runs, a rapidly increasing efficiency is observed initially. It was found that it requires approximately 9 hours for the radon concentration to completely reach equilibrium in the emanation system, this effect can be seen in figure 4.26. The inset is fit with $\epsilon(\text{t}) = \epsilon_0(1 - \text{e}^{-\lambda \text{t}})$ used to determined the time constant for equilibrium. Because of this, the efficiency is determined by a constant fit performed after

the first 10 hours to determine the efficiency.

In addition to radon measurements from polonium-214, the polonium-218 decay channel can be used to measure radon emanation rates. This channel contains events that are associated with decays from bismuth-212 decay contaminating the polonium-218 signal however due to the high activity of the radon source, the bismuth-212 decays are a very small fraction of the polonium-218 signal in calibration runs. Therefore the signal can be approximated as a pure polonium-218 signal in calibration runs. This results in an efficiency of polonium-218 detection of (4.784 +/- 0.002)% and is shown in figure 4.27 with a constant fit. The inset is fit with $\epsilon(t) = \epsilon_0(1 - e^{-\lambda t})$ used to determined the time constant for equilibrium.

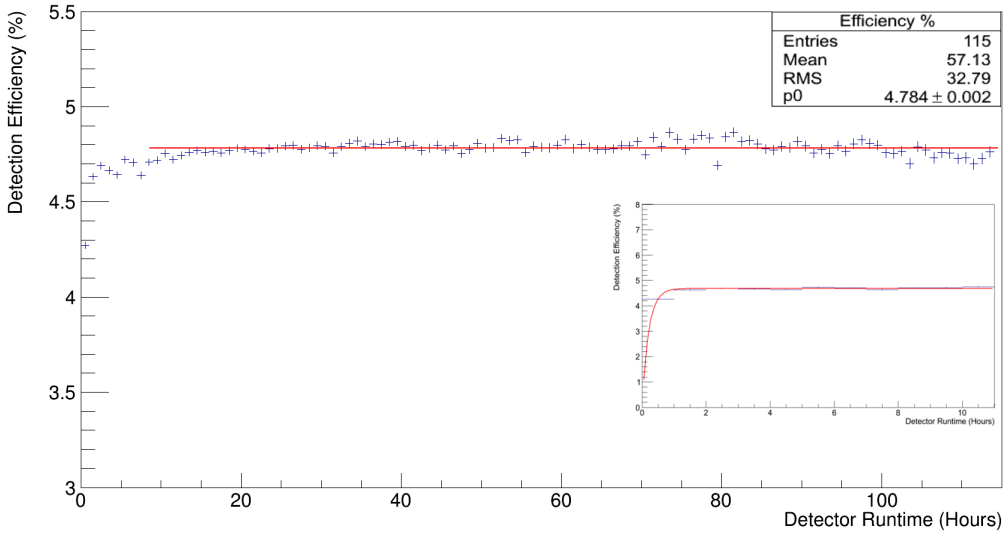

Figure 4.27: Efficiency of detecting radon-222 from the polonium-218 decay channel (Run 920 had a source activity of 421 Bq). The inset shows the effects of the initial radon mixing and shorter delay in polonium-218 production in the emanation system with a time constant of (4.87±0.09)hr^{-1}.

The efficiency for polonium-218 was determined using the same approach as the polonium-214 efficiency. The effects of radon mixing is visible however the time required for polonium-218 to reach secular equilibrium is shorter in this

signal which is due to polonium-218 being the direct daughter of radon-222. The effects of the radon mixing can still be seen in the polonium-218 decays. The efficiency is determined after the initial 10 hours of run-time as the radon mixing constrains a fit to lower times which is observed in both figure 4.26 and 4.27. In addition, the polonium-218 efficiency is smaller than the polonium-214 efficiency. This is consistent with what was expected when comparing the two efficiencies for the emanation chambers alone. This discrepancy is due to the increased capture time of polonium-214. The polonium-214 has a higher probability of being attracted to the photodiode due to the longer decay time that is needed to produce polonium-214. The polonium-214 parent nuclei are charged and thus also attracted to the diode increasing the chances that the polonium-214 when produced will decay on the diode and be detected. This effect is not as prevalent in polonium-218 as it is produced directly by radon-222 and has a short half-life lowering the chances that it will have been collected at the diode.

One important aspect of the emanation system is the removal and purging of all ambient radon gas that is introduced when a new sample is tested from room air exposure. Due to the purging process a parameter that varies from detector run to detector run is the pressure of the emanation system[8]. Because the radon is collected through the collection of charged ions, it is expected that the efficiency is dependent on the ion mobility. Since ion mobility is directly related to pressure, it is important to study the effect that pressure has on the detection efficiency of radon through both the polonium-214 and 218 decay channels. This was done by using the radon source, in which the emanation system was evacuated to $\sim$200 mBar and nitrogen flushed through the radon source until a pressure of $\sim$400 mBar was reached. From this pressure an incremental increase of nitrogen pressure of $\sim$100 mBar was performed until

[8]The purging process consists of evacuating the emanation chamber to $<$0.5 mBar and refilling with nitrogen gas. This is performed three times to remove nearly all ambient radon.

the normal operating pressure of ∼850 mBar was reached. The results for the pressure dependence of the efficiency for both the polonium-214 and polonium-218 decay channels can be seen in figure 4.28. The source activity was 930 Bq in calibration run 988 which ran for ∼10 days. The fit equation used is shown in equation 4.20:

$$\epsilon(\mathrm{p}) = \epsilon_0 + \mathrm{P}_0(\mathrm{p} - \mathrm{p}_{\mathrm{default}}); \tag{4.20}$$

where P_0 is a fit determined geometric correction factor, p is the operating pressure, $\mathrm{p}_{\mathrm{default}}$ is fixed at the default operating pressure of 850 mBar, ϵ_0 is the default operating efficiency.

The pressure of the emanation chamber is continually monitored during the detector run-time. This allows the efficiency of each detector run to be determined through the resulting parameters of the fit determined from figure 4.28. Simply applying the operational pressure of the emanation system to equation 4.20 using the fit determined parameters P_0 and P_1, the detector efficiency can be determined for a wide range of pressures. In the data of figure 4.28 the efficiency increases with decreasing pressure. An optimal running pressure of around 450 mBar to maximize detection efficiency can be used, however it was found that operating the emanation system much lower than atmospheric pressure results in increased wear on the diaphragm pump circulating air between the emanation chamber and sample holding tank. This increased wear can cause the diaphragm to rupture and introduce a leak. The effects of a diaphragm rupture has been shown in section 4.2.4[9]. The default operating pressure therefore was chosen to be 850 mBar.

[9]The run analyzed here was a monitored leak caused by a ruptured/leaking diaphragm in the circulation pump, where the introduced leak produces a signal consistent with emanation.

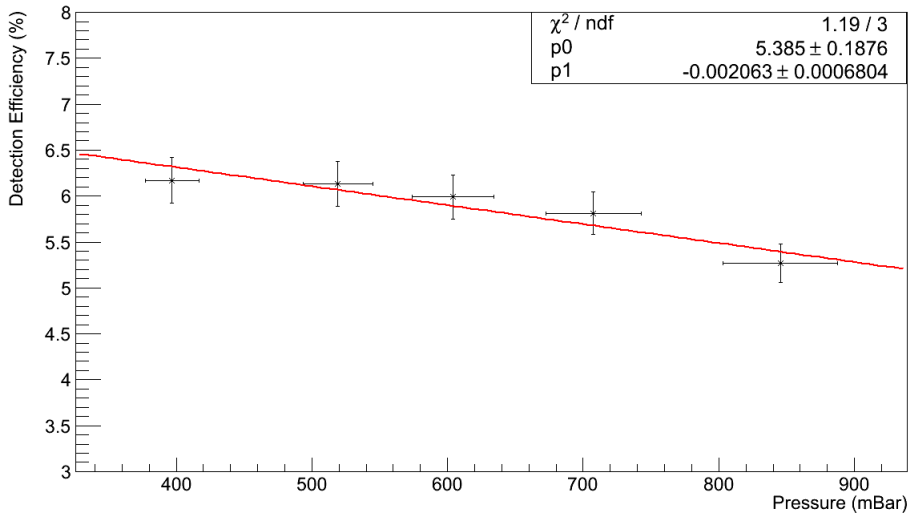

(a) Efficiency as a function of system pressure for the polonium-214 decay channel.

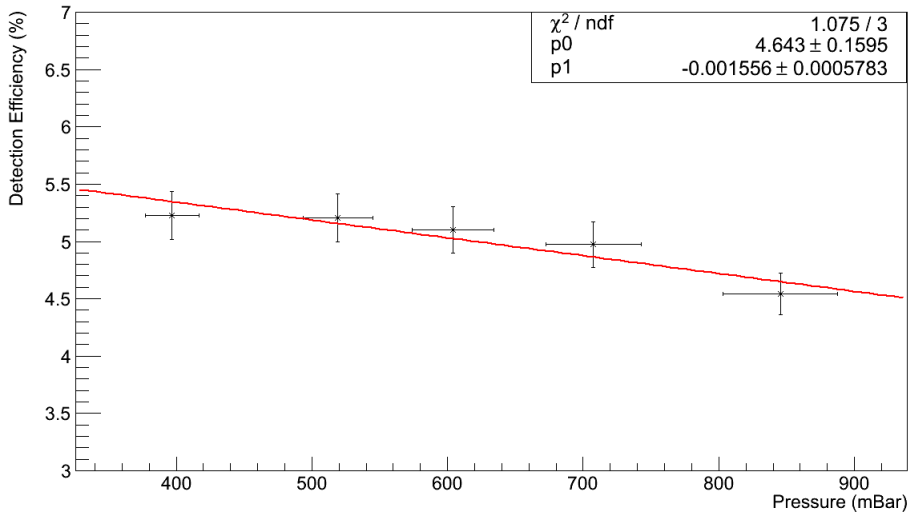

(b) Efficiency as a function of system pressure for the polonium 218 decay channel.

Figure 4.28: Efficiency of detecting radon-222 from the polonium-214 and 218 decay channels with the vacuum tank system.

Efficiency of the Beam-Pipe System

Since the efficiency is intrinsic to the emanation system volume/design and associated operating pressure, the efficiency of the beam-pipe system needs to

be determined in addition to the vacuum holding tank system. The pressure dependence of the efficiency for the beam-pipe emanation system for both the polonium-218 and polonium-214 decay channel are shown in figure 4.29. The efficiencies were determined using the same approach as the vacuum tank system. The beam-pipe system underwent the purging process to ∼200 mBar and the source was flushed into the system with nitrogen until a pressure of ∼400 mBar was reached and incrementally increased up to the normal operating pressure of ∼850 mBar. The source activity was 930 Bq in calibration run 1117 which ran for ∼12 days. The fit equation used is equation 4.20.

The beam-pipe system has a volume that is approximately $\frac{1}{10}$ the volume of the vacuum tank. The volume difference results in a larger fraction of the total detector volume being sampled. Due to this volume difference, it is expected that the detection efficiency is larger by approximately a factor of two for the beam-pipe system than for the vacuum tank system. This can easily be seen in figure 4.30.

The difference in efficiency can be understood as the difference in a dilution factors between the two systems. The dilution factor represents the decrease in radon concentration in the emanation system caused by the volume increase from the addition of the sample holding tanks. The dilution factor for the detection systems is as follows:

$$\mathrm{F_{Dilution}} = \frac{\mathrm{V_{Chamber}}}{\mathrm{V_{Chamber}} + \mathrm{V_{SampleTank}}} \tag{4.21}$$

The dilution factor can therefore be used to determine the relative efficiency of the detection system based on the additional volumes added to the emanation systems. The efficiency for the emanation chamber without the additional sample holding tanks can then be calculate from the volume differences. Both systems can be used to check for a consistent efficiency of the emanation chamber based on the experimentally determined efficiencies.

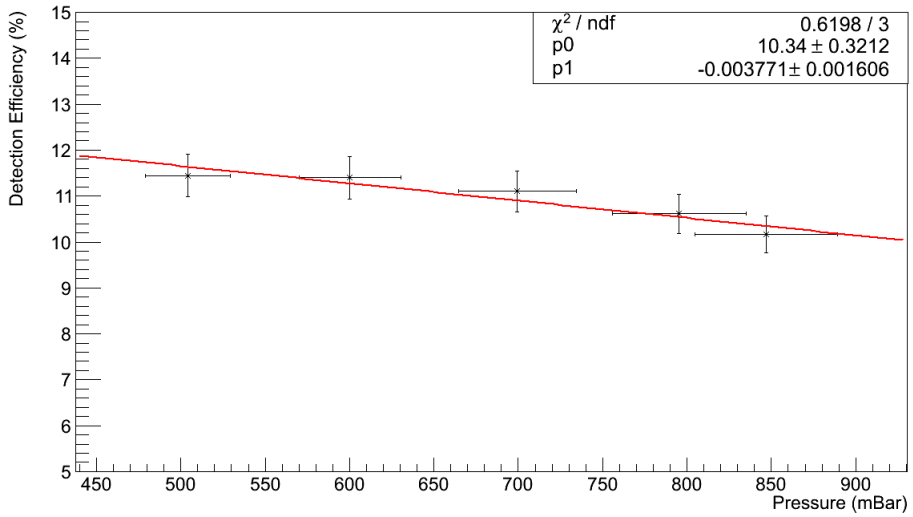

(a) Efficiency as a function of system pressure for the polonium 214 decay channel.

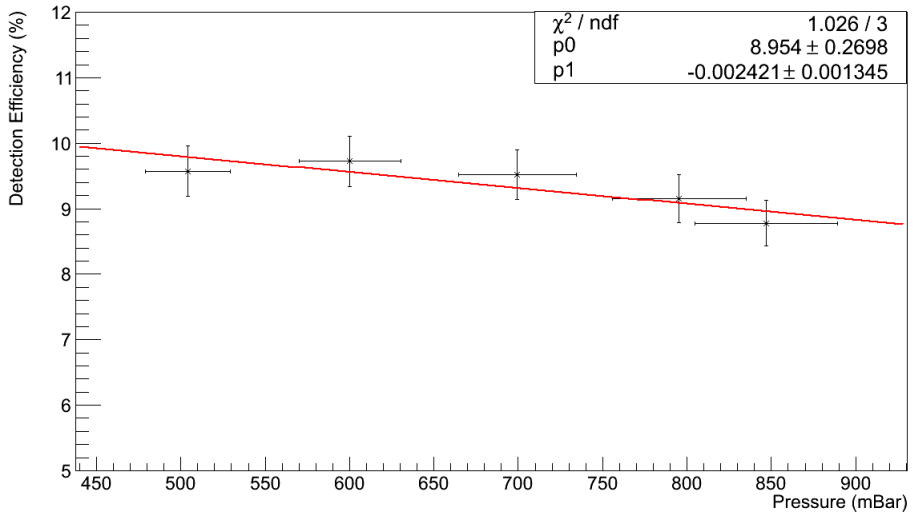

(b) Efficiency as a function of system pressure for the polonium 218 decay channel.

Figure 4.29: Efficiency of detecting radon-222 from the polonium-214 and 218 decay channels with the beam-pipe system. The source activity was 930 Bq.

This can be accomplished using:

$$\epsilon_{\text{System}} = \text{F}_{\text{Dilution}} \cdot \epsilon_{\text{Chamber}} \tag{4.22}$$

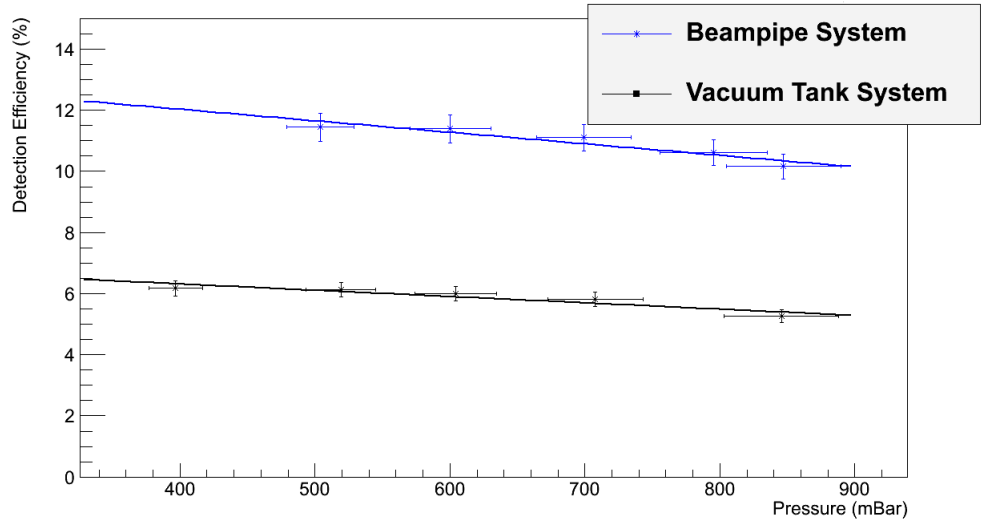

(a) Polonium 214 decay channel.

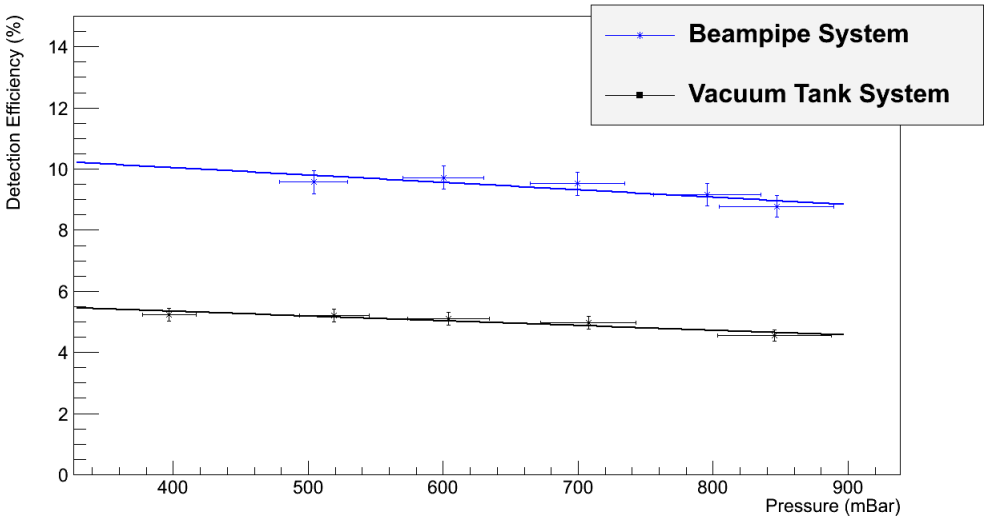

(b) Polonium 218 decay channel.

Figure 4.30: Efficiency of the two emanation systems as a function of system pressure.

and with equation 4.22 we get for the chamber efficiency:

$$\epsilon_{\text{Chamber}} = \frac{(\text{V}_{\text{Chamber}} + \text{V}_{\text{SampleTank}})}{\text{V}_{\text{Chamber}}} \cdot \epsilon_{\text{System}} \tag{4.23}$$

From equation 4.23 the efficiency for the emanation chamber without the holding tanks can be found from both the beam-pipe and vacuum tank systems. The efficiencies for each system are calculated using equation 4.20 and the corresponding operational pressure and fit parameters. The efficiency calculated for the emanation chamber using the vacuum tank system efficiency of (5.38 $\pm$ 0.21)% at normal operating conditions(850 mBar) was found to be (12.09 $\pm$ 0.82)%. Using the same approach with the beam-pipe system a value of (11.78 $\pm$ 1.08)% was found. For comparison a value of (12.96 $\pm$ 0.22)% was calculated for the emanation chamber separately at normal operating conditions. This shows that all modes of operation produce consistent efficiency values[10]. In addition, representing the efficiencies of the two systems as the same calibration factor that is defined by Super-K as equation 3.1, a calibration factor of (5.94 $\pm$ 0.24) cpd/(mBq/m^3) for the vacuum tank system and a calibration factor of (11.48 $\pm$ 0.46) cpd/(mBq/m^3) for the beam-pipe system can be obtained for the polonium-214 decay channel.

4.2.7 Detector Sensitivity

The detector sensitivity is an important parameter that can be obtained for the emanation system. The sensitivity represents the lowest limit at which the emanation system can differentiate a sample signal from a background signal. The sensitivity is proportional to the background activity of the detector. That is, a larger background activity will introduce larger statistical fluctuations in the background and therefore the sensitivity will become worse. The background fluctuations determine at which point an emanation signal can be attributed to sample emanation. This introduces the limit for the lowest radon emanation rate that can determined for the emanation system.

The emanation system underwent upgrades in which the background activ-

[10]All efficiency values presented are through the polonium-214 decay channel which presents the clearest radon signal.

ity of the system was lowered through material selection and extensive cleaning which was covered in section 4.2.5. This caused a decrease in the background activity by a factor of over 3. As a result an improvement in the detector sensitivity is also achieved. The background activity before and after the improvements are shown in figure 4.31.

The sensitivity of the emanation system is obtained statistically through the background fit results. By taking a one standard deviation limit of the background, the sensitivity can be found. The sensitivity limit ensures that an activity above this limit can be differentiated from the background signal. The emanation system before the upgrade had a sensitivity limit of 11 ± 5 radons/hr. With the improvements to the emanation system discussed in section 4.2.5 the sensitivity was lowered by a factor of approximately 3 to 4 ± 2 radons/hr. Although work on reducing the background activity is still needed, this shows that the cleaning and material selection have had a significant influence on the detector sensitivity. Further reduction through a rigorous material selection is necessary to achieve the high sensitivity desired for the detector.

4.2.8 Radon Emanation Analysis

With the efficiency and the background activity of the emanation systems determined it is possible to extract radon emanation rates from sample runs. The emanation rates can be extracted from the polonium-214 channel and represent the clearest signal for measuring radon emanation from samples. In addition to the polonium-214 channel, the polonium-218 channel can be used to extract radon emanation rates as a consistency check for the polonium-214 decay channel. The polonium-218 channel however contains bismuth-212 contamination and requires an additional method for signal separation. This section will cover the analysis techniques used to extract measured radon emanation rates from the data using both signal decay channels making use of the experimentally measured detection efficiency and background activity.

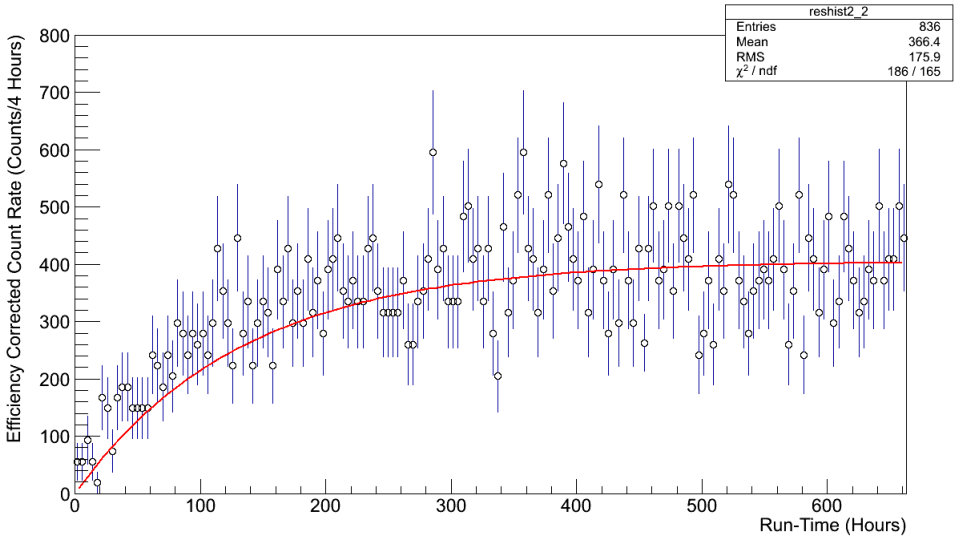

(a) Background pre-cleaning and material screening.

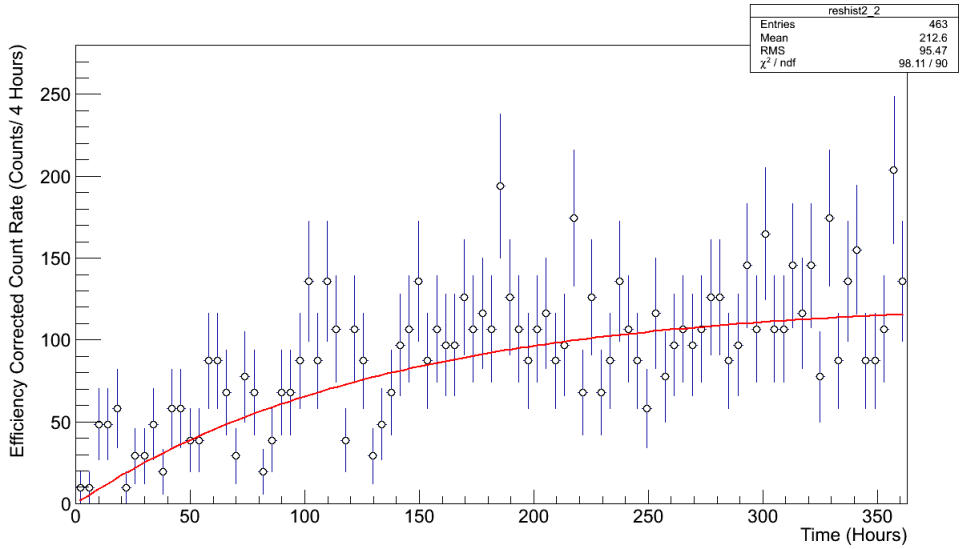

(b) Background post-cleaning and material screening.

Figure 4.31: Comparison of background activity before and after the detector was cleaned and the internal materials were screened for strong radon emitters. Plots show a background run before and after this process. Rates are efficiency corrected so a direct comparison can be seen.

The analysis that is shown below is performed on a sample run consisting of one 100' 18 gauge 4-conduit electronics cable and one 100' 18 gauge 2-conduit

electronics cable. These cables were a candidate for use in the University of Alberta's radon clean-room. The radon emanation from the cables is above the limits set for the radon clean-room. This high radon emanation makes it a prime sample in which to show a sample analysis because it is well above the background activity of the detector discussed in section 4.2.4 and produces a clear radon emanation signal.

Emanation Analysis Using Polonium-214 Decay Channel

The analysis of radon emanation using the polonium-214 decay channel uses the emanation equation shown in equation 4.10. This equation represents the behavior of radon activity within the emanation system assuming that the emanation system is free of all ambient radon and leaks after the nitrogen purge process.

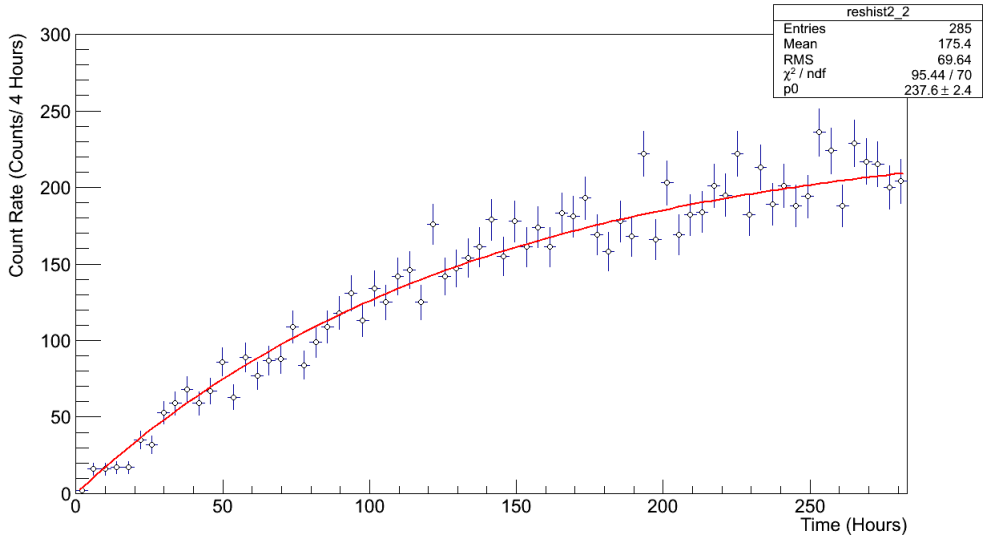

Figure 4.32: Emanation run 975 tested a 100' 18 gauge 4-conduit cable and a 100' 18 gauge 2-conduit cable candidates for the radon clean-room. The sample shows high levels of radon emanation making it a poor choice for the clean-room. Fit shown corresponds to equation 4.10.

A χ^2 fit is performed to the time evolution of the detected radon activity

using the emanation equation. The equation used is as follows:

$$A_{Rn}(t) = P_0(1 - \exp(-P_1 t)) \tag{4.24}$$

Parameter P_0 was permitted to vary. The one parameter fit determines the radon emanation rate. It was chosen to fix parameter P_1, the decay constant λ_{Rn} as this parameter is well measured and allows a constraint to be applied to the fit[2]. From this fit the emanation rate is extracted and the efficiency correction is applied to the emanation rate. This results in the corrected emanation rate as:

$$E_{Corrected} = E_{Extracted} \cdot \epsilon_{Efficiency} \tag{4.25}$$

Once the extracted emanation rate is corrected for the efficiency loss, the background activity of the emanation system must be removed because the corrected emanation rate represents the emanation rate of the sample and emanation rate of the detector. More specifically, the extracted emanation rate once efficiency corrected represent:

$$E_{Corrected} = E_{Sample} + E_{Background} \tag{4.26}$$

The processes which produce both sample emanation and detector background emanation are the same. This means that a subtraction of the background emanation rate measured for the detector results in the emanation rate of the sample. The measurement of radon emanation from a sample however is not a good value to report as it is represents the emanation rate of the sample based on the geometry of the sample. The emanation rate can be better presented by adjusting the sample emanation rate in units of the surface area of the sample whenever possible. This is relevant for a sample in which the radon is emitted from a very thin layer of surface area of the sample. All radon below a thin layer on the surface is trapped within the material and cannot escape.

The measurement of radon emanation rates are then best presented as:

$$E_{Rn} = E_{Sample}/A_{Sample} \tag{4.27}$$

where A_{Sample} is the surface area of the tested sample.

By presenting radon emanation rates in this form, the measured rates can be extrapolated to estimate radon emanation rates from sample with other geometries[11]. This is very important as it allows a selection of materials which only emanate low levels of radon, and materials from the same manufacturer with low radon emanation can be used to construct low background detectors. In addition an estimate on a detectors radon emanation background can be obtained by extrapolating the radon emanation rates based on the surface area of the materials used.

Emanation Analysis Using Polonium-218 Decay Channel

Using the methods described in section 4.2.8 a consistency check for the radon emanation can be obtained from the polonium-218 decay channel. This channel requires the effects of the bismuth-212 decay contributions present in the polonium-218 channel to be removed. This is accomplished by applying the separation analysis method discussed in section 4.2.4 which obtained a proportionality constant relating the bismuth-212 and polonium-212 events. Using this ratio it is possible to estimate the bismuth-212 signal within the polonium-218 channel.

Equation 4.16 represents the behavior of the bismuth-212 and polonium-212 decays. Using this equation and fitting to the polonium-212 decays obtains the radon-220 emanation curve. For the sample tested, a χ^2 fit is performed and the fit results to the polonium-212 data can be seen in figure 4.33. Because

[11] These rates are only estimates as the emanation rate is characteristic of many variables such as type of material, the manufacturer who made the sample, etc.

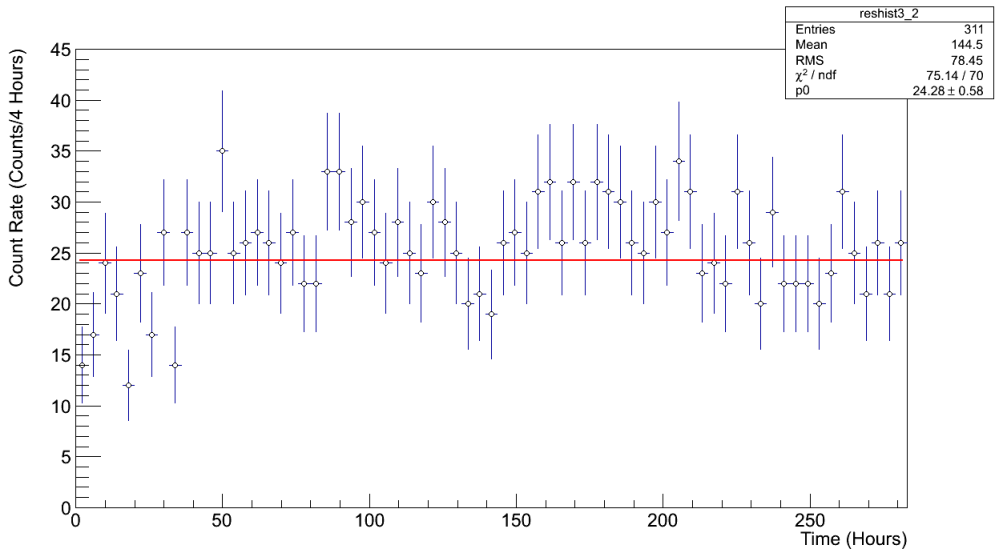

Figure 4.33: Emanation run 975 tested a 100' 18 gauge 4-conduit cable and a 100' 18 gauge 2-conduit cable candidates for the radon clean-room. Fit to the polonium-212 rates using equation 4.16. Data rebinned to 4 hour bins.

this equation applies to both polonium-212 and bismuth-212 it can be rescaled using the proportionality constant obtained from section 4.2.4. This method constrains the expected bismuth-212 evolution in the polonium-218 signal region and can be applied alongside the radon-222 emanation curve to obtain a radon-222 emanation rate. The equation representing the new fitting function is shown in 4.17 in section 4.2.4.

A χ^2 fit is applied to the time evolution of the polonium-218 decay channel for the same sample that was shown in section 4.2.8 using equation 4.17. This can be seen in figure 4.34: From the fit value for the emanation rate for radon-222 using the polonium-218 channel the emanation rate can be found. With the emanation rate found, the methods used in section 4.2.8 can be applied and the corrected radon emanation rate using the polonium 218 decay channel can be determined. The value found is consistent with the radon-222 emanation rate determined through the polonium-214 decay channel and this will be shown in the following chapter.

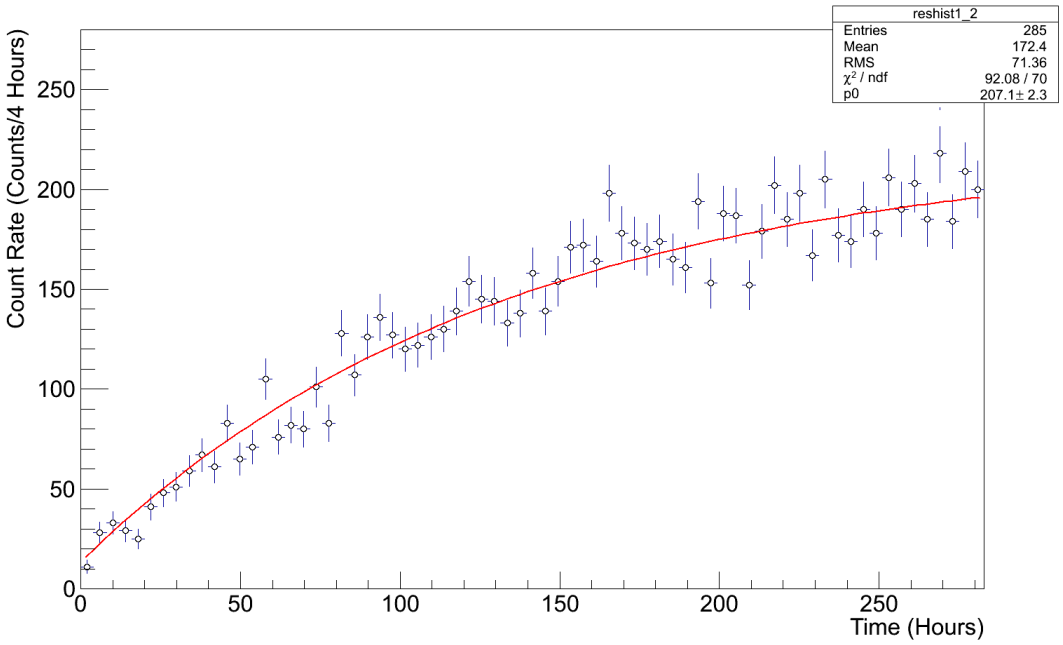

Figure 4.34: Emanation run 975 tested a 100' 18 gauge 4-conduit cable and a 100' 18 gauge 2-conduit cable candidates for the radon clean-room. The sample shows high levels of radon emanation making it a poor choice for the clean-room. Fit shown corresponds to equation 4.17.

Chapter 5

Analyzed Run and List of Emanated Samples

This chapter will present a fully analyzed run using the techniques discussed in chapter 4 and the sample preparation procedure. In addition, the tabulated results from the analysis of a variety of tested samples will be given. The complete analysis will be shown for a sample of electronics cabling that was selected for use in the University of Alberta radon clean-room. This sample was selected due to a clear radon emanation signal. The results of this analysis and there implications with the clean-room will be briefly discussed.

5.1 Analyzed Run

The run analyzed corresponds to run 975 which operated for ∼285 hours. This emanation run consists of one grey 2-conduit and one grey 4-conduit 18 gauge 100' electronic cables that were tested for use in the clean-room. The cabling was found to emanate radon strongly making it a poor choice for use in the radon clean-room. The vacuum emanation system was used in the testing of these cables. The samples were placed within the vacuum sample holding tank and the emanation system underwent the purging process discussed in section

4.2.

5.1.1 Sample Preparation and Setup

The preparation of a test sample is an important procedure for radon emanation measurements. As samples are exposed to radon contaminated air, dust and small particulates can accumulate on the surface of the sample. The contamination from the dust/particulates can cause an increase in the measured radon emanation rates. In order to minimize any effects caused by dust contamination, all samples are cleaned thoroughly with an ethanol wipe procedure. The sample above is cleaned by performing an ethanol wipe consisting of a thorough cleaning using latex gloves and lint free wipes with ethanol to remove dust and any other surface contaminates.

The clean sample is placed in the vacuum holding tank. All ambient radon introduced from opening the emanation system is removed using a rotary vacuum pump and the nitrogen purging process begins. The full purging process involves the evacuation and refilling of the emanation system through three purging cycles. Each purge cycle includes a $\sim$2 hour evacuation period that drops the emanation chamber pressure from atmospheric pressure[1] to less than 1mBar. After the two hour period the emanation system's pressure is increased by injecting nitrogen gas up to a pressure betwen 600-700 mBar. The nitrogen gas is added because it acts as a transport medium for the removal of any remaining radon during the next purging cycle. Once the purging is completed, the emanation system is filled with nitrogen up to the operational pressure of approximately 850mBar. At this pressure the emanation system begins taking data.

[1]The ambient atmospheric pressure within the lab is $\sim$939mBar.

5.1.2 Sample Analysis

The calibrated spectrum of the electronic cables is shown in figure 5.1. From the spectrum it is easy to see that the sample produces a strong radon signal that is higher than the background from the emanation system. From the spectrum, it

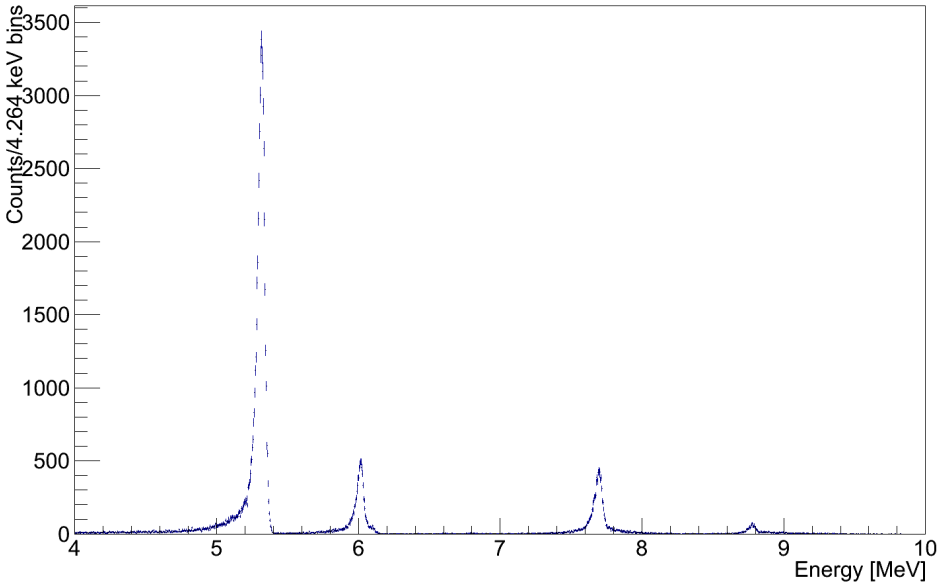

Figure 5.1: Calibrated spectrum for run 975. This run sampled two grey electronic cables that were proposed for use in the radon clean-room. The spectrum contains ∼285 hours of detector data.

can be estimated that this sample is a strong source of radon emanation. This makes it a poor choice for use in a radon free environment. This however does not provide any additional information in terms of a quantitative value for the radon emanation rate. To obtain a quantitative value for the radon emanation rate the radon emanation rate has to be determined.

As described in section 4.2.4, the clearest radon signal is found from the polonium-214 decay signal. This decay channel is therefore the primary choice used to determine the radon emanation rates from the sample. The radon emanation signal from the sample can be seen in figure 5.2.

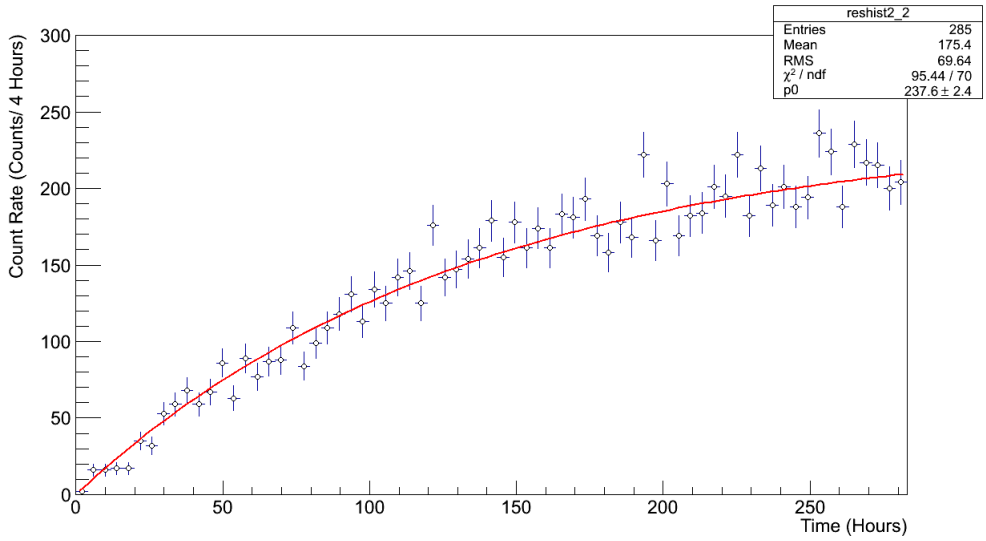

Figure 5.2: The evolution of the radon activity detected through the polonium 214 decay channel.

The fit shown in figure 5.2 is equation 4.10 from section 4.2.3. The fit applies a one parameter fit with a fixed decay constant λ_{Rn} at a value of 0.007553 hr^{-1}[2]. The value determined through the fit is the radon emanation rate (P_0). From the above fit results the radon emanation rate using the polonium-214 decay channel was found to be (59 ± 1) radons/hr.

The value determine above directly reflects what is detected by the emanation system. It was shown in section 4.2.6 that the emanation system does not have a 100% detection efficiency. As a result, the emanation rate must be corrected for the efficiency loss of the emanation system. In addition, it was found that the emanation system efficiency is strongly affected by pressure and thus the efficiency must be determined for the operating pressure of this run. The pressure for the run was recorded manually over its duration[2] and was stable at (874 ± 44) mBar. Applying the pressure correction discussed in section 4.2.6 for the vacuum tank system, the detector efficiency can be determined.

[2]The pressure monitoring system had not been installed at this time.

The detector efficiency for this run was determined as (5.33±0.21)%.

The efficiency correction can be applied to the radon emanation rate extracted above. After applying the efficiency correction an emanation rate of (1113 ± 45) radons/hr is found. This value corresponds to the total radon emanation within the emanation system volume. This value then reflects radon emanation of the cables sample in addition to the radon emanation background of the emanation system. The contribution from the background can be removed by applying a background subtraction to the measured value of the total radon emanation for the run. The background activity of the emanation system using the polonium-214 decay channel was determined in section 4.2.4. The background activity for the vacuum tank system was (101±11) radons/hr. After background subtraction the samples emanation rate was measured to be (1012 ± 46) radons/hr through the polonium-214 channel.

The emanation rate is also calculated for the polonium-218 channel. This channel is used as a consistency check for the polonium-214 and because it follows a similar analysis only its result will be reported. The fit used to determine the radon emanation rate can be seen in figure 5.3 and follows equation 4.17. Through the polonium-218 channel a radon emanation rate of (1005 ± 41) radons/hr was extracted. This value is consistent with the value reported through the polonium-214 channel. From this it is evident that the radon emanation rate from the electronic cables are high. Since these cables are a source of radon emanation they were discarded for the construction of the clean room.

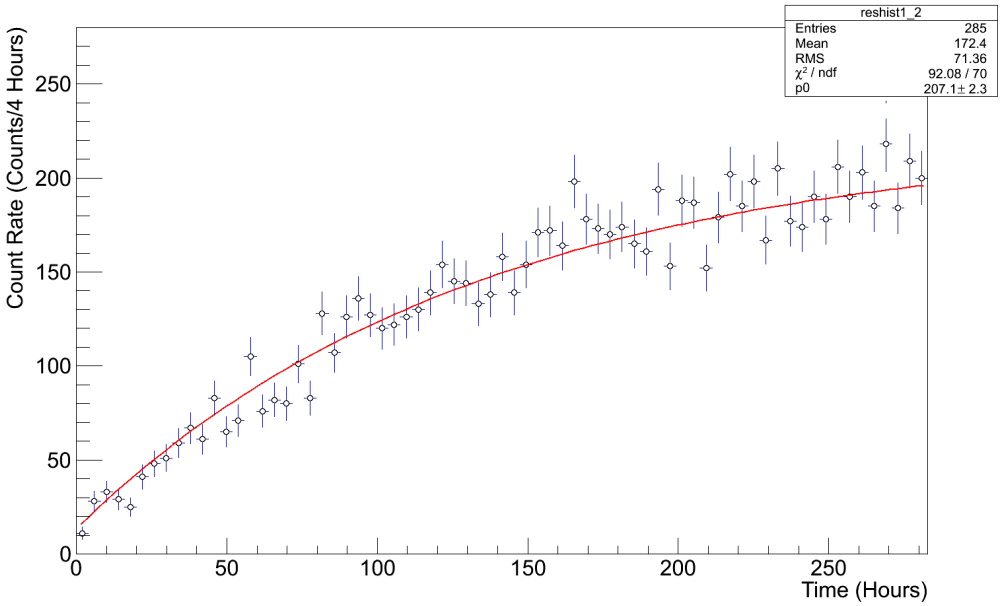

Figure 5.3: The evolution of the radon activity detected through the polonium-218 decay channel.

5.2 Results of Analysis of Samples

This section reports on the various samples tested within the emanation system. The tabulated results from various samples are shown below is table 6.2 and a short assessment of each sample will be give. For reference, the desired total radon emanation tolerance within the radon clean-room is 16920 radons/hr[35].

The results extracted from run 1031 show high levels of radon emanation for these components. The level of emanation from the components is too high for use in the radon clean-room. The sample consists of multiple components and as a result of the high radon emanation levels, these components must be individually tested to determine whether the source of the radon emanation is a single component or distributed evenly between the components. Further testing will determine whether a single component or all components are sources of the radon emanation and which can be used for the clean-room.

Run 1073 results show radon emanation from an electronics cable that is too

high for the radon clean-room. These results imply that the cables analyzed in section 5.1 which have an emanation rate of (1012 $\pm$ 46) radons/hr should be chosen over this sample. A cable of the sample tested in run 1073 of equivalent length to the sample tested in section 5.1 produces radon emanation that is above the two cable sample and as a result this cable was discarded.

The gasket sample of run 1082 has radon emanation comparable to the backgrounds within the emanation system. This sample shows low levels of radon emanation and is a good choice for the radon clean-room. The emanation from this sample is not negligible however it will not greatly influence the radon level within the clean-room in comparison to total desired radon emanation tolerance for the radon clean-room.

The radon emanation rate extracted from run 1130 shows that the majority of the radon emanation of the components tested in run 1031 is from the black mats. As a result the aluminium wheels tested in this sample can be used in the clean-room. The radon emanation from the wheels is low but not negligible, however the quantity of these wheels within the clean-room is low (4 wheels for 1 toolbox) and as a result they will not significantly influence the radon levels.

The sample from run 1381 has low radon emanation, however this sample was tested and was to be used for the background reduction of the emanation system. The sample shows radon emanation that is above the level of the radon background of the emanation system. This makes the sample a poor choice in lowering the background of the detector. As a result a more suitable material must be found for the emanation system in order to lower the background to the desired level.

For the larger list of emanated samples refer to the appendix.

Table 5.1: Report on the various samples tested and the resulting emanation rates and additional information regard the tested samples. All results are obtained through the polonium-214 decay channel.

Run Number	Emanation System	Background Rate (Radons/hr)	Corrected Emanation Rate (Radons/hr)	Adjusted Emanation Rate	Sample Description
1031-1047	Vacuum Tank System	101 ± 11	1112 ± 68	N/A	4 aluminum and plastic toolbox wheels and 5 black mats.
1073-1082	Vacuum Tank System	101 ± 11	248 ± 21	37 ± 3 (Radons/hr/m)	20' black 6P6C cable.
1082-1096	Vacuum Tank System	101 ± 11	143 ± 14	17 ± 2 (Radons/hr/m)	Gasket for clean-room door.
1130-1137	Vacuum Tank System	101 ± 11	226 ± 19	N/A	4 aluminum and plastic toolbox wheels.
1381-1404	Emanation Chamber Only	29 ± 4	43 ± 7	1141 ± 169 (Radons/hr/m^2)	Testing brown viton o-ring material.

Chapter 6

Conclusion

A high sensitivity radon emanation detector is currently in operation at the University of Alberta . The detector uses the method of electrostatic attraction to collect radon daughters onto a single photo-diode contained within a large stainless steel vessel. A +5 kV potential is applied to the stainless steel vessel to produce the electrostatic collection field. The data acquisition system and the analysis software were custom developed for this project and were shown to be stable. The main system was measured to have an efficiency of 5.4% at 850 mBar. The detectors absolute pressure was shown to decrease the efficiency by 2.1x10^{-3}%/mBar for increasing pressures. The detector sensitivity was improved by reducing the background activity of the emanation systems. The intrinsic background activity within the detector was reduced by a factor of larger than 3. With the reduced background levels, a senstivity of $\sim(4 \pm 2)$ radons/hr at 68% confidence was achieved. This was accomplished through passivation of the stainless steel walls along with careful cleaning of all parts to remove possible sources of radon such as dust within the emanation system. Measurements of multiple samples used in the SNO+ experiment, University of Alberta clean room, and various other smaller experiments were conducted and reported.

Further study of this detector is required as certain effects have not been

studied. The effects include possible pumping speed variations of the circulation pump. In addition a full Monte Carlo simulation of this detector would be of further benefit to verify the efficiency determined for the polonium channels. This detector can also be improved further with a carefully designed vessel which minimizes drift field dead spots similar to what was done in the SNO ESC[19]. In closing, the current radon emanation system is well understood, in full operation and producing radon emanation measurements.

Appendix

Labview Software Setup

In this section a detailed explanation of the software setup required to operate the emanation system is provided along with a description of the software required. It will outline a detailed step by step procedure which will allow interfacing the emanation system with any Windows based computer. The computer must have a Windows operating system installed, however only Windows XP and Windows 7 have been tested.

Required Software and Setup

To interface a computer with the emanation system Microsoft Visual Studio C++ must be installed. It can be downloaded and installed from:
http://www.microsoft.com/visualstudio/en-us/products
There is no specification on which to use. The free version is adequate for its purpose. Microsoft Visual Studio C++ will be used to open/modify/build the custom C++ library that is used to interface Labview with ROOT.

The ROOT library is required and can be found at:
http://root.cern.ch/drupal/content/downloading-root
The binary verson for windows operating systems must be used. ROOT must be installed directly in C:/ drive or some modification to the Labview to ROOT library are required. A procedure on what modifications are necessary will be

discussed below.

The emanation system uses a custom 8 channel MCA which interfaces with the computer through a USB connection. It uses the QuickUSB libraries that must be installed. They can be found at:
www.quickusb.com
Follow the installation prompt is all thats required.

The emanation system DAQ is written in Labview which must be installed. Labview can be downloaded from:
www.ni.com/labview/
The latest version of Labview Development should be chosen. Labview requires a license key that must be obtained. When installation is complete it will ask for links to Labview drivers, this can be skipped. They will be installed afterward. With Labview installed, the required drivers are needed. The Labview driver can be found at:
http://www.ni.com/drivers/
Download and install the latest versions of both the NI-488.2 and NI-VISA.

With Labview installed a complete copy of the emanation system DAQ software must be installed. The complete software includes the Labview code in addition to the custom c++ library. The two folders needed are called *Labview* and *labview_root_project*. To install the DAQ software copy these folders into *DocumentandSettings/Users/Username* folder. This location will be required below so take note of this path. With the DAQ software installed open visual c++ and open the project for the *labview_to_root* software. If ROOT was not installed directly into C:/ drive, then some modifications are necessary. You must right click *Solution* in the *SolutionExplorer* and set the paths that point to ROOT, to the location where ROOT was installed. There are two instances where they must be changed, they are located under the General tab and Linker tab. If ROOT was installed directly into C:/ drive then no changes are required. With the correct paths a solution must be built

in Visual Studios C++. This will build the Labview.dll library that is used by Labview to save data into the ROOT file format. The solution must be built on the computer you run the DAQ software on or potential problems can occur.

Once the above is completed, the Labview DAQ can be opened. The main Labview file is *Radon_DAQ.vi* that must be opened. A prompt may ask for the the location of the Labview.dll file built from visual studios C++. This can be found in the labview_root_project under the debug or release folder. With this the data acquisition software is setup and data can be taken.

Software Modification

If modifications to the software are made, there is one instance where ROOT CINT must be called to recompile certain files. If any changes are made to the visual c++ files in *labview_root_project* such as adding addition information to the ROOT files, ROOT CINT must be called. To do this, a command prompt must be opened to the *src* folder in *labview_root_project*. From here ROOT CINT can be called with the command line code below:

rootcint -f MCA_DATADict.cxx -c MCA_DATA.h MCA_DATA.cpp
MCA_DATALinkDef.h

Once this command has been used, the Labview.dll must be rebuilt in Visual C++ and the changes to the files will take affect.

Operation of time_analysis Code

The time_analysis code analyzes all three run type discussed in section 4.2. The analysis code can be called with the following command line in linux:

./time_analysis -r # -c # -d # -e # -k # -s # -t # -a # -f #

Below is a description of the nine arguments above represented by # and what they do.

-r #

This option is used to specify the run number in which to start the analysis on. It is used to find the first file with the corresponding run number given. The run number of the data files increment daily and this is used for file tracking

-c #

This option is used to specify which detectors data you will be analyzing. Channel 0 or -c 0 represents the MCA input for channel 0 (typically tunnel detector), and channel 2 is the channel which has the emanation chamber data. So -c 2 represents the emanation chamber data. Default is -1, which means a channel must be chosen

-t #

This option specifies what binning time you want to analyze at in minutes. So for binning times of 30 minutes the argument would be -t 30. The default is set to 60 (hourly) minutes,-t 60.

-d #

This specifies how many days you would like to analyse. In the case that a detector run is longer then a day this is used to combine the additional files. time_analysis will output the files that are combined together in the terminal window. Default is -d 1

-s #

This argument has two options, it must be 0 or 1. In the first case that 0 is chosen, then the run being analyzed is not a calibration run, thus it skips certain analysis that only involves calibration runs with known source activity. If 1 is chosen, then the run is assumed to be a calibration run and all calibration analysis is completed. The default is 0. Note: Calibration runs can still be run with -s 0, if it has already been processed with -s 1 argument previously.

-f #

This argument is similar to the -s 0 argument, however you instead specify what calibration data you want to use on the current data set with the calibration data run number. So for example you want to analyze run 670 and the closest calibration data is from run 660, but want to use calibration data from 580, then you must include -f 580 in the command line, otherwise the calibration data from run 660 will be used.

-a #

Used to reconstruct Alpha Aria counter data. If this option is chosen the analysis will be run on the Alpha Aria data, which is the alpha counter. Default is 0(Off)

-e #

This runs the emanation analysis on the data, this will run with the tunnel data however it is a meaningless analysis for the tunnel data and should only be used on the emanation chamber data(channel 2) and will calculate emanation rates and will require an input for the surface area of the sample.

-k 2,1,0,-1

This argument incorporates background subtraction from data as well as background calculations. If nothing is chosen the default is -1. This will look up background values from previous runs and apply background subtraction to the current data. If 0 is chosen, then all backgrounds are ignored, that is no background subtraction to the current data. The only time to choose -k 1 is when the data being analyzed is a background run. This will run through background calculations(it assumes the data is a background run) on the data and fits the rates to determine background rates and stores the results in three possible root files depending on the detector for use by other runs. If k is set as 2, you will be asked to speicify which background data to use, that is it will not look at the nearest background run but rather at the run you specify.

Commandline Examples

./time_analysis -r 780 -c 2 -d 4 -s 1

This will look at run 780 for the emanation chamber(channel 2) and will combine 4 data files, the data file for run 780 and the next 3 days of data. The run is specified as a source(-s 1) run so the calibration analysis will be conducted on the data.

./time_analysis -r 780 -c 2 -d 4 -e 1 (-k 0)

This will look at run 780 for the emanation chamber(channel 2) and will combine 4 data files, the data file for run 780 and the next 3 days of data files. It will also preform the emanation analysis with background subtraction incorporated. If the -k 0 argument is included then background subtraction is skipped.

./time_analysis -r 780 -c 2 -d 4 -k 1

This will look at run 780 for the emanation chamber(channel 2) and will combine 4 data files, the data file for run 780 and the next 3 days of data files. It will also preform background analysis calculations. NOTE: Background analysis and emanation analysis cannot be run simultaneously, either the run is an emanation run or it is a background run.

Sample Emanation Results

Below is a list of emanated samples that were tested using the vacuum sample holding tank system. The adjusted emanation rates are only known for samples where the geometry of the samples were recorded.

Table 6.1: Extracted emanation rates for the samples tested since the connection of the vacuum tank to the emanation system. All results are obtained through the polonium-214 decay channel.

Run Number	Emanation System	Background Rate (Radons/hr)	Corrected Emanation Rate (Radons/hr)	Adjusted Emanation Rate	Sample Description
841-846	Vacuum Tank System	101 ± 11	33 ± 12	N/A	White, green and red wire samples
857-860	Vacuum Tank System	101 ± 11	282 ± 23	N/A	Duct Silencer
860-863	Vacuum Tank System	101 ± 11	395 ± 31	N/A	Mist Buster
863-865	Vacuum Tank System	101 ± 11	1465 ± 115	N/A	Grey RJ45 LED panel control cables
869-873	Vacuum Tank System	101 ± 11	21 ± 11	N/A	BX cable
873-877	Vacuum Tank System	101 ± 11	286 ± 23	N/A	Roll of blue one-sided tackbed filter
877-881	Vacuum Tank System	101 ± 11	84 ± 12	N/A	full roll of regular filter material
881-884	Vacuum Tank System	101 ± 11	64 ± 12	N/A	eggcrate sound dampener foam
887-892	Vacuum Tank System	101 ± 11	1366 ± 93	N/A	signal cable wire, 4 rolls, 18 gauge
903-907	Vacuum Tank System	101 ± 11	707 ± 59	116 ± 9 (Radons/hr/m)	6P6C telephone cables 20'
911-916	Vacuum Tank System	101 ± 11	545 ± 43	N/A	single roll of 18 gauge wire

Table 6.2: Extracted emanation rates for the samples tested since the connection of the vacuum tank to the emanation system. All results are obtained through the polonium-214 decay channel.

Run Number	Emanation System	Background Rate (Radons/hr)	Corrected Emanation Rate (Radons/hr)	Adjusted Emanation Rate	Sample Description
933-938	Vacuum Tank System	101 ± 11	59 ± 13	N/A	2 Compressed air silencers
962-975	Vacuum Tank System	101 ± 11	578 ± 43	N/A	White 6P6C cable
998-1011	Vacuum Tank System	101 ± 11	617 ± 46	18 ± 1 (Radons/hr/m)	4 conduit 18 shield 100 ft cable
1011-1020	Vacuum Tank System	101 ± 11	318 ± 24	N/A	steam humidifier
1054-1058	Vacuum Tank System	101 ± 11	8702 ± 627	N/A	SNO+ electronics cable
1096-1107	Vacuum Tank System	101 ± 11	38 ± 12	N/A	Quartz glass sample

Bibliography

[1] J. Beringer *et al.* (Particle Data Group). *Phys. Rev. D 86*, 010001, (2012).

[2] National Nuclear Data Center. Information extracted from the chart of nuclides database, 2013. URL `http://www.nndc.bnl.gov/chart/`.

[3] U.S. Environmental Protection Agency. Radon, February 2013. URL `http://www.epa.gov/radiation/radionuclides/radon.html`.

[4] Agency for Toxic Substances and Disease Registry. Toxicological Profile for Radon. May 2012. URL `http://www.atsdr.cdc.gov/toxprofiles/`.

[5] United Nations Scientific Committee on the Effects of Atomic Radiation. Sources and Effects of Ionizing Radiation. *Unscear 2000 Report to the General Assembly*, 1:111, 2000.

[6] World Health Organization. WHO Handbook on Indoor Radon - A Public Health Perspective. 2009. URL `http://www.who.int/ionizing_radiation/env/9789241547673/en/`.

[7] Samuel S. M. WongKrane. *Introductory Nuclear Physics*. "John Wiley and Sons; WILEY-VCH Verlag Gmbh and Co. KGaA. Weinheim ", second edition, 2004.

[8] Durridge Company Inc. *RAD7 Radon Detector - User Manual*. "Durridge Company", revision 7.2.2 edition, 2013.

[9] V.C. Negro and Sidney Watnick. "fungi" - a radon measuring instrument with fast response. *Nuclear Science, IEEE Transactions on*, 25(1):757–761, 1978. ISSN 0018-9499. doi: 10.1109/TNS.1978.4329405.

[10] A. Alessandrello *et al.* Measurements of internal radioactive contamination in samples of Roman lead to be used in experiments on rare events. *Nucl. Instrum. Meth. B*, 142(1-2):163–172, JUN 1998.

[11] E. Aprile et al. Design and Performance of the XENON10 Dark Matter Experiment. *Astropart.Phys.*, 34:679–698, 2011. doi: 10.1016/j.astropartphys.2011.01.006.

[12] G.J. Alner et al. First limits on WIMP nuclear recoil signals in ZEPLIN-II: A two phase xenon detector for dark matter detection. *Astropart.Phys.*, 28:287–302, 2007. doi: 10.1016/j.astropartphys.2007.06.002.

[13] E. Aprile et al. Response of the XENON100 Dark Matter Detector to Nuclear Recoils. *Phys.Rev.*, D88:012006, 2013. doi: 10.1103/PhysRevD.88.012006.

[14] X. Chen. Monte Carlo Study of Beta-Gamma Backgrounds from ^{208}Tl and ^{214}Bi. SNO-STR-96-003, JAN 1996.

[15] H.H. Chen. Direct approach to resolve the solar-neutrino problem. *Phys. Rev. Letters*, 55(14), (1985).

[16] Lino Miramonti and Vito Antonelli. Advancements in solar neutrino physics. *Int.J.Mod.Phys.*, E22:1330009, 2013. doi: 10.1142/S0218301313300099.

[17] J. Boger et al. The Sudbury neutrino observatory. *Nucl.Instrum.Meth.*, A449:172–207, 2000. doi: 10.1016/S0168-9002(99)01469-2.

[18] The Sudbury Neutrino Observatory, accessed january 2014. URL `http://www.sno.phy.queensu.ca/sno/`.

[19] Jian-Xiong Wang, Tom C. Andersen, and John J. Simpson. An electrostatic radon detector designed for water radioactivity measurements. *Nucl.Instrum.Meth.A*, 421(3):601 – 609, 1999. ISSN 0168-9002. doi: 10.1016/S0168-9002(98)01230-3.

[20] T.C. Andersen et al. Measurement of radium concentration in water with Mn coated beads at the Sudbury Neutrino Observatory. *Nucl.Instrum.Meth.*, A501:399–417, 2003. doi: 10.1016/S0168-9002(03)00616-8.

[21] R. Falk, H. More, and L. Nyblom. Calibration of rn-222 reference instrument in sweden. *National Institute Standard Technol.*, 95:115, 1990. doi: http://dx.doi.org/10.6028/jres.095.011.

[22] A.J. Howard, B.K. Johnson, and W.P. Strange. A high-sensitivity detection system for radon in air. *Nucl.Instrum.Meth.A*, 293(3):589 – 595, 1990. ISSN 0168-9002. doi: http://dx.doi.org/10.1016/0168-9002(90)90328-4.

[23] Alessandra Carlotta Re. The Borexino impact in the global analysis of neutrino data. *J.Phys.Conf.Ser.*, 375:042031, 2012. doi: 10.1088/1742-6596/375/1/042031.

[24] Kevin B. Mccarty. The borexino nylon film and the third counting test facility. *Princeton University*, PHD Thesis, 2006. URL `http://borex.lngs.infn.it/Thesis/`.

[25] G. Bellini et al. Lifetime measurements of 214Po and 212Po with the CTF liquid scintillator detector at LNGS. *Eur.Phys.J.*, A49:92, 2013. doi: 10.1140/epja/i2013-13092-9.

[26] G Alimonti et al. A large-scale low-background liquid scintillation detector: the counting test facility at gran sasso. *Nucl.Instrum.Meth.A*, 406(3):

411 – 426, 1998. ISSN 0168-9002. doi: http://dx.doi.org/10.1016/S0168-9002(98)00018-7.

[27] Lee Ka Pik. Study of the neutrino mass hierarchy with the atmospheric neutrino data observed in Super-Kamiokande. *Tokyo University*, PHD Thesis, 2012. URL `http://www-sk.icrr.u-tokyo.ac.jp/doc/sk/pub/`.

[28] Super-Kamiokade Collaboration: Y. Takeuchi et al. Measurement of radon concentrations at super-kamiokande. 1999. doi: 10.1016/S0370-2693(99)00311-1.

[29] Super-kamiokande, accessed december 2013. URL `http://www-sk.icrr.u-tokyo.ac.jp/sk/index-e.html`.

[30] Hamamatsu Photonics. Si pin photodiode - s3204/s3584 series, 2012. URL `https://www.hamamatsu.com/resources/pdf/ssd`.

[31] C. Mitsuda et al. Development of super-high sensitivity radon detector for the Super-Kamiokande detector. *Nucl.Instrum.Meth.*, A497:414–428, 2003. doi: 10.1016/S0168-9002(02)01923-X.

[32] Y Takeuchi et al. Development of high sensitivity radon detectors. *Nucl. Instrum. Methods Phys. Res., A*, 421(1-2):334–341, 1999.

[33] P. Kotrappa et al. Electret - a new tool for measuring concentrations of radon and thoron in air. *Health Phys.*, 41(35), 1981.

[34] U.S. Army Public Health Command. Radiation hazards with the use of tungsten welding rods containing thorium. URL `http://phc.amedd.army.mil/`.

[35] D. Grant et al. Low radon cleanroom at the university of alberta (presentation). *Low Radon Techniques (LRT)*, 2010. URL `www.snolab.ca/lrt2010/talks/Session6/Hallin%20LRT2010.pptx`.

[36] D. Grant et al. Low radon cleanroom at the university of alberta. *AIP Conference Proceedings*, pages 161–163, 2011. doi: 10.1063/1.3579575.

[37] National Instruments. Labview system design software, 2014. URL `http://www.ni.com/labview/`.

[38] Bitwise Systems. Quickusb, 2014. URL `http://www.bitwisesys.com/quickusb`.

[39] Brun, R. and Rademakers, F. ROOT - An Object Oriented Data Analysis Framework. *Nucl.Instrum.Meth.*, A(389):81–86, 1996.

[40] ROOT Version 5.30. see for example TTree, 2014. URL `http://root.cern.ch/root/html530/TTree.html`.

[41] Pylon Electronics Inc. Radioactive sources - datasheet, 2014. URL `http://www.pylonelectronics.com/pylonpdfs/DS123R3.pdf`.

[42] R. D. Evans. *The Atomic Nucleus*. Norton and Company, 1985.

[43] A. T. McGarry P. A. Colgan. Radon monitoring and control of radon exposure. Radiological Protection Institute of Ireland, 2012.

[44] G. F. Knoll. *Radiation Detection and Measurement*. "John Wiley and Sons", 3rd edition edition, 1999.

[45] W. R. Leo. *Techniques for Nuclear and Particle Physics Experiments - A How-to Approach*. "Springer Verlag", 2nd edition edition, 1994.

[46] ROOT Version 5.30. see for example TSpectrum, 2014. URL `http://root.cern.ch/root/html530/TSpectrum.html`.

[47] James F. Ziegler, M.D. Ziegler, and J.P. Biersack. {SRIM} the stopping and range of ions in matter (2010). *Nucl.Instrum.Meth.B*, 268(1112):1818 – 1823, 2010. ISSN 0168-583X. doi: http://dx.doi.org/10.1016/j.nimb.2010.02.091.

[48] T. Spencer. Improving Resolution for the KATRIN Detector Prototype. August 2004.

[49] L. Landau. On the energy loss of fast particles by ionization. *J.Phys.(USSR)*, 8:201–205, 1944.

[50] P.V. Vavilov. Ionization losses of high-energy heavy particles. *Sov.Phys.JETP*, 5:749–751, 1957.

[51] J.E. Moyal. Theory of ionization fluctuations. *Philosophical Magazine Series 7*, 46(374):263–280, 1955.

[52] DJ. Steck RS. Lively. Long-term Radon Concentrations Estimated from 210Po Embedded in Glass. *Health Physics*, 64(5):485–490, 1993.

[53] INFICON. Pirani Capacitance Diaphragm Gauge - PCG550 PCG552 PCG554 . *Operating Manual*, Feb 2010.

[54] Stellar Solutions Inc. Citrisurf 2250 product information, 2014. URL `http://citrisurf.com/cs2250info.htm`.

[55] Joseph R. Davis. Stainless Steel. *ASM International*, pages 137–139, Jan 1994.

[56] J.A. Favre. Removal of radon from hydrocarbon streams, February 24 1976. US Patent 3,940,471.